SRNL-STI-2012-00018
Revision 0

Keywords: *Alternative Reductant, DWPF, CPC, glycolic acid, hydrogen*

Retention: *Permanent*

Glycolic-Nitric Acid Flowsheet Demonstration of the DWPF Chemical Processing Cell with Matrix Simulants and Supernate

D.P. Lambert
M.E. Stone
J.D. Newell
D.R. Best

May 2012

Savannah River National Laboratory
Savannah River Nuclear Solutions, LLC
Aiken, SC 29808

Prepared for the U.S. Department of Energy under contract number DE-AC09-08SR22470.

SRNL
SAVANNAH RIVER NATIONAL LABORATORY

DISCLAIMER

Printed in the United States of America

Prepared for
U.S. Department of Energy

SRNL-STI-2012-00018
Revision 0

Keywords: *Alternative Reductant, DWPF, CPC, glycolic acid, hydrogen*

Retention: *Permanent*

Glycolic-Nitric Acid Flowsheet Demonstration of the DWPF Chemical Processing Cell with Matrix Simulants and Supernate

D.P. Lambert
M.E. Stone
J.D. Newell
D.R. Best

May 2012

Savannah River National Laboratory
Savannah River Nuclear Solutions, LLC
Aiken, SC 29808

Prepared for the U.S. Department of Energy under contract number DE-AC09-08SR22470.

SRNL
SAVANNAH RIVER NATIONAL LABORATORY

REVIEWS AND APPROVALS

AUTHORS:

D.P. Lambert, Process Technology Programs Date

M.E. Stone, Process Technology Programs Date

J.D. Newell, Process Technology Programs Date

D.R. Best, Process Technology Programs Date

TECHNICAL REVIEW:

D.C. Koopman, Process Technology Programs Date

APPROVAL:

C.C. Herman, Manager Date
Process Technology Programs

S.L. Marra, Manager Date
Environmental & Chemical Process Technology Research Programs

J.E. Occhipinti, Manager Date
Waste Solidification Engineering

EXECUTIVE SUMMARY

Testing was completed to demonstrate the viability of the newly developed glycolic/nitric flowsheet for processing in the Defense Waste Processing Facility's (DWPF) Chemical Process Cell (CPC). The Savannah River National Laboratory (SRNL) initiated a sludge matrix study to evaluate the impact on CPC processing. Four sludge simulants were designed to cover a broad insoluble solid composition range to bracket future sludge batches. The first pair of sludge parameters was high iron/low aluminum versus low iron/high aluminum (referred to as HiFe or LoFe in this report). The second pair of sludge parameters was high calcium-manganese/low nickel, chromium, and magnesium versus low calcium-manganese/high nickel, chromium, and magnesium (referred to as HiMn or LoMn in this report). In addition, a simple supernate simulant was prepared to match the composition of the matrix simulants.

Four planned experiments (GF34 to GF37) and four additional experiments (GF36b, GF36c, GF37b and GF38) were completed to demonstrate the glycolic-nitric flowsheet viability. Also, four supernate experiments (GF39a-GF39d) were performed to better understand the reaction sequence, particularly the reduction and stripping of mercury.

Composition and physical property measurements were made on the Sludge Receipt and Adjustment Tank (SRAT) and Slurry Mix Evaporator (SME) products. Composition measurements were made on the composited condensates from the Mercury Water Wash Tank (MWWT), and Formic Acid Vent Condenser (FAVC), on the ammonia scrubber solution, and on SRAT samples pulled throughout the SRAT cycle. Updated values for glycolate and formate loss, nitrite-to-nitrate conversion, and oxalate formation were found that can be used in the acid calculations for future sludge matrix process simulations with the glycolic-nitric flowsheet.

Preliminary results of the initial testing indicate:

- Hydrogen generation rate was below detection limits (<7.6E-4 lb/hr DWPF-scale or <0.001 vol%) throughout all SRAT cycles.
- Hydrogen generation rate was below 0.0258 lb/hr DWPF-scale throughout all SME cycles. Hydrogen was produced in the SME cycles because formic acid was added with the frit slurry.
- Mercury was both reduced and stripped without formic acid. The mercury concentration of the SRAT product was below 0.8 wt % limit in four of the runs and below 0.92 wt % in the other four runs.
- Nitrite in the SRAT product was <100 mg/kg slurry for all runs
- Foaminess was not an issue using the nominal antifoam addition strategy in these tests.
- High wt % total solids were achieved while staying within rheological limits which makes the glycolic acid/nitric acid flowsheet an improvement for processing more viscous sludges. However, there may be a tradeoff between excessive dissolution of metals and thinner rheology.
- The pH remains steady throughout processing (i.e. no pH rebound) potentially leading to more consistent processing during the CPC. The SRAT product pH varied from 3.5-4.5 for the 100% acid stoichiometry runs, significantly lower than is typical of the baseline nitric acid/formic acid flowsheet.

- The testing apparatus has been significantly modified to improve processing with high viscosity slurries. Testing of the old style and new style rig identified no differences in CPC processing, including steam stripping of Hg.

Recommendations:
The glycolic-nitric flowsheet is recommended as a viable flowsheet alternative to the baseline DWPF flowsheet. In the testing that has been performed to date, this flowsheet meets or outperforms the current flowsheet in minimizing off-gas generation, removing mercury, and producing a rheologically thinner product. Previous testing with glycolic/formic acid mixtures demonstrated a wide processing window regarding both the glycolic-formic ratio and acid stoichiometry. The addition of glycolic acid leads to SRAT products that are rheologically less viscous which means that more concentrated products can be produced, leading to potentially higher waste throughput per batch. In addition, the combination of lower pH processing and the complexing power of glycolic acid leads to the dissolution of more metals, which may minimize deposits in the CPC processing vessels and prevent the fouling of steam coils. Follow on testing is recommended in the following areas:

- Improve glycolate and oxalate analyses. The majority of the glycolate results reported were correct. However, there are issues with anion and cation deposition on the Ion Chromatograph's (IC) column, causing higher than expected glycolate and oxalate in blanks and some samples. Both Process Science and Analytical Laboratory (PSAL) and Analytical Development (AD) have reported results that have varied significantly from expectations. Modification to the sample preparation method is likely needed to improve analytical accuracy and minimize the cleaning and replacement of the IC column. An alternative to the IC measurement of glycolate should also be considered.
- Determine the appropriate REDOX model for the glycolic-nitric flowsheet. The REDOX model may need more terms due to the more extensive reduction of some metals, including Mn and Fe. In addition, accurate measurement of glycolate (and possibly oxalate) and nitrate is needed to accurately predict REDOX. REDOX testing of the matrix sludges should be repeated using acceptable frits that meet Product Composition Control System (PCCS) limits.
- Testing should be completed with alternate forms of ruthenium to determine whether the elimination of the chloride added as ruthenium chloride would improve the reduction and stripping of the mercury. Testing should be completed with the baseline and glycolic-nitric flowsheets.
- Test the glycolic-nitric flowsheet at acid stoichiometries of less than 100%. Demonstration of this flowsheet at an acid stoichiometry of <100% is recommended and might be useful for mercury stripping.
- Demonstrate the glycolic-nitric flowsheet with actual waste in SRNL Shielded Cells SRAT and SME processing, to include periodic slurry sampling throughout the SRAT and SME processing along with a glass REDOX measurement.
- Increase both the nitric and glycolic acid flowrate to the same scaled molar flowrate as formic acid to minimize glycolic-nitric flowsheet batch time.
- Complete a supernate experiment without nitrite to determine whether nitrite is needed to reduce mercury.
- Measure SME condensate anions and cations in future glycolic-nitric flowsheet runs.

TABLE OF CONTENTS

LIST OF TABLES

LIST OF FIGURES

LIST OF ABBREVIATIONS

AD	Analytical Development
CPC	Chemical Process Cell
DWPF	Defense Waste Processing Facility
GC	Gas Chromatograph
FAVC	Formic Acid Vent Condenser
HM	H-Canyon Modified (PUREX)
IC	Ion Chromatography
ICP-AES	Inductively Coupled Plasma-Atomic Emission Spectroscopy
MWWT	Mercury Water Wash Tank
PSAL	Process Science Analytical Laboratory
PUREX	Plutonium - URanium EXtraction
REDOX	Reduction/Oxidation
SME	Slurry Mix Evaporator
SMECT	Slurry Mix Evaporator Condensate Tank
SRAT	Sludge Receipt and Adjustment Tank
SRNL	Savannah River National Laboratory
SRR	Savannah River Remediation
SRS	Savannah River Site
TOC	Total Organic Carbon Analysis
TT&QAP	Task Technical and Quality Assurance Plan
XRD	X-ray Diffraction

1.0 Introduction

Savannah River Remediation (SRR) is evaluating changes to its current DWPF flowsheet to improve processing cycle times. This will enable the facility to support higher canister production while maximizing waste loading. Higher throughput is needed in the CPC since the installation of the bubblers into the melter has increased melt rate. Due to the significant maintenance required for the DWPF gas chromatographs (GC) and the potential for production of flammable quantities of hydrogen, reducing or eliminating the amount of formic acid used in the CPC is being developed. Earlier work at Savannah River National Laboratory has shown that replacing formic acid with an 80:20 molar blend of glycolic and formic acids has the potential to remove mercury in the SRAT without any significant catalytic hydrogen generation.[1,2,3] This report summarizes the research completed to determine the feasibility of processing without formic acid.

In earlier development of the glycolic-formic acid flowsheet, one run (GF8) [2] was completed without formic acid. It is of particular interest that mercury was successfully removed in GF8, no formic acid at 125% stoichiometry. Glycolic acid did not show the ability to reduce mercury to elemental mercury in initial screening studies, which is why previous testing focused on using the formic/glycolic blend.

The objective of the testing detailed in this document is to determine the viability of the nitric-glycolic acid flowsheet in processing sludge over a wide compositional range as requested by DWPF.[4] This work was performed under the guidance of Task Technical and Quality Assurance Plan (TT&QAP).[5] The details regarding the simulant preparation and analysis have been documented previously.[6]

2.0 Experimental Procedure

The experimental apparatus used in these experiments is typical for DWPF SRAT/SME testing. The four experiments were performed in 4-L kettles. The test equipment included a GC to measure off-gas composition, an ammonia scrubber, and a pH meter. In all runs, the SRNL acid calculation spreadsheet[7] used the Koopman equation[8] to determine acid addition quantities and dewater targets.

2.1 CPC Simulation Details

The SRAT 4-L rigs were assembled following the guidelines of SRNL-3100-2011-00127.[9] The intent of the equipment is to functionally replicate the DWPF processing vessels. Each glass kettle is used to replicate both the SRAT and SME, and it is connected to the SRAT Condenser, the MWWT, and the FAVC. The Slurry Mix Evaporator Condensate Tank (SMECT) is represented by a sampling bottle that is used to remove condensate through the MWWT. For the purposes of this paper, the condensers and wash tank are referred to as the off-gas components. A sketch of the experimental setup is given in Figure 2-1.

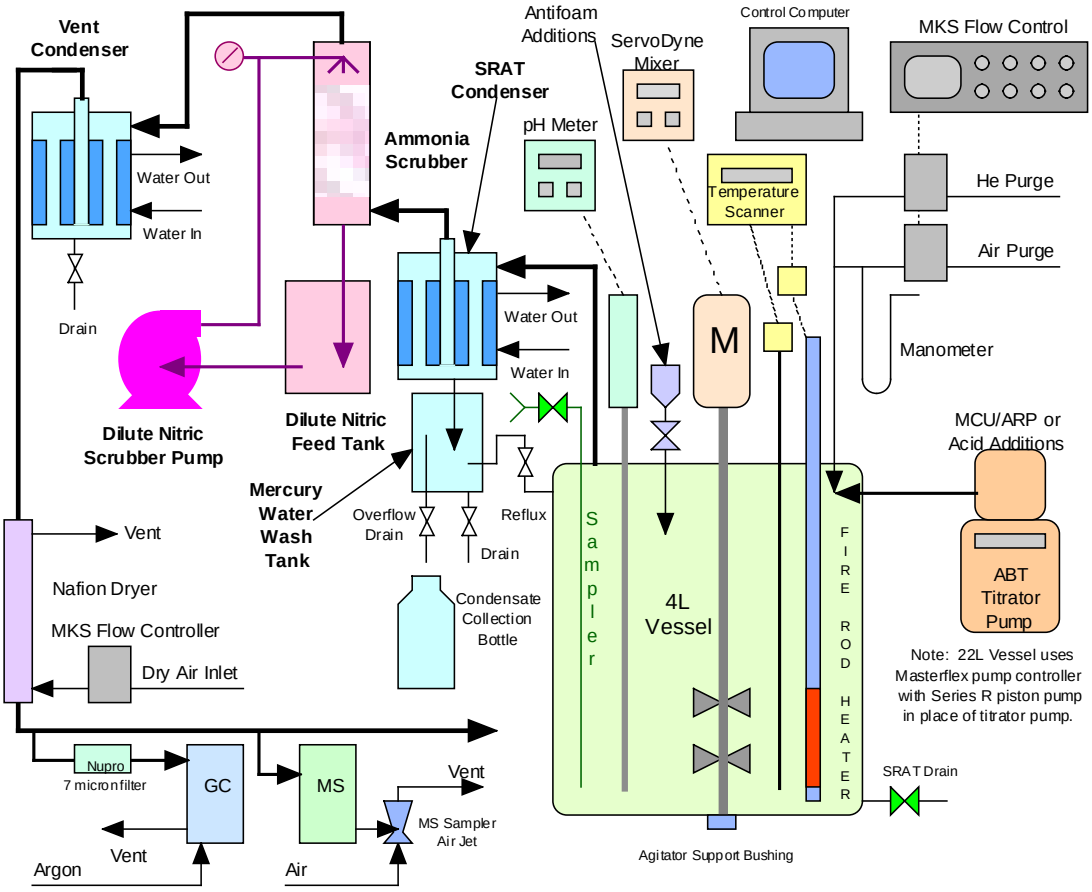

Figure 2-1. Schematic of CPC Equipment Set-Up

There were several notable changes to the CPC equipment set-up:

1. Used two heating rods to better simulate the steam coils instead of a heating mantle
2. Used Series R piston pump instead of titrator pump
3. The control system was modified to control the heating rod so that it could not reach a temperature of >160°C, the approximate maximum temperature of the DWPF steam coils

The runs were performed using the guidance of Procedure ITS-0094 [10] ("Laboratory Scale Chemical Process Cell Simulations") of Manual L29. Off-gas hydrogen, oxygen, nitrogen, nitrous oxide, and carbon dioxide concentrations were measured during the experiments using in-line instrumentation. Helium was introduced at a concentration of 0.5% of the total air purge as an inert tracer gas so that total amounts of generated gas and peak generation rates could be calculated. This approach eliminates the impact of fugitive gas losses through small leaks on the calculated outlet gas flowrates. During the runs, the kettle was visually monitored to observe process behavior including foaming, air entrainment, rheology changes, loss of heat transfer capabilities, and off-gas carryover. Observations were recorded on data sheets and pasted into laboratory notebooks.[11]

Quality control measures were in place to qualify the data in this report. Helium and air purges were controlled using mass flow controllers calibrated by the SRNL Standards Lab using

traceable standards and methods. Thermocouples were calibrated using a calibrated dry block calibrator. The GCs were calibrated with standard calibration gases before and after the runs and the data reprocessed based on these data. The pH probes were calibrated with pH 4 and pH 10 buffer solutions and rechecked at the conclusion of each run using pH 4, 7 and 10 buffer solutions.

The automated data acquisition system developed for the 4-L SRAT rigs was used to collect data electronically. Data included SRAT temperature, bath temperatures for the cooling water to the SRAT condenser and FAVC, slurry pH, heating rod temperature and watts, SRAT mixer speed and torque, and air and helium purge flows. Cumulative acid addition flowrate and volume data are calculated from the acid pump rotation speed. Raw GC data were acquired on a computer dedicated to the GCs.

Dual column Agilent 3000A micro GC's were used on both runs. The GC's were baked out before and between runs. Column-A can collect data related to He, H_2, O_2, N_2, NO, and CO, while column-B can collect data related to CO_2, N_2O, and water. Calibrations were performed using a standard calibration gas containing 0.499 vol% He, 1.000 vol% H_2, 20.00 vol% O_2, 51.0 vol% N_2, 25.0 vol% CO_2 and 2.50 vol% N_2O. Instrument calibration was verified prior to starting the SRAT cycle. Room air was used to give a two point calibration for N_2. Calibration status was rechecked following the SRAT cycle.

Concentrated nitric acid (~50 wt %) and glycolic acid (~70 wt %) were used to acidify the sludge and perform neutralization and reduction reactions during processing. The total amount of acid (in moles) to add for each run was determined using the Koopman acid equation[8]. The Koopman minimum acid equation was used with a 100% stoichiometric factor for all tests except GF 38 (125%).

The acid mix was partitioned between nitric and glycolic acid by utilizing the latest REDOX equation[12] with a term added for glycolate ion (see below). A coefficient of 6 was used on the glycolate term based on electron equivalence.[13] The REDOX target ($Fe^{2+}/\Sigma Fe$) was 0.1. Process assumptions were made to predict SME product anion concentrations. In addition to the standard assumptions needed for formate and oxalate loss and nitrite to nitrate conversion, a factor was added to the acid calculation for glycolate loss. Process assumptions for the stoichiometric window testing were adjusted based on results from earlier testing.

$$REDOX=0.2358+0.1999*((2*C_{formate}+4*C_{oxalate}+4*C_{Carbon}+6*C_{glycolate}-5*(C_{Nitrate}+C_{Nitrite})-5*C_{Mn}))*(45/TS)$$

Where C_x = species concentration of component x, g-mole/kg melter feed, TS = total solids in melter feed in wt %, and REDOX is a molar ratio of $Fe^{2+}/\Sigma Fe$

A standard 4-L SRAT/SME apparatus with an ammonia scrubber was used for these simulations. The scrubber solution consisted of 749 g of de-ionized water and 1 g of 50 wt% nitric acid. The solution was recirculated through the column by a MasterFlex pump at 300 mL/min through a spray nozzle at the top of the packed section. Glass rings were used as packing and did not significantly add to the back pressure on the SRAT vessel as has been seen in earlier tests with different packing. The SRAT condenser was maintained at 25 °C during the run, while the vent condenser was maintained at 4 °C.

In experiments with sludge simulants, 200 ppm antifoam was added prior to acid addition, 100 ppm was added after nitric acid addition, 500 ppm was added before boiling and 100 ppm was added before the SME cycle and every 12 hours during boiling.

In supernate experiments, no antifoam was added. SRAT processing was abbreviated to include a two hour dewater time and about three hours at reflux.

2.2 Sludge Matrix

SRNL produced four matrix sludge simulants in order to improve the understanding of how changing sludge composition impacts DWPF waste processing. These simulants have been used in other SRNL studies, and the composition has been previously measured. [6,14] These simulants were used to demonstrate the flowsheet across a broad compositional range.

There are many elements in the insoluble solids. The two major insoluble elements in Savannah River Site (SRS) high activity waste slurries are iron and aluminum, corresponding to Plutonium - URanium EXtraction (PUREX) and H-Canyon Modified (HM) wastes respectively. The first solids concentration parameter was chosen to reflect variations between these two elements. There are a number of elements that occur at about an order of magnitude lower concentration than Al and Fe in SRS waste slurries including Ca, Hg, Mg, Mn, Ni, and Si (also U, but that is outside the scope of this study). These can be defined as the semi-major elements. Creating high-low pairs from all of these elements in addition to Al and Fe would have led to a prohibitively large study. The size of the study was controlled by grouping some of the semi-major elements into two sets. Manganese was paired with Ca, and Mg was paired with Ni. This defined the second concentration parameter in the study. Silicon, as SiO_2, was seen as essentially inert and not included in the pairings with the other semi-major elements.

Mercury has been studied in other contexts. Therefore, mercury was held at 1.5 wt% in the starting sludge total solids in all tests in the sludge matrix study. The noble metals were added at the same concentrations as were used in previous high noble metal tests of the matrix sludges.[15] Cr is typically at least an order of magnitude lower in concentration than the semi-major elements. It was considered potentially significant, however, due to its several oxidation states and was added to the Mg-Ni pair. Another constraint on handling the semi-major elements was that the oxides must sum to 100%. Suppressing or enhancing the concentrations of all of the semi-major elements simultaneously would have led to unreasonably high or low concentrations of either Al or Fe. Conceptually, the second concentration parameter represents reasonable compositional variations within each of the two main waste types, PUREX or HM (Figure 2-2).

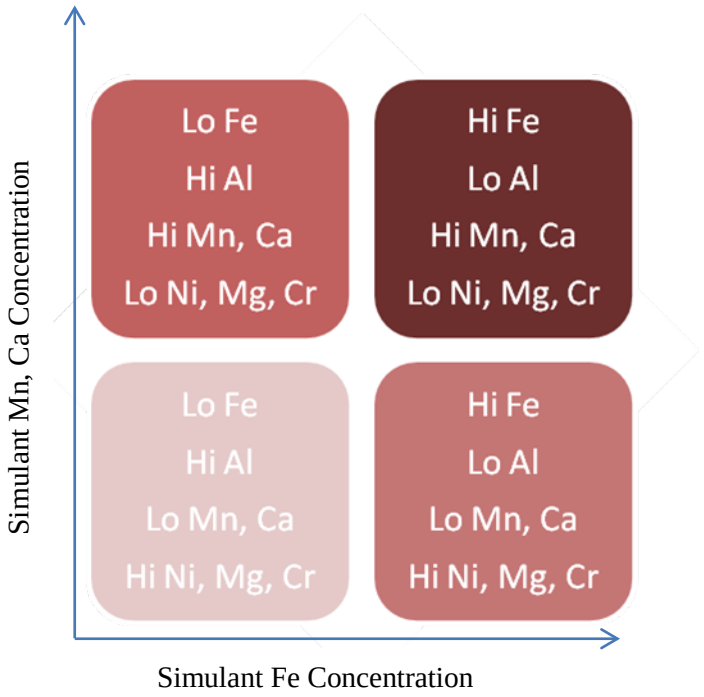

Figure 2-2. Definition of Sludge Matrix Simulants

The three primary parameter groups drawn from the insoluble solids are summarized below:

1. High iron or high aluminum (representing PUREX and HM wastes respectively). This parameter is referred to as either Hi Fe or Lo Fe in the discussion below.
2. High Mn and Ca or high Mg, Ni, and Cr (representing the semi-major insoluble species). This parameter is referred to as either Hi Mn or Lo Mn below.
3. The other (minor) sludge species, such as Ba, Zn, Zr, Cu, La, etc., were to be held in constant relative proportions in the simulants.

The measured slurry composition is summarized in Table 2-1.The supernate compositions of the matrix sludge simulants were maintained nearly constant.

The sludge simulations had identical mercury and noble metal targets, given in Table 2-2 as wt% in the total solids of the trimmed slurry. The noble metals concentrations are comparable to the high noble metal case in the Rh-Ru-Hg matrix study, while mercury was held constant during this study at the midpoint value of the Rh-Ru-Hg matrix study.[15]

Table 2-1. Composition of Sludge Simulants

Result	GF34 HiFeHiMn	GF35 SB7An	GF36 LoFeLoMn	GF37/GF3 LoFeLoMn	Units
Total Solids	23.70	18.02	22.81	23.07	wt%
Calcined Solids	17.81	13.61	16.95	16.00	wt%
Insoluble Solids	16.70	12.57	16.35	16.05	wt%
Soluble Solids	7.00	5.45	6.47	7.01	wt%
Slurry Density	1.185	1.142	1.189	1.176	kg / L slurry
Supernate density	1.057	1.053	1.055	1.057	kg / L supernate
Aluminum	9.000	15.65	9.130	23.755	wt % calcined basis

Table 2-1. Composition of Sludge Simulants					
Result	**GF34 HiFeHiMn**	**GF35 SB7An**	**GF36 LoFeLoMn**	**GF37/GF3 LoFeLoMn**	**Units**
Boron	<0.100	<0.100	<0.100	<0.100	wt % calcined basis
Barium	0.077	0.102	0.101	0.0705	wt % calcined basis
Calcium	3.83	0.836	2.22	1.97	wt % calcined basis
Cadmium	<0.010	NM	<0.010	<0.010	wt % calcined basis
Cerium	0.104	0.148	0.108	0.0965	wt % calcined basis
Chromium	0.015	0.0455	0.285	0.244	wt % calcined basis
Copper	0.045	0.033	0.045	0.048	wt % calcined basis
Iron	32.4	19.2	31.5	12.2	wt % calcined basis
Potassium	0.120	0.125	0.0905	0.0955	wt % calcined basis
Magnesium	0.396	0.366	2.69	2.42	wt % calcined basis
Manganese	4.04	4.37	0.721	0.661	wt % calcined basis
Sodium	12.9	15.3	13.1	14.2	wt % calcined basis
Nickel	0.213	3.37	2.6345	2.312	wt % calcined basis
Phosphorus	<0.100	<0.100	<0.100	<0.100	wt % calcined basis
Lead	0.071	0.025	0.047	0.0715	wt % calcined basis
Sulfur	0.289	0.371	0.340	0.374	wt % calcined basis
Silicon	1.580	1.91	1.52	1.32	wt % calcined basis
Tin	<0.010	0.013	0.106	0.0925	wt % calcined basis
Titanium	<0.010	0.025	<0.010	<0.010	wt % calcined basis
Zinc	0.065	0.047	0.0775	0.0705	wt % calcined basis
Zirconium	0.054	0.252	0.1175	0.049	wt % calcined basis
Nitrite	17,900	9,140	17,800	13,250	mg/kg slurry
Nitrate	13,550	6,470	13,400	13,250	mg/kg slurry
Formate	<100	<100	<100	<100	mg/kg slurry
Sulfate	1,770	1,460	1,575	1,585	mg/kg slurry
Chlorine	116	<100	131	127	mg/kg slurry
Phosphate	0	<100	<100	<100	mg/kg slurry
Oxalate	300	8,500	275	295	mg/kg slurry
Glycolate	<100	NM	<100	<100	mg/kg slurry
Total or Slurry TIC	2,751	1,066	2,492	2,403	mg/kg slurry
Supernate TIC	1,080	664	1,310	1,280	mg/L supernate
Total Base pH = 7	0.590	0.580	0.562	0.522	moles/L

Table 2-2. Mercury and Noble Metal Composition Added to Sludge Simulants

Noble Metal	Concentration Weight Percent Total solids basis
Target wt% Hg dry basis	1.5000
Target Ag metal content	0.0014
Target Pd metal content	0.0790
Target Rh metal content	0.0380
Target Ru metal content	0.2170

An additional supernate simulant was prepared to supplement the four slurry simulants above. The purpose of this simpler simulant was to improve understanding of the mercury reduction chemistry. The simulant was similar to the supernate used in the matrix slurry preparation. The only soluble species added were sodium hydroxide, sodium nitrite, sodium nitrate, sodium sulfate, sodium oxalate, sodium carbonate and potassium nitrate. The resulting concentration is summarized in Table 2-3. The added noble metal and mercury target of these runs is summarized in Table 2-4. Note that because of the lower total solids of the supernate, the added mass of noble metals and mercury is approximately one-third that added in the slurry experiments.

Table 2-3. Composition of Supernate Simulant

Anion or Cation	Concentration mg/kg
Nitrite	21,561
Nitrate	15,784
Carbonate	6,051
Oxalate	351
Sulfate	1,888
Free Hydroxide	3,556 (0.221 M)
Na	27,067
K	153

Table 2-4. Mercury and Noble Metal Composition Added to Supernate Simulants

Noble Metal	Concentration Weight Percent Total solids basis
Target wt% Hg dry basis	1.5000
Target Ag metal content	0.0014
Target Pd metal content	0.0790
Target Rh metal content	0.0297
Target Ru metal content	0.2170

2.3 CPC Run Details

The eight nitric-glycolic acid flowsheet tests were performed at the ACTL using the four-liter kettle setup. Table 2-5 identifies each run and its corresponding assumptions.

Table 2-5. CPC Simulation Process Assumptions

Run	Sludge	Cycles	Date	% Koopman Acid Stoichiometry	Actual % Hsu Acid Stoichiometry	Labware
GF34	HiFeHiMn	SRAT/SME	16-Nov-11	104.0	108.0	New
GF35	SB7A	SRAT/SME	17-Nov-11	100.0	102.2	New
GF36	HiFeLoMn	SRAT/SME	16-Nov-11	106.1	125.1	New
GF36b	HiFeLoMn	SRAT	25-Jan-12	106.1	125.1	New
GF36c	HiFeLoMn	SRAT	25-Jan-12	106.1	125.1	Old
GF37	LoFeLoMn	SRAT/SME	2-Feb-12	100.0	112.3	New
GF37b	LoFeLoMn	SRAT	17-Nov-11	100.0	112.3	New
GF38	LoFeLoMn	SRAT	2-Feb-12	125	140.4	New

DWPF design basis processing conditions were scaled down and used for most processing parameters including SRAT/SME air purges and boil-up rate. SRAT product total dried solids were targeted at 27 wt% for the slurry simulant runs. Final SME total dried solids were targeted at 45% at 36% waste loading.

Because nitric and glycolic acid are more dilute acids than formic acid, both acids were added at the same molar flowrate as formic acid. Thus nitric acid was added at a DWPF scaled flowrate of 4.572 gallons per minute and glycolic acid was added at a DWPF scaled flowrate of 3.948 gallons per minute to maintain acid addition times. It is recommended that DWPF modify the acid feed pumps to deliver the higher flow rates before implementing the glycolic flowsheet.

The following constraints must be met by the current DWPF CPC flowsheet:

- SRAT hydrogen <0.65 lb/hr
- SME hydrogen <0.223 lb/hr
- Reduce mercury to elemental form
- Steam strip mercury below 0.8 wt% in the SRAT product dried solids
- SRAT product less than 1000 mg nitrite/kg product slurry
- SRAT product rheology* design basis 1.5 to 5 Pa yield stress and 5 to 12 cP consistency
- SME product rheology* 2.5 to 15 Pa yield stress and 10 to 40 cP consistency
- Glass REDOX of 0.09-0.33 $Fe^{2+}/\Sigma Fe$
- Minimize water in SME product (55 wt% typical)
- Minimal foaming

Data are presented in Section 3 showing how the nitric-glycolic flowsheet met or exceeded the processing constraints in the list above with the possible exception of mercury removal and REDOX.

2.4 Off-gas Analytical Methods

Process samples were analyzed by various methods. Slurry and supernate elemental compositions were measured by inductively coupled plasma-atomic emission spectroscopy (ICP-AES) at PSAL. Soluble anion concentrations were measured by IC. Mercury concentration was

* Processing limits are the same for both SRAT and SME as agitator and drive are identical

measured by ICP-AES. Ammonium ion concentration on selected samples was measured by cation chromatography by SRNL AD. Slurry and supernate densities were measured using an Anton-Parr instrument at PSAL. Dewater and condensate samples were submitted to PSAL for IC. A gradient method using the Dionex AG-11HC and AS-11HC, 2mm microbore columns was used to analyze fluoride, glycolate, formate, chloride, nitrite, nitrate, sulfate, oxalate and phosphate on SRAT/SME samples.[16]

SME product samples were vitrified in nepheline sealed crucibles, and the resulting glasses were measured for REDOX ($Fe^{2+}/\Sigma Fe$).[17] The REDOX target for all the simulations in this study was 0.1. The target is achieved by predicting the SME product anion concentrations and adjusting the split of acids between nitric and glycolic. Therefore the ability to control REDOX at the target value is highly dependent on being able to accurately predict anion behavior in the SRAT and SME cycles. Inserting the actual SME product data into the latest REDOX correlation gave a "predicted" REDOX that was different than the target. It should be noted that frit 418 was used for all runs. No attempt was made to produce a frit that was optimized for each of the four sludges. The glass produced was nonhomogeneous and this may have impacted the redox results.

3.0 Results and Discussion

Four SRAT simulations with supernate and eight SRAT/SME process simulations with slurry feeds were completed to demonstrate the feasibility of using only glycolic acid as the reducing acid in SRAT processing. The elimination of formic acid has the potential to eliminate the catalytic generation of hydrogen, which could lead to the reduction of the air purge in the DWPF CPC. The main concern in eliminating formic acid[1] is that the mercury won't be effectively reduced, and won't be removed by steam stripping to meet the DWPF SRAT mercury target and minimize the mercury sent to the melter. The discussion begins with the supernate results followed by the slurry results.

3.1 Supernate Testing

Four SRAT process simulations were completed with a simple supernate solution with added mercury and noble metals. These runs were performed after the slurry runs in order to better understand the processing chemistry. In particular, it was important to understand when the mercury is reduced in processing. Samples were pulled during glycolic acid addition and for several hours during the dewater and reflux phases to better understand the process chemistry using a simpler mixture than sludge simulants.

3.1.1 *Mercury Reduction and Stripping*

Approximately 3.4 g of mercury were added to each simulation. The mercury recovery results are summarized in Table 3-1.

Table 3-1. Supernate Testing with Mercury and Noble Metals

Run	GF39a	GF39b	GF39c	GF39d
Hg, wt %	1.5	1.5	1.5	1.5
Rh, wt %	0	0.0297	0.0297	0.0297
Pd, wt %	0	0.079	0.079	0.079
Ag, wt%	0	0.0014	0.0014	0.0014
Ru, wt %	0	0.3358	0	0.3358
% Koopman Acid Stoichiometry	100	100	100	80
% Hsu Acid Stoichiometry	74	74	74	60
Hg Collected, g	0.617*	None	0.434#	None

* Found 1.455 g of elemental Hg in kettle
# Found 1.939 g of black solids in kettle

The runs demonstrated that the mercury could be reduced and stripped with only glycolic acid (no formic acid). The exception to this is that in the runs with added ruthenium chloride (GF39b, GF39d), no mercury was recovered. In runs with added ruthenium, 0.765 g Ru was added as $RuCl_3 \cdot 1.93H_2O$ (1.832 g or 0.0227 g-moles of Cl). In all runs, 3.689 g of HgO were added (0.0170 g-moles of Hg). In previous testing, the presence of Cl led to the production of calomel (Hg_2Cl_2), which is not steam stripped. It is recommended that these runs should be repeated with another form of Ru such as ruthenium oxide hydrate to see if adding the Ru without Cl has the same impact on mercury reduction and stripping.

The mercury (II) contained in the starting slurry as mercuric oxide was reduced during the glycolic acid addition at a pH of 4.5. The photographs below (Figure 3-1) show the slurry both before and after the run from Run GF39a (mercury was added but no noble metals). The kettle contents quickly changed from the orange HgO slurry to a transparent silver colored solution over a period of several minutes. The silver color slowly disappeared during boiling when the mercury was being steam stripped and recovered in the MWWT.

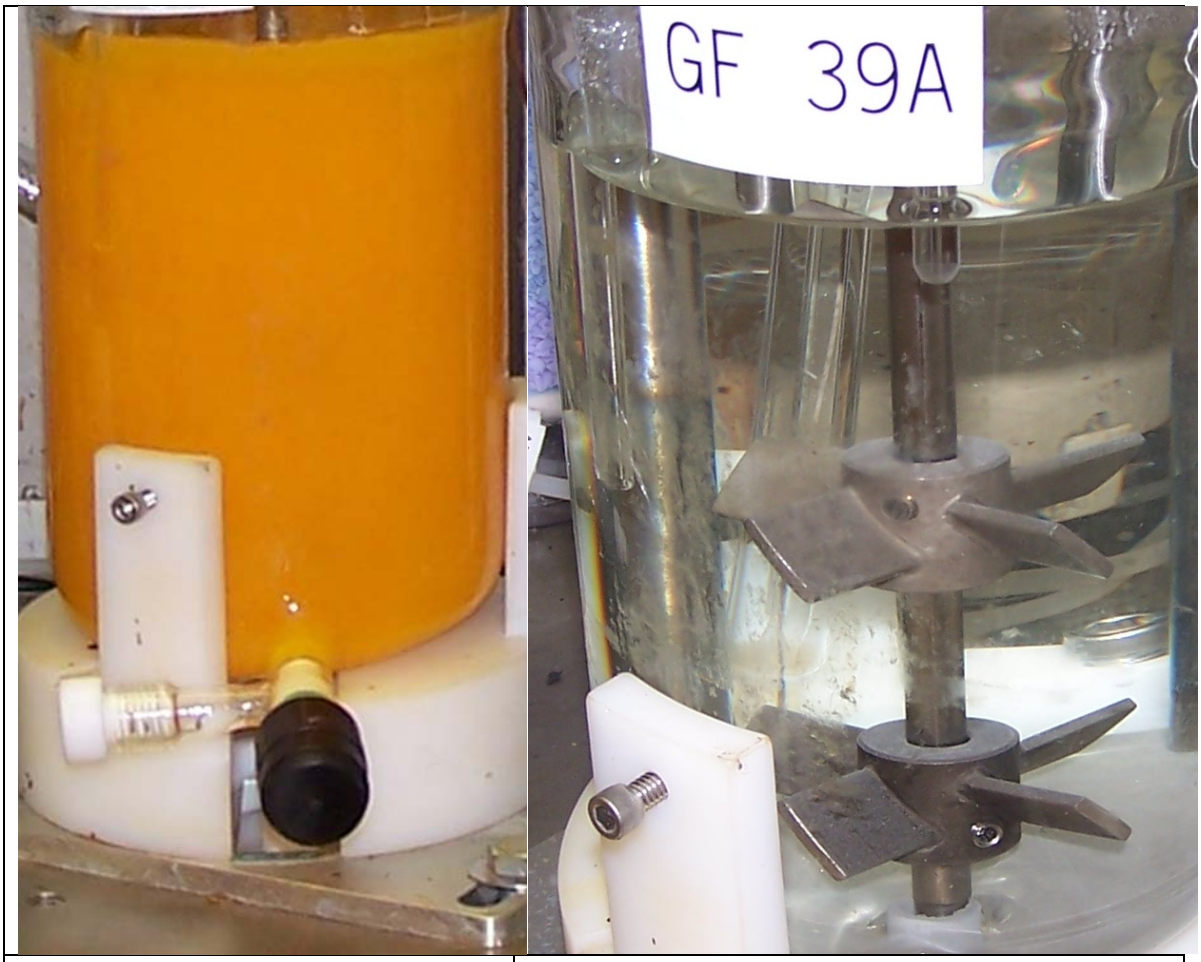

Figure 3-1. Photographs of GF39a before and after SRAT cycle (Supernate plus HgO)

In the runs with added noble metals and mercury, the slurry looked very much like sludge. The photographs below (Figure 3-2) show the slurry both before and after the run from Run GF39b (mercury and noble metals were added). The kettle contents quickly changed from the brown slurry to a transparent brown colored solution over a period of several minutes at a pH of 4.3. No mercury was recovered in the MWWT.

Figure 3-2. Photographs of GF39b before and after SRAT cycle (Supernate plus HgO and noble metals)

A mass balance was performed for each run to predict the concentration of all cations and anions throughout the run. In run GF39b (100% Koopman Stoichiometry, added noble metals and mercury), there was an apparent mass loss of 986 g (expected mass loss 151 g). This was calculated to match the final sodium concentration measured in the SRAT product sample. Using this mass loss, the predicted mercury concentration in the SRAT product is 2,306 mg/L and the measured mercury concentration was 2,315 mg/L. In other words, the mercury was completely soluble in the SRAT product and no mercury was recovered (not reduced, not stripped) in the MWWT. In contrast, run GF39a (100% Koopman stoichiometry, add mercury only), the final mercury concentration in the SRAT product was 14.9 mg/L compared to a predicted concentration of 1,433 mg/L (1.04% of the mercury was soluble). In addition, of the 3.4 g of mercury added initially on an elemental basis, 0.6 g was collected in the MWWT and 1.5 g was found in the SRAT product slurry as elemental mercury.

3.1.2 *Nitrite and Carbonate Destruction*

Nitrite and carbonate were below detection limits by the first hour of reflux in supernate testing. The results are summarized in Table 3-2.

Table 3-2. Nitrite Data, mg/L

Anion	GF39a	GF39b	GF39c	GF39d
Post Nitric Acid	20,000	19,700	21,800	21,700
Mid Glycolic Acid	10,800	6,560	4,540	11,700
Post Glycolic Acid	<100	1,070	1,150	2,615
1 hour dewater	<100	<100	<100	224
Post Dewater	<100	<100	<100	<100
Post Run	<100	<100	<100	<100

3.1.3 *Anion and Cation Mass Balance*

Anions and cations were measured (solid lines in graphs below) throughout the supernate runs. A mass balance was completed for each run based on the known amounts added in preparing the supernate and the mass of added noble metals and mercury. These predictions (dotted lines), calculated by mass balance, were plotted along with the measured result in Figure 3-3 and Figure 3-4 (GF39b is presented as an example of this data). It should be noted that the measured nitrate agrees well with the nitrate prediction but the measured glycolate is approximately 20% of that measured by PSAL. In addition, oxalate is also much higher than predicted. It is likely that some oxalate is produced from glycolate decomposition. The measured nitrate is greater than prediction during glycolic acid addition due to the oxidation of nitrite to nitrate but is lower than prediction during reflux and boiling due to nitrate destruction. The sulfate concentration as measured by IC was very different than predicted. However, the measured sulfate, as calculated from ICP-AES S, was approximately 30% higher than predicted.

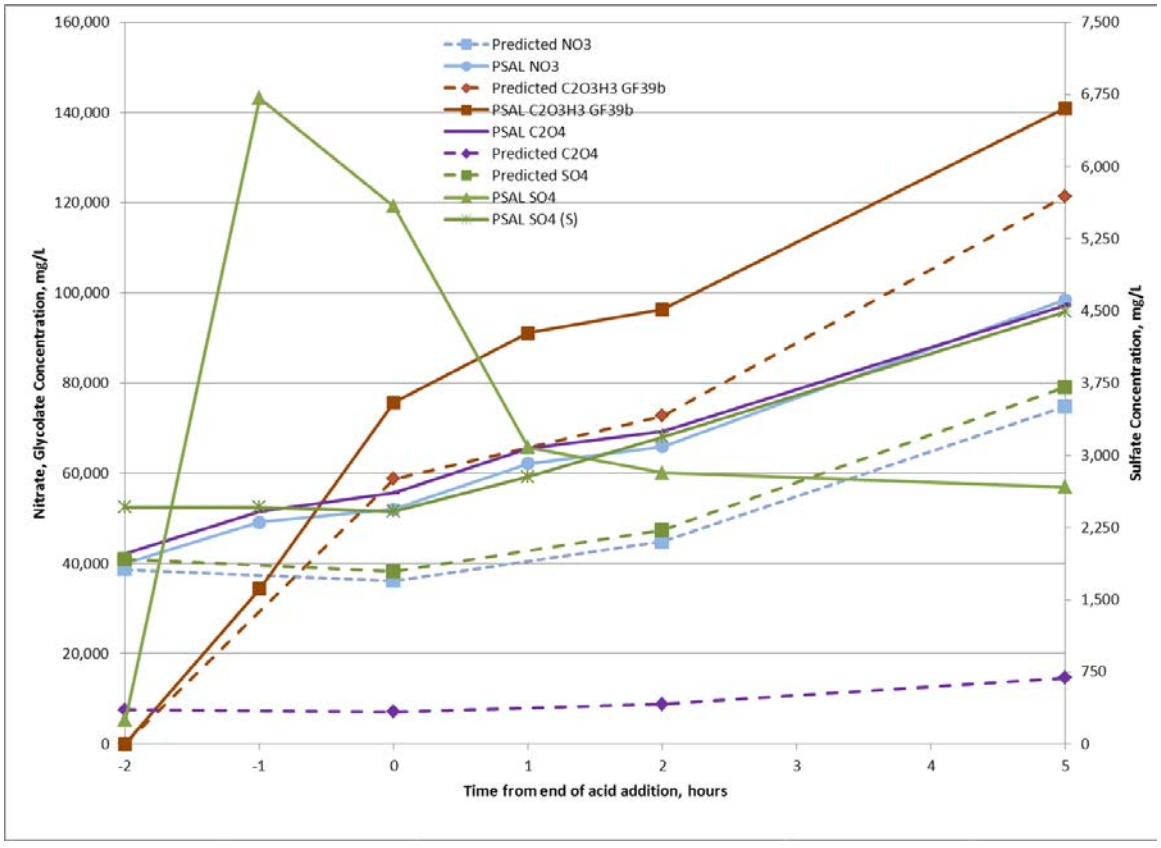

Figure 3-3. Supernate Run GF39b Predicted and Measured Anion Concentration

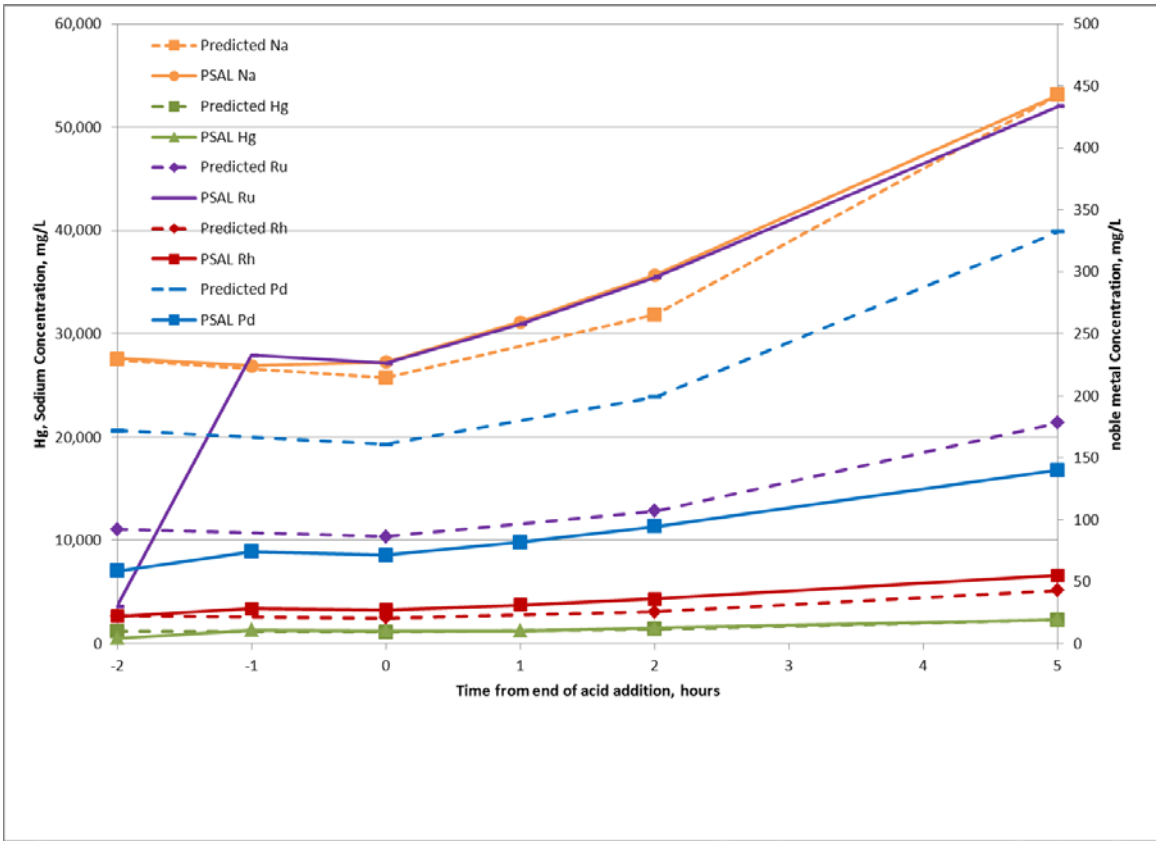

Figure 3-4. Supernate Run GF39b Predicted and Measured Cation Concentration

The measured sodium and mercury concentrations agreed well with predictions throughout run GF39b. The concentration of Pd and Ru were higher than predicted in Run GF39b. The Rh was approximately 80% of the predicted value and the Ag was below the detection limit. In Run GF39a (no added noble metals), the noble metals were all below detection limits.

3.1.4 *Conclusions from Supernate Testing*

The new SRAT apparatus is capable of keeping the noble metals and mercury suspended prior to acid addition. In runs with all noble metals (GF39b, GF39d), no mercury was reduced or collected. In runs without ruthenium chloride (GF39a, GF39c), mercury was collected in the MWWT and mercury was found in the SRAT product as an insoluble mercury compound.

The concentration of Pd and Ru were higher than predicted in Run GF39b. The Rh was approximately 80% of predicted and the Ag was below the detection limit. In Run GF39a (no added noble metals), the noble metals were all below detection limits.

Another interesting observation is that although the runs had no added Al, Ca, Cu, Fe, Mn, Mg, Ni or Si, these compounds were detected in samples throughout the runs (most of these have concentrations of approximately 10 mg/L, although Si was 40-80 mg/L). Although the glassware and agitator is cleaned by soaking in 8 M nitric acid overnight, the runs cleaned the equipment by dissolving up these metals. This is further demonstration that the glycolic-nitric flowsheet will help to keep the DWPF processing vessels cleaner than the current flowsheet.

3.2 Slurry Testing

Eight SRAT process simulations were completed with the matrix sludges and with added mercury and noble metals. Runs GF34, GF35, GF36 and GF37 were completed first and also included SME cycles. Runs 36b and 36c were duplicates of the GF36 SRAT cycle to compare the old and new processing rigs and determine whether the changes had impacted process chemistry. Run 37b was a duplicate of GF37 and GF38 was a higher acid stoichiometry repeat of GF37. The main reason for the four repeat runs was to better track mercury as the mercury recovery in the first four runs was poor. Some data from the supernate runs is included in this section for completeness if they were not reported in Section 3.1.

3.2.1 *Off-gas*

Besides essentially eliminating hydrogen generation, the glycolic acid flowsheet also appears to stop or significantly slow down other off-gas generating reactions. Data is presented to summarize the results of these analyses. More detailed data is included in Appendix B.

3.2.1.1 Hydrogen

A main objective of this testing was to show that hydrogen generation could be mitigated or eliminated by the use of the glycolic/nitric flowsheet. No hydrogen was detected in any of the SRAT cycles. When formic acid was added with the frit in the SME cycle, hydrogen generation on the order of 0.05 volume percent was measured (Figure 3-5). Table 3-3 compares SRAT and SME cycle hydrogen on a DWPF scale.

Table 3-3. Peak Hydrogen Generation

Run	Sludge Composition	SRAT H_2, lb/hr	SME H_2, lb/hr
DWPF	Current Limit	0.65	0.223
GF34	HiFeHiMn	0	0.017
GF35	SB7A	0	0.00759
GF36	HiFeLoMn	0	0.019
GF37b	HiFeLoMn	0	No SME
GF37c	HiFeLoMn	0	No SME
GF37	LoFeLoMn	0	0.0258
GF37b	LoFeLoMn	0	No SME
GF38	LoFeLoMn	0	No SME
GF39a, b, c, d	Supernate Hg and/or noble metals	0	No SME

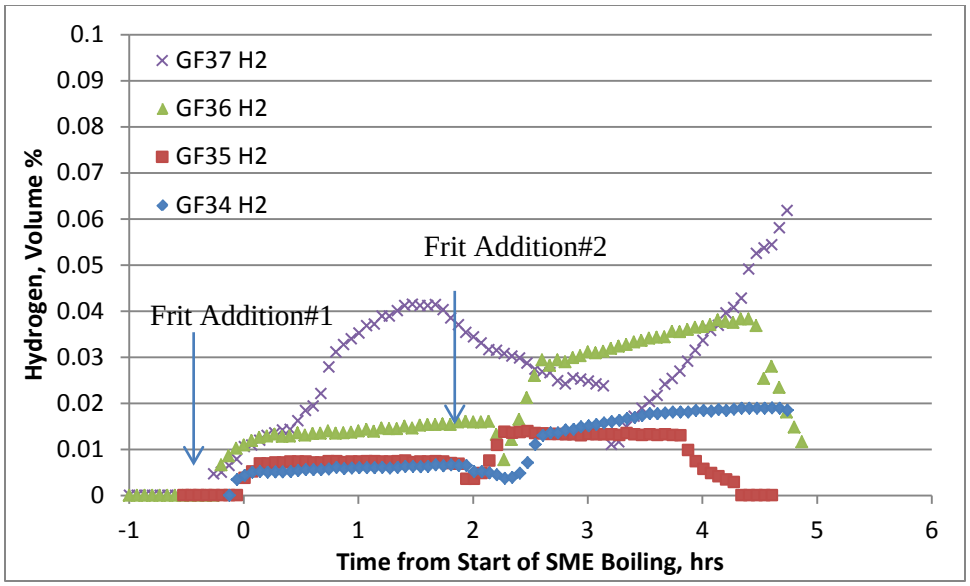

Figure 3-5. SME Cycle Hydrogen Generation

3.2.1.2 Other Off-gas Components

In addition to generation of hydrogen, other gases including carbon dioxide, carbon monoxide, and a number of oxides of nitrogen are produced. Only carbon dioxide and nitrous oxide (N_2O) can be quantified using the gas chromatographs and calibration gas standards.

Carbon dioxide is the major off-gas generated, produced by the decomposition of carbonate species during acid addition. Table 3-4 and Figure 3-6 summarizes the carbon dioxide generation in the SRAT cycle. Table 3-5 and Figure 3-7 summarizes the carbon dioxide generation in the SME cycle. The small generation of CO_2 in the SME cycle is triggered by the addition of formic acid with the frit in the frit-slurry. This could be eliminated by not adding formic acid with frit in the SME cycle.

Table 3-4. Comparison of SRAT Carbon Dioxide Generation Data

Run	CO_2 from Carbonate, g	CO_2 in off-gas, g
GF34	29.2	38.0
GF35	12.5	26.1
GF36	26.5	34.9
GF36b	26.5	29.0
GF36c	26.5	30.5
GF37	25.5	36.5
GF37b	25.5	32.8
GF38	25.5	19.5
GF39a (Hg)	12.9	17.2
GF39b (Hg + NM)	12.9	22.0
GF39c (Hg+NM-Ru)	12.9	18.6
GF39d (Hg + NM)	12.9	16.2

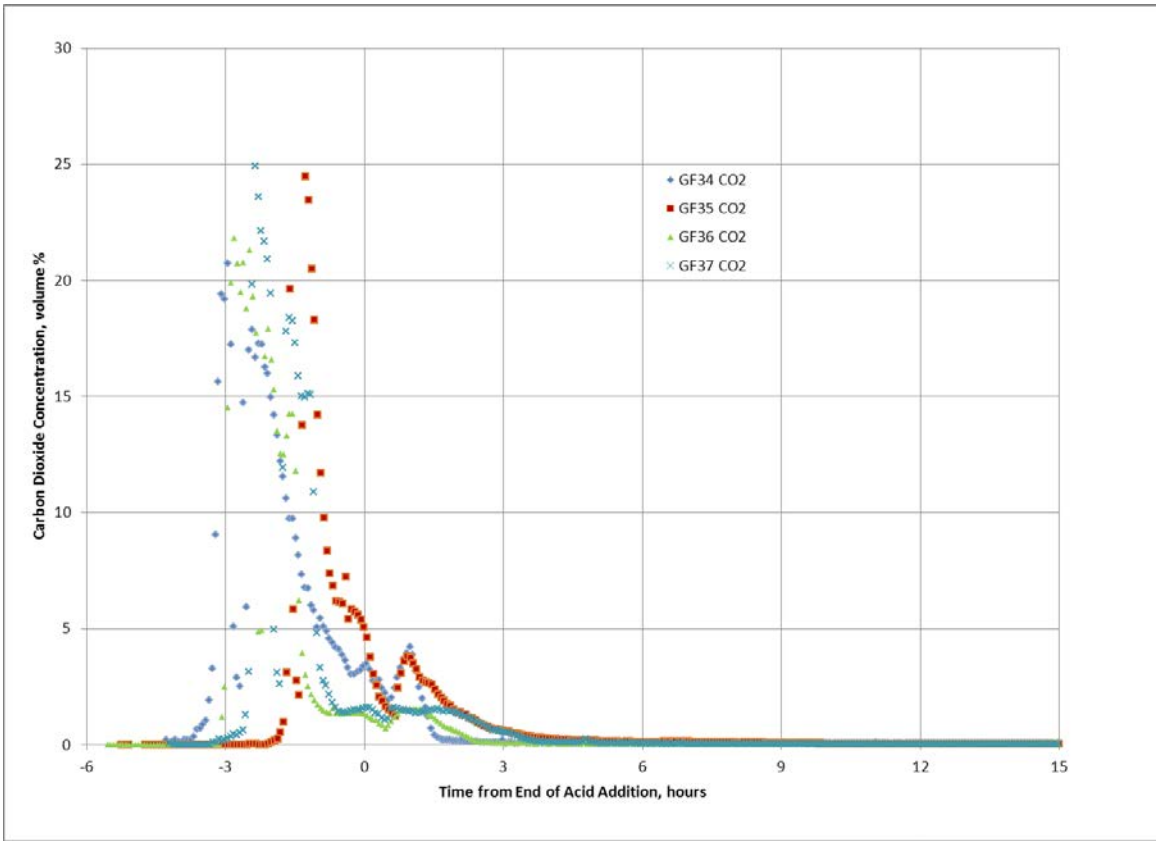

Figure 3-6. Carbon Dioxide Generation in SRAT cycles, lb/hr DWPF Scale

Table 3-5. Comparison of SME Carbon Dioxide Generation Data

Run	CO_2 from Formate, g	CO_2 in off-gas, g	CO_2 left as formate, g
GF34	10.2	5.1	5.9
GF35	7.3	1.4	7.1
GF36	9.6	7.1	7
GF37	9.1	6.8	6.6

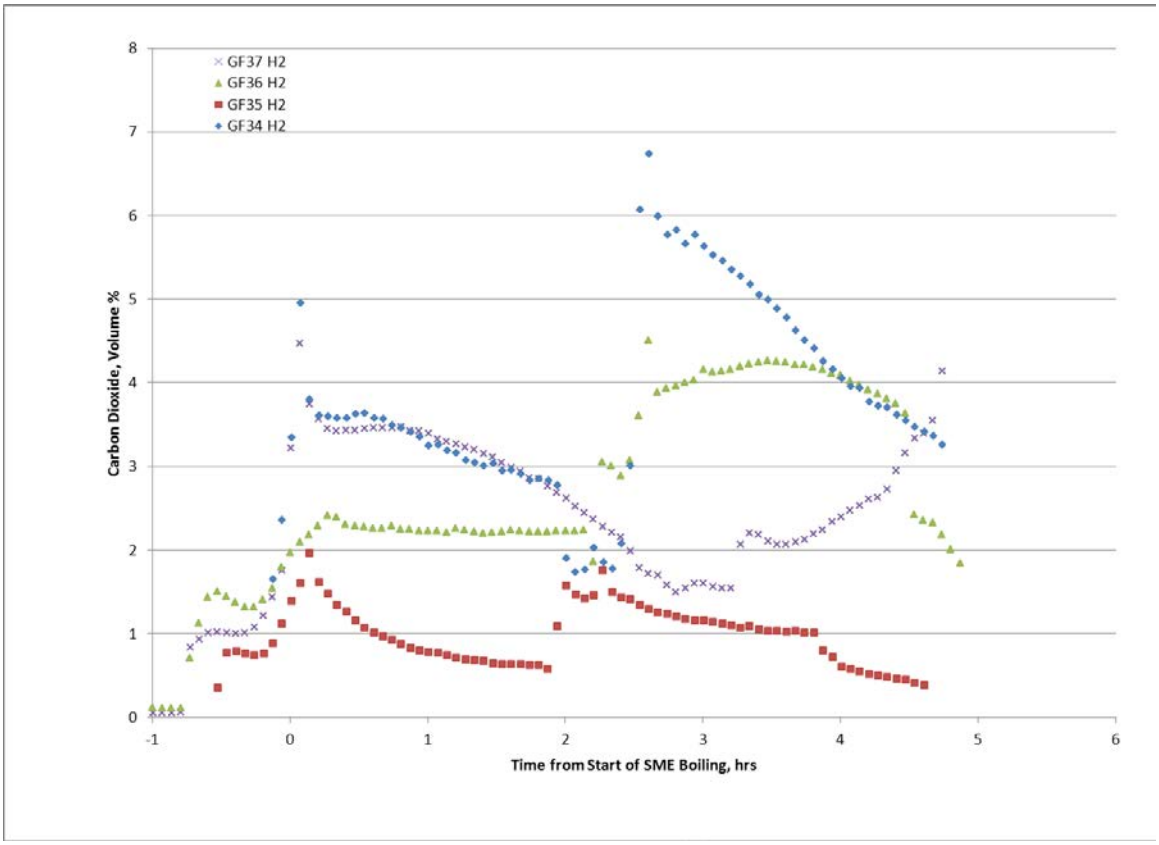

Figure 3-7. Carbon Dioxide Generation in SME cycles, lb/hr DWPF Scale

Most of the nitrite in the feed is converted to NO or NO_2 during the SRAT cycle. However, these cannot be quantified with the gas chromatographs, although the yellow off-gas is indicative of significant NO_2 in the off-gas. The production of N_2O is minor, 1.6% - 4.5% of the nitrite was converted to N_2O. Table 3-6 and Figure 3-8 summarizes the nitrous oxide generation in the SRAT cycle.

Table 3-6. Comparison of SME Nitrous Oxide Generation Data

Run	NO_2^- in feed , g	Potential N_2O from feed, g	Measured N_2O in off-gas, g
GF34	51.9	24.8	0.77
GF35	27.9	13.3	0.59
GF36	51.6	24.7	0.38
GF36b	51.6	24.7	0.35
GF36c	51.6	24.7	0.34
GF37	52.5	25.1	0.67
GF37b	52.5	25.1	0.45
GF38	52.5	25.1	0.21

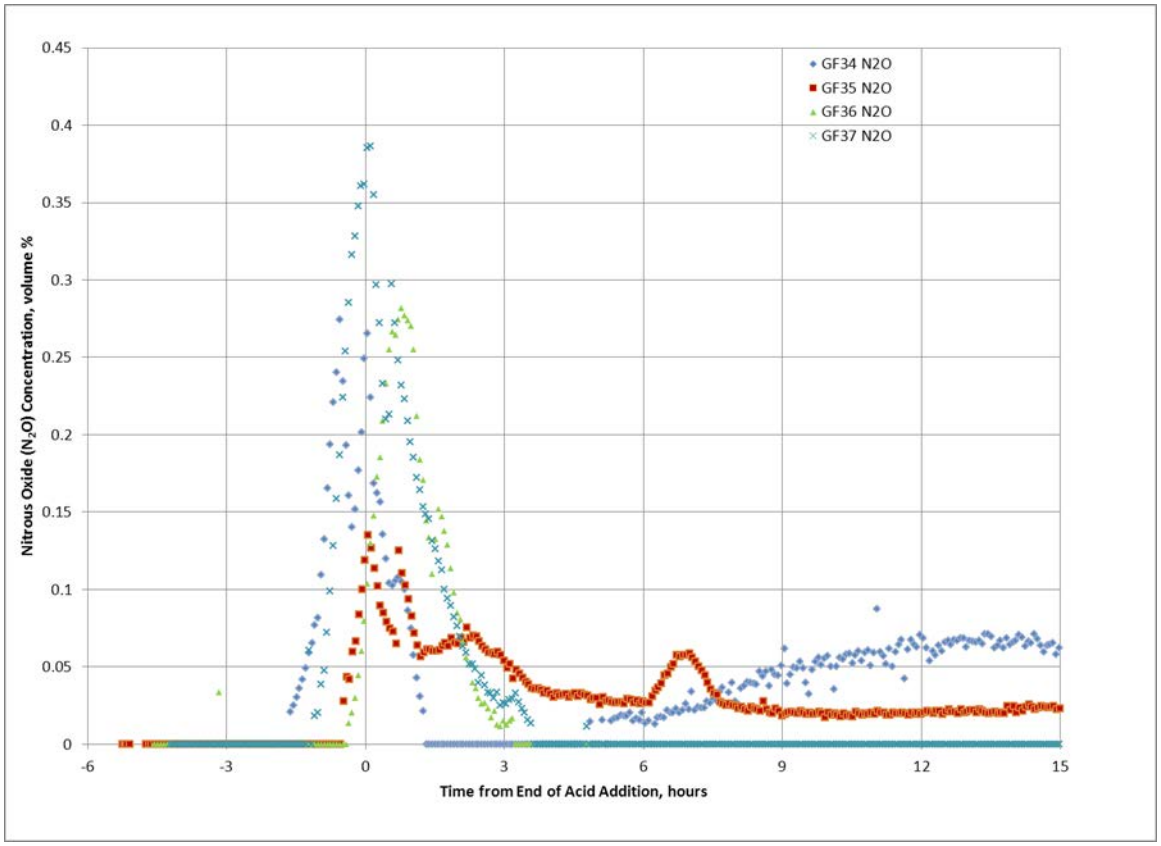

Figure 3-8. Nitrous Oxide Generation in SRAT cycles, volume %

3.2.2 *SRAT Mercury Reduction and Stripping*

One of the most important questions to resolve concerning the glycolic-nitric acid flowsheet is whether mercury could be effectively reduced and steam stripped in the SRAT cycle without formic acid. In the baseline flowsheet, mercury is reduced to elemental mercury during formic acid addition and then removed from the slurry by steam stripping during the concentration and reflux periods in SRAT processing.

The starting sludge was trimmed to 1.5 wt% Hg in the total solids. This required a theoretical boiling time of 12 hours to remove mercury to less than 0.80 wt% in the SRAT product total

solids using lab-scaled DWPF design basis boil-up rates and a stripping efficiency of 750 g steam/g Hg.

A mass balance was completed for each of the runs to attempt to determine where the mercury had accumulated. The mercury mass balance is summarized in Table 3-7. In three of the first four runs, GF34, 35, 36 and 37, the mercury recovery was poor in the MWWT. As a result, Runs 36 and 37 were repeated (Runs GF36b, 36c, 37b and 38). The mercury recovery in the second set of runs was typical for lab-scale SRAT cycles[18]. No cause for the differences in duplicate runs has been identified, but it is possible that there was technician error in collecting the mercury. It is recommended that SRAT cycles are performed with SB8 simulant to demonstrate that mercury can be reduced without formic acid in glycolic flowsheet runs with typical (not matrix) sludge simulant. Run GF35 (SB7A sludge) was not repeated, since the sludge was consumed in Run GF35. Run GF38 was performed at 125% acid stoichiometry to determine if acid stoichiometry impacted mercury recovery. Note that about 50% less mercury was recovered in the MWWT in run GF38 (125% acid stoichiometry) than was recovered in run GF37b (100% acid stoichiometry), as is seen in baseline flowsheet runs.

Table 3-7. Mercury Balance in SRAT and SME Cycle, g

Run	% Acid Koopman	Added	MWWT	Slurry	Condensate	Total	% Recovery
GF34	104.0	10.56	2.27	12.12	2.27	16.66	160%
GF35	100.0	8.25	0.02	0.19	0.17	0.38	4.6%
GF36	106.1	10.17	0.14	5.85	0.53	6.52	64%
GF36b	106.1	10.17	2.27	6.59	NA	8.85	87%
GF36c	106.1	10.17	2.35	7.17	NA	9.53	94%
GF37	100.0	10.28	0.01	7.13	0.48	7.62	74.%
GF37b	100.0	10.28	4.10	4.75	NA	8.56	86%
GF38	125	10.28	1.99	7.40	NA	9.15	91%

Samples were taken periodically throughout the runs for mercury analysis. The chart below (Figure 3-9) shows the concentration of mercury in the slurry as a function of time for the eight runs. It is expected that the mercury concentration will decrease linearly during SRAT steam stripping and collect in the MWWT. A linear decrease of Hg concentration in the slurry assumes a constant boil-up rate and a constant approach to thermodynamic vapor-liquid equilibrium between the slurry and off-gas phases. The general trend of the mercury profile curves is a linear decrease as expected. It was expected that the SRAT product would have a mercury concentration of 0.8 wt% or 2160 mg/kg. The SRAT product Hg concentration ranged from 0.01-0.92 wt % total solids basis. Results are summarized in Table 3-8.

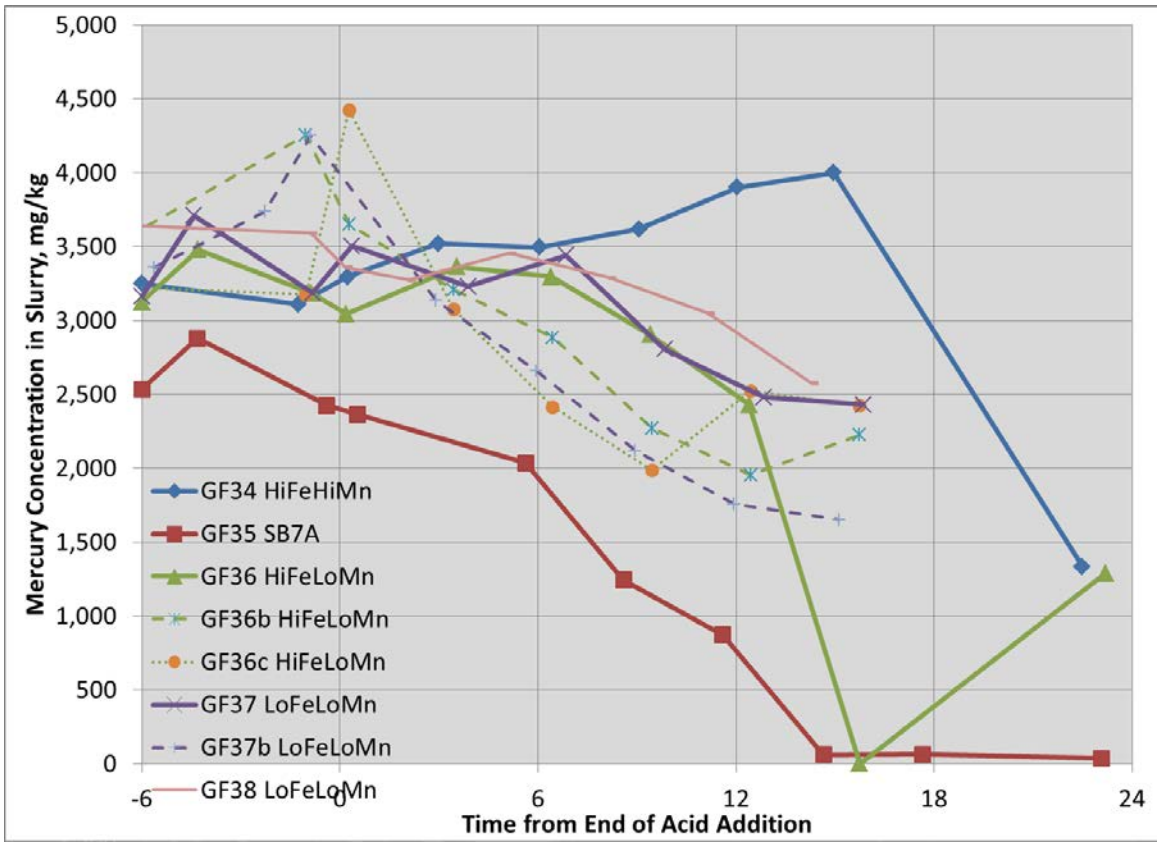

Figure 3-9. Mercury concentration versus time in SRAT and SME cycles

Mercury is added to the sludge as HgO. In these runs the HgO was slurried with water and homogenized using the vortex mixer to break up any clumps and allow an even dispersal of the mercury. During SRAT processing the mercury is first dissolved and may later be reduced to elemental mercury. Once it is reduced, it is insoluble and can be steam stripped. In Runs GF37b and GF38, extra samples were pulled during the acid addition and dewater phase to understand when these reactions occur. In both runs, approximately 90% of the mercury was dissolved prior to the completion of nitric addition and the Hg was completely dissolved by midway through the glycolic acid addition. The mercury then is reduced during the first two hours of dewatering (faster during GF38, the 125% acid stoichiometry run, than during GF37b, the 100% acid stoichiometry run). The dissolution and reduction of mercury was very similar to that seen for Pd. The concentration of Hg and Pd are summarized in Figure 3-10.

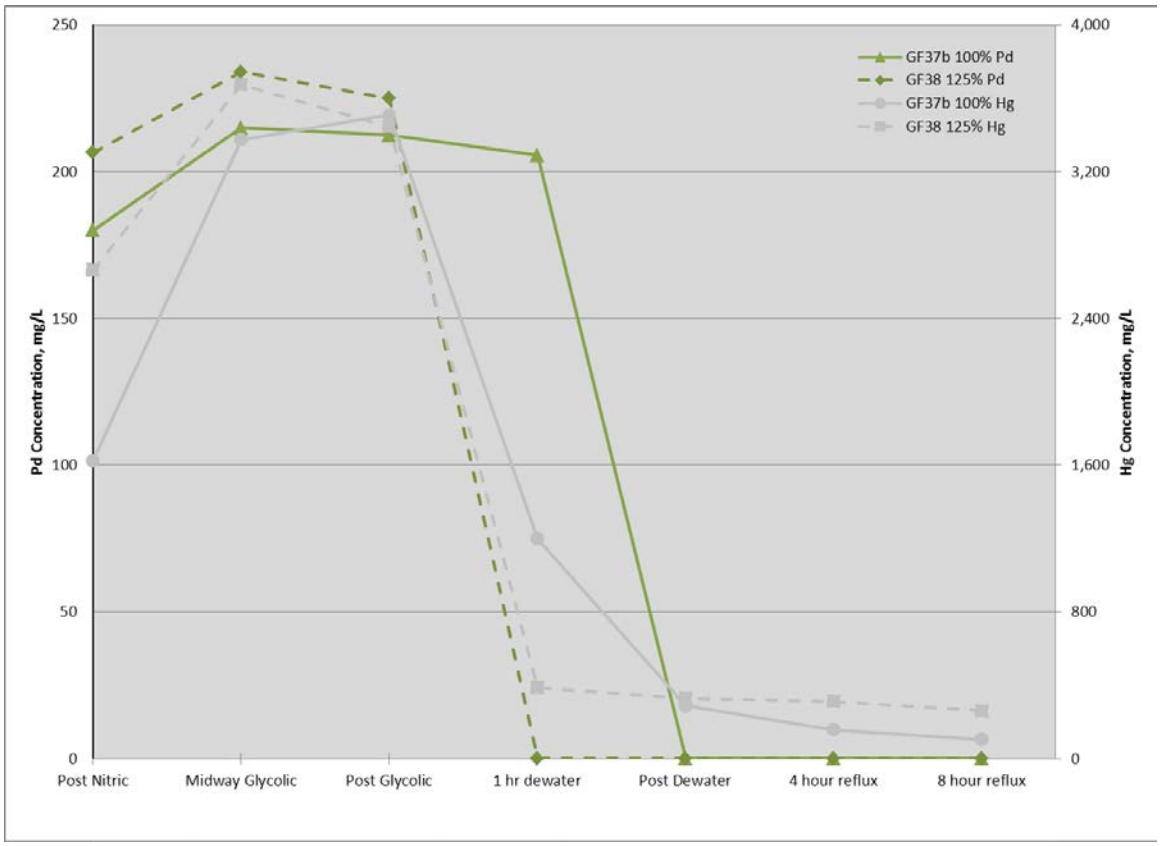

Figure 3-10. Mercury and Palladium Concentration for GF37b and GF38 SRAT Cycles

3.2.3 *SRAT and SME Product Data*

3.2.3.1 SRAT Elemental Data

General SRAT product slurry data for the eight runs are tabulated below. Analyses were completed of both the slurry and supernate from all SRAT and SME products. The slurry results are summarized in Table 3-8. Conversion of the elemental data to the expected oxide form allows summing the oxides as a measure of both complete sample dissolution and accurate analysis of the major elements in the sludge product. The sum of oxides range from 98.2-100.5 over this data set (95-105 is considered acceptable). The slurry samples were filtered and the supernate results of these analyses are summarized in Table 3-9.

Table 3-8. SRAT Product Slurry PSAL Elemental Data, wt % calcined solids basis

Run	GF34	GF35	GF36	GF36b	GF36c	GF37	GF37b	GF38
Al	9.01	15.2	9.1	9.2	9.1	23.7	23.5	23.9
B	<0.100	<0.100	<0.100	<0.100	<0.100	<0.100	<0.100	<0.100
Ba	0.080	0.108	0.095	0.094	0.092	0.063	0.064	0.063
Ca	3.58	0.80	2.12	1.95	1.94	1.68	1.66	1.69
Cd	<0.010	<0.010	<0.010	<0.010	<0.010	<0.010	<0.010	<0.010
Cr	0.017	0.067	0.273	0.269	0.269	0.223	0.224	0.220
Cu	0.070	0.052	0.054	0.043	0.040	0.051	0.040	0.041
Fe	32.3	20.5	32.0	32.9	32.9	12.6	12.3	12.3
Hg@	0.42	0.01	0.43	0.81	0.87	0.82	0.59	0.92
K	0.080	0.075	0.061	0.077	0.083	0.071	0.079	0.086
Li	<0.100	<0.100	<0.100	NM	NM	<0.100	<0.100	<0.100
Mg	0.410	0.382	2.57	2.77	2.76	2.36	2.40	2.43
Mn	4.01	5.02	0.706	0.640	0.631	0.666	0.600	0.596
Na	14.2	15.5	13.5	13.4	13.2	15.3	14.1	14.4
Ni	0.212	3.42	2.69	2.73	2.73	2.37	2.35	2.37
P	<0.100	<0.100	<0.100	<0.100	<0.100	<0.100	<0.100	<0.100
Pb	0.080	0.023	0.056	0.049	0.041	0.058	0.050	0.039
Pd	<0.100	<0.100	<0.100	<0.010	<0.010	<0.100	<0.010	<0.010
Rh	0.031	0.032	0.033	<0.100	<0.100	0.047	<0.100	<0.100
Ru	0.032	0.031	0.032	<0.100	<0.100	0.030	<0.100	<0.100
S	0.276	0.347	0.276	0.264	0.269	0.294	0.283	0.260
Si	1.48	1.70	1.95	1.82	1.76	1.30	1.42	1.39
Sn	<0.010	0.029	0.107	0.102	0.102	0.089	0.094	0.093
Ti	0.010	0.025	0.010	<0.010	<0.010	0.010	<0.010	<0.010
Zn	0.062	0.064	0.072	0.071	0.070	0.061	0.062	0.062
Zr	0.055	0.236	0.117	0.110	0.110	0.045	0.040	0.044

@ Hg reported on a total solids basis

Table 3-9. SRAT Product Supernate PSAL Elemental Data, mg/L supernate basis

Run	GF34	GF35	GF36	GF36b	GF36c	GF37	GF37b	GF38
Al	292	217	411	2,280	2,255	554	2,205	4,040
B	1.22	1.28	1.23	<10.0	<10.0	1.49	<10.0	<10.0
Ba	2.18	0.99	1.65	3.28	3.32	1.26	2.69	3.37
Ca	2,390	109	2,390	3,345	3,485	2,145	3,040	2,865
Cd	<0.010	<0.010	<0.010	<0.100	<0.100	<0.010	<0.100	<0.100
Cr	2.58	3.52	32.04	54.85	53.75	85.98	103.00	198.00
Cu	11.6	1.33	11.9	25.9	24.6	15.1	24.7	38.5
Fe	1,665	141	1,040	2,815	3,290	328	1,490	3,560
K	392	321	272	16.4	5.23	290	265	247
La	27.8	2.84	18.6	239	269	39.2	NM	NM
Li	<10.0	<10.0	<10.0	<1.00	<1.00	<10.0	<1.00	<1.00
Mg	309	203	4,830	4,460	4,040	4,410	4,090	4,180
Mn	8,855	2,670	1,330	1,280	1,154	1,300	1,280	922
Na	30,100	33,700	26,500	28,200	25,900	30,400	29,800	28,500
Nd	7.13	0.61	4.58	10.77	9.84	10.71	NM	NM
Ni	121	100	2,940	3,160	2,845	3,165	3,180	3,965
P	0.86	1.04	1.13	1.54	1.86	1.56	<10.0	<10.0
Pb	4.10	0.17	0.61	2.29	2.01	2.31	4.15	18.95
Pd	0.16	0.21	0.16	0.18	0.13	0.18	<0.100	<0.100
Rh	2.97	9.21	10.7	18.4	15.0	12.0	36.0	78.3
Ru	106	25.6	181	229	206	289	330	453
S	645	880	572	453	482	672	599	513
Si	23.5	38.3	17.4	132	68.8	67.4	121	103
Sr	4.17	2.32	3.06	NA	NA	2.99	41.6	77.3
Ti	<0.010	<0.010	<0.010	<0.100	<0.100	<0.010	<0.100	<0.100
Zn	25.7	0.40	28.6	34.1	34.0	39.6	42.8	64.6
Zr	6.29	22.6	14.5	60.9	62.0	17.7	38.3	50.7

3.2.3.2 SRAT Anion Data

Ion Chromatography was completed using weighted dilutions (not the AD acid strike oxalate method) for both the slurry and supernate from all SRAT and SME products. The slurry results are summarized in Table 3-10. The slurry samples were filtered and the supernate results of these analyses are summarized in Table 3-11. Anion balance data for nitrite, nitrate, formate and glycolate are presented in the table below for all runs (Table 3-12).

The SRAT and SME product oxalate results are of particular interest. The starting sludge contained about 800 mg/kg oxalate, which could be partially destroyed catalytically during the SRAT cycle. In the glycolic/formic flowsheet runs, however, oxalate was being created. The glycolic acid is likely oxidized to glyoxylic acid ($HCOCO_2H$) by nitrite, which is further oxidized to oxalic acid by the reduction of mercury. However, more experiments are needed to pinpoint the reaction pathways.

Table 3-10. SRAT Product Slurry PSAL Anion Data, mg/kg Slurry Basis

Run	GF34	GF35	GF36	GF36b	GF36c	GF37	GF37b	GF38
Formate	<100	<100	<100	<100	<100	<100	<100	<100
Chloride	650	572	622	591	602	821	590	583
Nitrite	<100	<100	<100	<100	<100	<100	<100	<100
Nitrate	57,150	43,450	57,500	56,650	56,350	56,550	52,500	56,900
Sulfate	1,250	1,910	1,210	1,280	1,240	1,500	1,445	1,420
Oxalate	1,990	4,370	3,955	3,190	3,210	2,755	2,420	2,655
Glycolate	44,850	39,850	37,250	51,250	53,100	42,200	55,450	77,850

Table 3-11. SRAT Product Filtrate PSAL Anion Data, mg/L Supernate Basis

Run	GF34	GF35	GF36	GF36b	GF36c	GF37	GF37b	GF38
Formate	<100	<100	<100	<100	<100	<100	<100	<100
Chloride	894	823	858	736	783	913	772	746
Nitrite	<100	<100	<100	<100	<100	<100	<100	<100
Nitrate	80,450	63,750	86,350	74,000	74,300	82,150	70,950	77,350
Sulfate	2,250	2,795	2,170	1,530	1,610	2,740	1,845	1,795
Oxalate	1,565	3,800	3,250	4,060	4,240	3,860	3,035	3,605
Glycolate	56,350	48,600	46,700	64,550	70,750	61,350	72,500	98,150

Table 3-12. SRAT Cycle Anion Balance Data, %

	GF34	GF35	GF36	GF36b	GF36c	GF37	GF37b	GF38
Nitrite Destruction	100	100	100	100	100	100	100	100
Glycolate Destruction	32.8	26.0	42.6	20.1	16.7	27.4	9.8	-12.4
Nitrite to Nitrate Conversion	54.7	14.7	27.1	32.9	31.9	49.5	19.9	18.3
SRAT Oxalate Generation	623	-49.4	1,420	1,140	1,150	867	-18	-11.1

As a result of uncertainty of the anion analyses, four samples were submitted to AD for both TOC and anion analysis. The data below (Table 3-13) shows the results from both PSAL and AD for comparison. The agreement is fairly good, with the exception of the glycolate and oxalate. In addition, the carbon species (formate, oxalate, glycolate) were converted to carbon concentrations and summed to estimate the Total Organic Carbon (TOC) result for each sample. These results were compared to the AD measured TOC result. It is obvious that the TOC predicted from the PSAL results agreed well with the TOC measurement.

Table 3-13. SRAT Product AD and PSAL Anion with Comparison to AD TOC, mg/kg

	GF36b	GF36c	GF37b	GF38
PSAL glycolate	50,200	55,100	55,500	77,900
AD Glycolate	33,900	34,400	35,900	54,500
PSAL Oxalate	3,160	3,300	1,340	2,390
AD Formate	<500	<500	<500	<500
PSAL Formate	<100	<100	<100	<100
PSAL Calculated TOC	20,900	24,100	24,100	32,400
AD Calculated TOC	11,500	11,500	11,900	18,100
AD Measured TOC	19,700	28,600	24,500	26,200

3.2.3.3 Other SRAT Data

Other SRAT product data are summarized in Table 3-14.

Table 3-14. Other SRAT Product Data

Run	GF34	GF35	GF36	GF36b	GF36c	GF37	GF37b	GF38
Total Solids, wt%	31.5	29.6	30.3	27.6	27.7	29.7	28.1	27.9
Insoluble Solids, wt%	17.7	17.7	17.0	13.7	13.3	14.9	13.4	12.4
Calcined Solids, wt%	18.0	17.6	16.7	15.0	15.1	16.1	15.1	14.0
Soluble Solids, wt%	13.8	12.0	13. 3	13.9	14.4	14. 8	14.8	15.5
pH	4.35	6.85	4.22	4.05	4.23	4.32	4.28	3.47
Slurry Density, g/mL	1.25	1.23	1.21	1.20	1.21	1.21	1.20	120
Supernate Density, g/mL	1.11	1.10	1.11	1.11	1.11	1.11	1.11	1.12
Ammonium, mg/L	30	9	18	NA	NA	20	NA	NA

Ammonia was below detection limit of 5 mg/L in ammonia scrubber samples. SRAT products were slightly above the detection limit (Table 3-14) as were some SME products, though the concentrations were smaller.

3.2.3.4 SME Elemental Data

General SME product sample data for the four runs (GF34, GF35, GF36 and GF37 had SME cycles) are tabulated below. The waste loading for these runs was targeted at 36% using frit 418. Elemental analyses were completed of both the slurry and supernate from all SME products. The slurry results are summarized in Table 3-15. Conversion of the elemental data to the expected oxide form allows summing the oxides as a measure of both complete sample dissolution and accurate analysis of the major elements in the sludge product. The sum of oxides range for 98.6-100.5 over this data set (95-105 is considered acceptable). The slurry samples were filtered and the supernate results of these analyses are summarized in Table 3-16.

Table 3-15. SME Product Slurry Elemental Data, wt % calcined solids basis

Run	GF34	GF35	GF36	GF37
Al	3.35	5.47	3.4	9.00
B	1.32	1.40	1.30	1.30
Ba	0.031	0.041	0.036	0.026
Ca	1.28	0.25	0.680	0.651
Cd	<0.010	<0.010	<0.010	<0.010
Cr	0.016	0.037	0.119	0.103
Cu	0.035	0.037	0.035	0.029
Fe	11.8	7.4	11.9	4.85
K	0.063	0.048	0.041	0.049
Li	2.20	2.31	2.27	2.18
Mg	0.152	0.145	0.924	0.858
Mn	1.4400	1.79	0.2305	0.2200
Na	8.6	9.23	8.6	9.06
Ni	0.073	1.210	1.00	0.92
P	<0.100	<0.100	<0.100	<0.100
Pb	0.038	0.014	0.036	0.035
Pd	<0.100	<0.100	<0.100	<0.100
Rh	0.017	0.018	0.027	0.025
Ru	0.015	0.024	0.034	0.023
S	0.099	0.116	0.102	0.114
Si	23.35	24.3	23.45	22.9
Sn	<0.010	0.013	0.044	0.038
Ti	0.007	0.013	0.012	0.008
Zn	0.026	0.027	0.028	0.026
Zr	0.026	0.103	0.051	0.024

Table 3-16. SME Product Supernate Elemental Data, mg/L supernate basis

Run	GF34	GF35	GF36	GF37
Al	178	343	320	922
B	54. 0	55.0	48.0	47.2
Ba	2.22	1.06	1.68	1.35
Ca	2,090	169	2,110	1,960
Cd	<0.010	<0.010	<0.010	<0.010
Cr	1.93	7.03	34.6	69.4
Cu	5.8	3.2	12.8	16.7
Fe	1,280	326	1,200	973
K	396	311	252	212
La	18	10	18	37
Li	2670	216	234	183
Mg	315	223	4,660	3,460
Mn	8,610	3,620	1,280	998
Na	29,500	37,000	24,750	25,500
Nd	4.21	2.50	4.24	10.2
Ni	114	226	2,800	2,490
P	0.77	2.49	1.02	1.87
Pb	4.01	0.30	0.81	2.01
Pd	0.18	0.24	0.14	0.13
Rh	2.83	12.2	12.6	7.95
Ru	87	35	166	205
S	679	874	575	516
Si	30.6	102	27.6	71.5
Sr	4.22	2.67	3.05	2.77
Ti	<0.010	<0.010	<0.010	<0.010

3.2.3.5 SME Anion Data

Ion Chromatography was completed for both the slurry and supernate from all SME products. The slurry results are summarized in Table 3-17. The slurry samples were filtered and the supernate results of these analyses are summarized in Table 3-18. Anion balance data for nitrite, nitrate, formate and glycolate are presented in the table below for all runs (Table 3-19).

The anion data is inconsistent. For example, in Run GF37, the data indicates there was high nitrite to nitrate conversion in the SRAT and high nitrate loss in the SME. Also, it indicates that glycolate was destroyed in the SRAT and generated in the SME. It is more likely that there was a lower nitrite to nitrate conversion and lower glycolate loss in the SRAT with minimal nitrate and glycolate loss in the SME. The inconsistent results are likely due to fouling of the IC columns by metals and oxalate that are soluble at pH 4 but insoluble at pH 10 (approximate pH of eluent). It is recommended that removal of metals with an appropriate guard column. An anion round robin has been initiated to better understand the analytical problems.

Table 3-17. SME Product Slurry Anion Data, mg/kg Slurry Basis

Run	GF34	GF35	GF36	GF37
Formate	<100	<100	<100	<100
Chloride	525	445	494	821
Nitrite	<100	<100	<100	<100
Nitrate	43,650	34,750	43,650	56,550
Sulfate	1,060	1,470	1,000	1,500
Oxalate	1,670	3,290	4,150	2,755
Glycolate	37,250	30,750	28,200	42,200
Formate	1,405	2,330	1,720	<100
Phosphate	<100	<100	<100	<100

Table 3-18. SME Product Filtrate Anion Data, mg/L Supernate Basis

Run	GF34	GF35	GF36	GF37
Formate	<100	<100	<100	<100
Chloride	892	770	884	726
Nitrite	<100	<100	<100	<100
Nitrate	79,100	58,200	84,750	60,100
Sulfate	2,345	2,825	2,710	2,570
Oxalate	1,620	4,845	3,960	3,395
Glycolate	59,400	42,150	45,550	45,600
Formate	1,715	3,785	2,251	1,940
Phosphate	<100	<100	<100	<100

Table 3-19. SME Anion Balance Data, %

	GF34	GF35	GF36	GF37
SME Nitrate Destruction	9.9	-2.5	10.1	21.8
SME Glycolate Destruction	5.3	15.1	4.9	35.8
SME Formate Destruction	41.5	61.8	42.6	62.2

3.2.3.6 Other SME Data

Other SME product data are summarized in Table 3-20. Of particular note is that the GF37 SME was not completed prior to kettle breakage. As a result, the total solid result of the recovered product is significantly lower than had been targeted. Also, no analyses were completed on the SME condensate. This should be completed in future flowsheet testing.

Table 3-20. Other SME Product Data

Run	GF34	GF35	GF36	GF37
Total Solids, wt%	48.8	46.3	45.8	39.3
Insoluble Solids, wt%	37.9	37.6	35.3	29.7
Calcined Solids, wt%	38.5	37.3	35.8	29. 7
Soluble Solids, wt%	10.9	8.71	10.5	9.53
pH	4.66	6.18	4.39	4.31
Slurry Density, g/mL	1.42	1.34	1.38	1.29
Supernate Density, g/mL	1.11	1.10	1.10	1.09
Ammonium, mg/L	14	<5	<5	7

3.2.4 *Supernate Chemistry -- Dissolution of Metals and Solubility of Anions*

One of the major unknowns revolving around the glycolic flowsheet is what is happening to the anions and cations during and after processing. The addition of glycolic acid and the ability to keep the pH low throughout SRAT and SME processing combine to dissolve insoluble metal species leading to higher concentrations of metals in solution. However in these runs, we have also seen crystalline solids form during storage, after the SRAT and SME cycles were complete. A photo below (Figure 3-11) shows the solids formation in some of the SRAT products.

Figure 3-11. Photo of SRAT Product Samples 11/30/2011 (4 days after SME cycle)

It should be noted that the solids formed primarily on the surface of the sample bottle and were easily reincorporated into the slurry by gentle mixing. The samples from GF34, GF35, GF36 and GF37 SRAT and SME products were submitted to SRNL/AD and identified as Gibbsite (γ-$Al(OH)_3$), Quartz (SiO_2), Bayerite (α-$Al(OH)_3$), Boehmite (γ-AlO(OH)), and Goethite (α-FeOOH). Note that there were no crystals noted in the GF35 (SB7A) simulant, only in some of the matrix simulants. The X-ray Diffraction (XRD) results are summarized in Appendix C.

3.2.4.1 SRAT Supernate Chemistry

The composition of the SRAT product slurry and supernate cations is summarized in Table 3-8 and Table 3-9. The composition of the SRAT product slurry and supernate anions is summarized in Table 3-10 and Table 3-11. Table 3-21 shows the amount of each element found in the SRAT product supernate expressed as a percentage of the total element present. These data are calculated by dividing the supernate concentration (converted to mg/kg on a slurry basis) by the total slurry fraction of each element (converted to mg/kg). Numbers greater than 100% are not physically possible and are a result of error in one of the analytical measurements used in the calculation.

Table 3-22 shows the amount of each anion found in the SRAT product supernate expressed as a percentage of the total anion present post acid addition. These data are calculated by dividing the

supernate anion concentration (converted to mg/kg on a slurry basis) by the total slurry concentration of each anion.

The % solubility of each anion is approximately 100% (80-120% based on method uncertainty), except for oxalate, which had a solubility of approximately 60% in the GF34 and GF35 runs. The solubility of Al and Fe was low in all runs. The solubility of Na, Mg, and Mn are all high in the glycolic flowsheet runs. For most of the metals, which are present primarily as hydroxides and oxides in the sludge, the concentration in the supernate increases throughout the SRAT cycle, but appear to be constant by the end of the SRAT cycle. Samples were pulled at the completion of nitric acid addition, midway through glycolic acid addition, after completing glycolic acid addition, one-hour into dewater, post dewater, 4 hours into reflux and 8 hours into reflux. These samples were centrifuged soon after being pulled to make sure no further reactions occurred due to insoluble solids. One interesting observation is that the centrifuged GF37b samples (100% acid stoichiometry) had almost no supernate after centrifuging at the completion of dewater (0.3 g of supernate typical in these samples). Prior to dewater and throughout run GF38 approximately 6-7 g of supernate was easily removed after centrifuging.

Based on this data, the order of dissolution for the "major components" is: Hg>Ca>Mn>Ni>Mg>Al>Fe. The data is summarized for major metals (>1,000 g/L) in Figure 3-12 and minor metals in Figure 3-13.

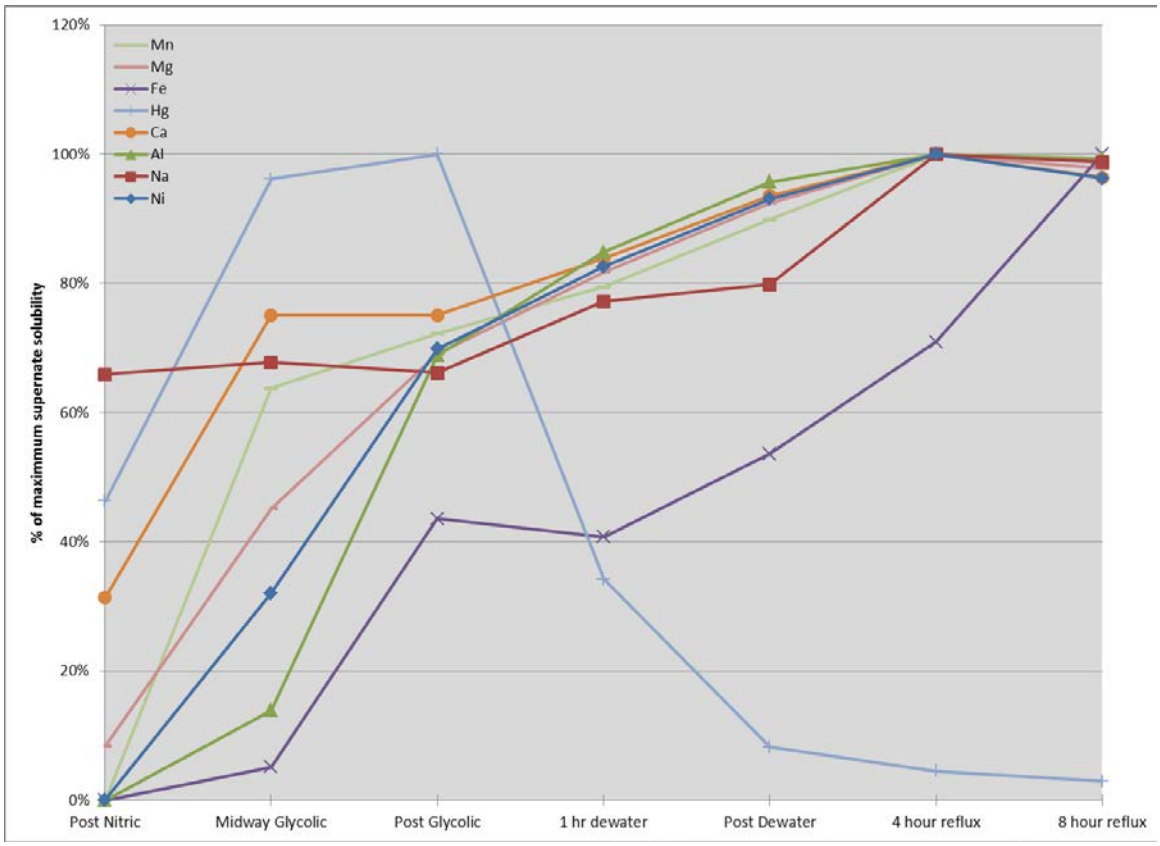

Figure 3-12. Order of Dissolution of "Major Metals" During SRAT Processing

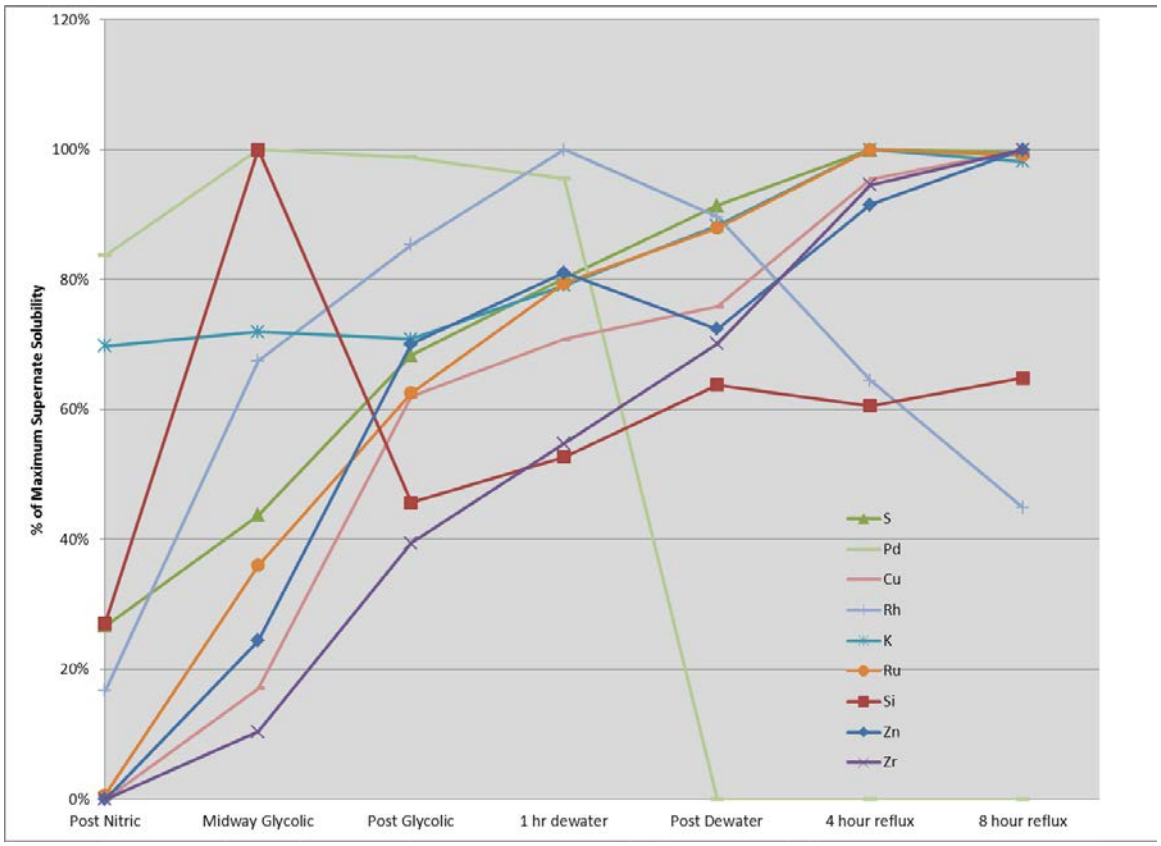

Figure 3-13. Order of Dissolution of "Minor Metals" During SRAT Processing

Several metals are of particular interest during SRAT processing. Note that mercury is discussed in Section 3.2.2. The reduction of Mn is important especially in the melter and cold cap in order to minimizing foaming in the melter. As can be seen in Figure 3-12, the Mn is dissolved (and likely reduced) early in the SRAT cycle and is >90% of the maximum solubility by the end of dewater. There are several metals that are essentially totally soluble such as Na, K, and Ca. The concentration of each metal changes as the metal is first diluted during acid addition, then concentrated during the dewater phase. In addition, the concentration of soluble metals should remain constant throughout the post dewater stage of the SRAT cycle. In GF37b, the concentration of both Na and Ca increased during this time, likely due to the extended centrifuge time necessary to squeeze out the 0.3 g of supernate from a 15 mL centrifuge tube. Note that for the lower acid run, GF37b, the calcium was not completely soluble until midway through glycolic acid addition. This may indicate that it may take more than 100% acid stoichiometry to produce a SRAT product that is easily filtered and concentrated in both the DWPF Analytical Lab and the SME.

Table 3-21. Major Components: SRAT Product % of Element Dissolved

Run	Al	Fe	Na	Mg	Mn
GF34 HiFeHiMn	1.3	2.1	87.5	31.0	90.8
GF35SB7A	0.6	0.3	92.9	22.7	22.7
GF36 HiFeLoMn	2.0	1.5	88.2	84.0	84.6
GF36b HiFeLoMn	12.9	4.4	88.2	84.0	84.6
GF36c HiFeLoMn	12.7	5.1	108.6	83.2	103.4
GF37 LoFeLoMn	1.1	1.2	94.9	89.0	93.1
GF37b LoFeLoMn	4.8	6.3	108.8	88.1	110.2
GF38 LoFeLoMn	9.4	16.2	109.6	95.8	86.0

Table 3-22. SRAT Product % of Anion Soluble

Run	GF34	GF35	GF36	GF36b	GF36c	GF37	GF37b	GF38
Chloride	101.7	108.2	103.2	96.8	101.3	85.2	101.9	99.7
Glycolate	92.9	91.7	93.8	97.9	103.8	111.4	101.8	98.3
Nitrate	104.1	110.4	112.4	101.6	102.7	111.3	105.2	105.9
Oxalate	58.2	65.4	61.5	99.0	102.9	107.3	97.7	105.8
Sulfate	133.1	110.1	134.2	92.9	101.1	139.9	99.4	98.5
Sulfate (S)	96.1	108.0	92.8	88.9	92.2	109.1	109.6	109.6

In order to understand the dissolution of metals and the timing of their dissolution, additional samples were pulled during runs GF37b and GF38 (LoFeLoMn sludge). The dissolution of Hg is discussed in the mercury section.

3.2.4.2 SME Supernate Chemistry

The main change in supernate chemistry during the SME cycle is that formic acid is added to the frit slurry to prevent caking. Formic acid is very reactive in DWPF SRAT and SME processing, ultimately leading to the noble metal catalyzed decomposition to hydrogen and CO_2. No formic acid was added or detected during the SRAT cycle. The solubility of the anions during the SME cycle is summarized in Table 3-23.

Table 3-23. Major Components: SME Product % of Anion Soluble

Run	GF34	GF35	GF36	GF37
Chloride	94.9	98.5	105	70.0
Formate	68.1	92.5	76.7	67.4
Glycolate	89.0	78.1	94.6	95.8
Nitrate	101	95.4	114	101
Oxalate	54.1	83.9	55.9	77.4
Sulfate	123	109	159	136
Sulfate (S)	98.9	115.0	91.9	98.4

Frit 418, nominally containing 8% B_2O_3, 8% Li_2O, 8% Na_2O, and 76% SiO_2, is added in the SME cycle. The added frit components are very insoluble, with the concentration of B, Li and Si <1%

in the four SME cycles. In addition, the Na solubility drops from near 100% in the SRAT cycle to 50-60% by the time the SME cycle is complete due to the insoluble sodium in the frit. The solubility of the elements is summarized in Table 3-24.

Table 3-24. Major Components: SME Product % of Element Dissolved

Run	Al	Fe	Na	Mg	Mn
GF34 HiFeHiMn	0.8	1.6	49.5	30.0	86.7
GF35SByA	1.0	0.7	61.1	23.4	30.8
GF36 HiFeLoMn	1.5	1.7	47.3	82.6	90.8
GF37 LoFeLoMn	2.2	4.4	61.2	87.5	98.5

3.2.4.3 Post Processing Supernate Chemistry

The formation of crystals in some of the SRAT and SME products could have been caused by continuing reactions after completion of CPC simulations or by changes in solubility caused by the lower temperature during storage. The addition of nitric and glycolic acid may have dissolved some species (i.e. Al and Fe) to solubility at 102°C, then the species became supersaturated upon cooling (15-20°C). Crystal growth can be slow, so it can take several days or weeks for the crystal growth to complete.

3.2.5 *SRAT and SME Rheology*

Flow curves for the four initial SRAT and SME slurry products were obtained by using a Haake RS600 rheometer and the current DWPF simulant rheology protocol.[19] The up and down curves were fit to a Bingham plastic model to determine yield stress and consistency. Down flow curve data are the generally preferred choice for comparisons between systems. The data for all runs are tabulated below for the SRAT (Table 3-25) and SME (Table 3-26).

Table 3-25. SRAT Product Rheology Summary

SRAT Product Sludge Type	Wt % Insoluble Solids	Up Yield Stress, Pa	Down Yield Stress, Pa	Up Consistency, cP	Down Consistency, cP
DWPF Ranges	10-15	1.5 to 5	1.5 to 5	5 to 12	5 to 12
GF34 Hi Fe-Hi Mn	17.7	1.9	1.9	11.7	11.7
GF35 Lo Fe-Hi Mn	17.7	0.3	0.3	5.7	5.8
GF36 Hi Fe-Lo Mn	17.0	3.7	3.6	16.2	16.8
GF37 Lo Fe-Lo Mn	14.9	10.8	11.0	13.4	13.0

Table 3-26. SME Product Rheology Summary

Sludge Type	Wt % Insoluble Solids	Up Yield Stress, Pa	Down Yield Stress, Pa	Up Consistency, cP	Down Consistency, cP
DWPF Ranges	20-35	2.5 to 15	2.5 to 15	10 to 40	10 to 40
GF34 Hi Fe-Hi Mn	37.9	9.1	12.2	33.1	26.4
GF35 Lo Fe-Hi Mn	37.6	-0.1	1.5	20.2	11.7
GF36 Hi Fe-Lo Mn	35.3	12.3	15.9	34.8	24.7
GF37 Lo Fe-Lo Mn*	29.7	8.9	11.1	24.6	18.0

The SME products from runs GF35-36 were further concentrated by evaporation to determine the extent of concentration that could be achieved with each SME product. Insufficient material was remaining from run GF37, so no concentration of this sample was completed. The data is summarized in Table 3-27.

Table 3-27. Post Concentration SME Product solids content

Sample	Total Solids	Sample	Total Solids
GF35-48%	39.7%	**GF36-48%**	37.4%
GF35-51%	43.1%	**GF36-51%**	39.0%
GF35-54%	46.6%	**GF36-54%**	43.2%
GF35-57%	49.4%	**GF36-57%**	41.6%
GF35-60%	50.6%		

The rheology of these concentrated SME products was analyzed to determine the rheology and the data is summarized in Figure 3-14.

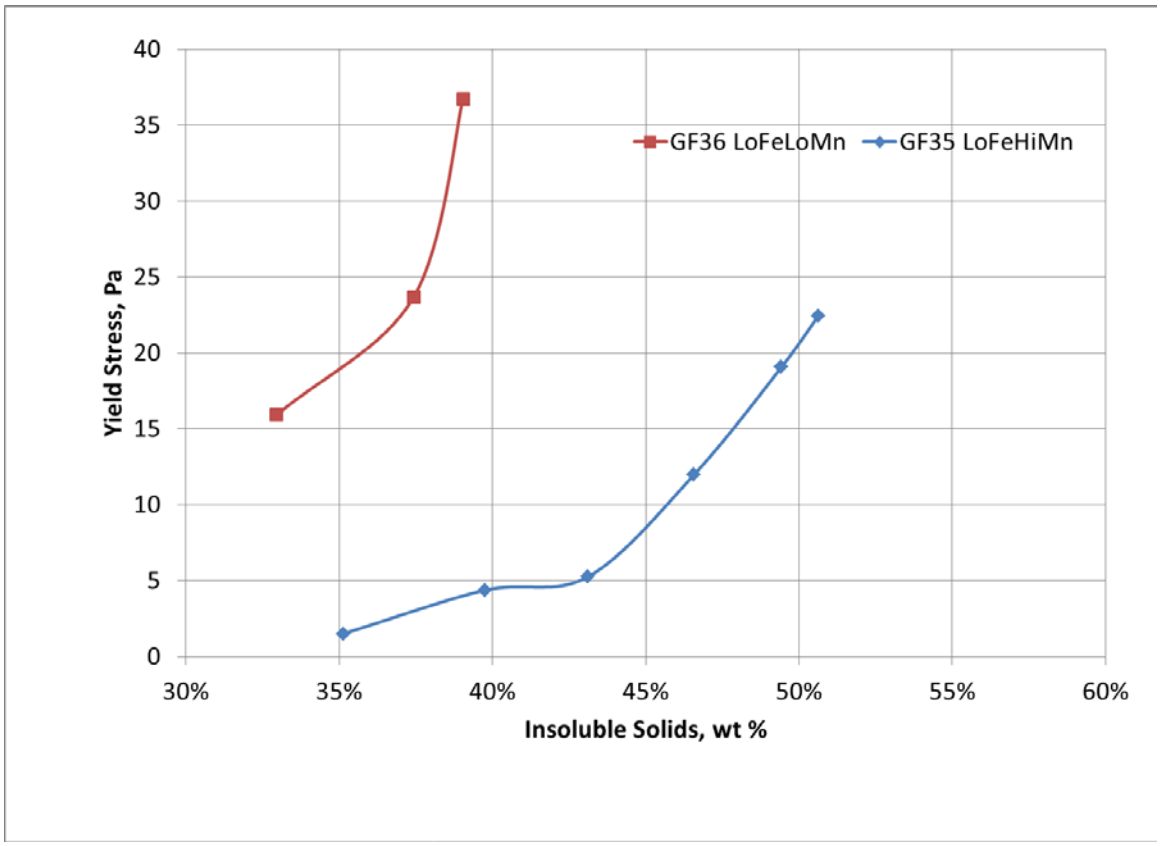

Figure 3-14. SME Product Rheology of Concentrated Subsamples

Lab-scale concentration of the two SME products to high wt% solids was problematic. Several laboratory rig kettles broke during concentration. It was important to mix well and to not have solids buildup during evaporation. The solids buildup led to localized overheating where the solids built up and to subsequent glass breakage. The high agitation speeds needed to mitigate solids buildup also led to breakage of the glassware, especially when the total solids exceeded 60 wt%.

3.2.6 *SRAT/SME REDOX*

SME products from GF34, GF35, GF36 and GF37 (SME products) were added to an alumina crucible, dried to peanut butter consistency, and vitrified in nepheline sealed crucibles. SRAT product samples from runs GF36b, GF36c, GF37b and GF38 were prepared for the redox measurement by taking the SRAT product and adding frit 418 to produce a waste loading of 36%. The resulting slurry was placed in a crucible, dried to peanut butter consistency and vitrified like the SME product samples from runs GF34, GF35, GF36 and GF37.

The REDOX prediction equation used in this study with an added term for glycolate is:

$$Fe^{2+}/\Sigma Fe = 0.2358 + 0.1999 * (2[F] + 4[C] + 6[G] + 4[O] - 5[N] - 5[Mn])*45/T$$

Where
[F] = formate (mol/kg feed)
[C] = coal (carbon) (mol/kg feed)
[O] = oxalate (soluble and insoluble) (mol/kg feed)

[G] = glycolate (mol/kg feed)
[N] = nitrate + nitrite (mol/kg feed)
[Mn] = manganese (mol/kg feed)

Values less than zero or greater than one can be calculated with the REDOX equation, because it is a linear regression equation fit to experimental data. Values outside the range of zero to one, however, are physically impossible. A number less than zero can be interpreted as fully oxidized and likewise a number greater than one as fully reduced.

Table 3-28 below shows the appropriate SME product data with the corresponding predicted REDOX values as well as the REDOX as measured. It should be noted that the REDOX equation underpredicts the measured REDOX. It should be noted that the glasses in this study were made with frit 418, not with a frit optimized for each slurry composition. The resulting REDOX may not be representative.

Table 3-28. SME product data for REDOX calculations, $Fe^{2+}/\Sigma Fe$

Run	Sludge	Predicted Redox*	Measured Redox
GF34	HiFeHiMn	0.069	0.319
GF35	SB7A	0.100	0.506
GF36	HiFeLoMn	0.025	0.280
GF36b	HiFeLoMn	0.111	0.286
GF36c	HiFeLoMn	0.000	0.226
GF37	LoFeLoMn	0.123	0.463
GF37b	LoFeLoMn	0.256	0.559
GF38	LoFeLoMn	0.524	0.665

* Predicted REDOX was calculated using measured sample results.

Both LoFe (HiAl) runs had significantly higher measured REDOX than the HiFe runs. The melter feed iron concentration may impact the percentage of iron that is reduced to Fe^{2+}. This may not be as evident in sludge batch processing, as the iron concentration doesn't change as much as the matrix sludges. This may be an important clue in developing a REDOX equation for the glycolic-nitric acid flowsheet.

It is possible that the anion analyses used to predict REDOX were inaccurate. As a result, the SME products were reanalyzed and the original results and reanalysis are summarized in Table 3-29.

Table 3-29. SME anion data for REDOX calculations, $Fe^{2+}/\Sigma Fe$

Result	Nitrate, mg/kg	Formate, mg/kg	Glycolate, mg/kg	Oxalate, mg/kg	SME Predicted Redox
GF34#1	43,650	1,405	37,250	1,670	0.064
GF34#2	44,000	1,420	38,200	5,220	0.106
GF35#1	34,750	2,330	30,750	4,370	0.119
GF35#2	33,300	2,710	29,850	4,525	0.133
GF36#1	43,650	1,720	28,200	4,150	0.031
GF36#2	46,150	1,785	31,450	5,700	0.057
GF36b	73,200	63,200	4,100	0.111	0.286
GF36c	65,700	53,100	3,340	0.073	0.226
GF37#1	38,450	1,855	30,700	2,830	0.147
GF37#2	39,850	1,680	29,850	4,540	0.125
GF37b	82,100	61,400	3,860	0	0.559
GF38	60,100	45,600	3,400	0.044	0.665

The reanalysis of the anions did not appreciably change the concentrations or the REDOX predications. A comparison of the original and reanalyzed results is summarized in Table 3-30. Note that oxalate concentrations of three of the four samples changed significantly.

Table 3-30. Change in Anion Concentration due to Reanalysis of SME Product Samples

Anion	GF34	GF35	GF36	GF37
Nitrate	0.8%	-4.2%	5.7%	3.6%
Formate	1.1%	16.3%	3.8%	-9.4%
Glycolate	2.6%	-2.9%	11.5%	-2.8%
Oxalate	212.6%	3.5%	37.3%	60.4%

A 10 ppm spike of nitrate, formate, glycolate, and oxalate was added to each diluted SME product subsample and analyzed by PSAL using the glycolate IC method[16]. The spiked samples were analyzed and the added spike was calculated (Table 3-31). Note that the calculated spike concentration of oxalate increased from 8.17 to 10.85 during this testing. It is likely that recovery of the oxalate from the IC column was not equal to the oxalate added, possibly because the column is “dirty”.

Table 3-31. Spiked Recovery of SME Product Samples, mg/kg slurry

Anion	GF34	GF35	GF36	GF37
Nitrate	9.81	9.89	9.82	10.0
Formate	10.35	10.11	10.55	10.7
Glycolate	10.05	10.05	10.2	10.25
Oxalate	8.17	9.34	9.64	10.85

The SME products were also analyzed for TOC. This was compared to calculated TOC concentration based on the analyzed glycolate, formate, and oxalate concentrations, converted to TOC. The data are summarized in Table 3-32. The good agreement between the measured and predicted TOC suggests that the analyses of the oxalate, formate, and glycolate concentrations are accurate enough to predict REDOX. No term was added to the TOC for the antifoam contribution since it was not measured. Based on the 800 ppm antifoam addition and the fact that the antifoam is about half carbon, the predicted TOC could be as much as 400 ppm higher if an antifoam term was added.

Table 3-32. TOC Analysis and Calculation of SME Product Samples, mg/kg slurry

Anion	GF36b	GF36c	GF37b	GF38
Measured TOC	19,700	28,600	24,500	26,200*
Predicted TOC	21,300	23,900	24,100	26,000

* The analytical result was corrected for added frit in preparing melter feed for REDOX testing.

Based on the anion results and using these to predict REDOX, it is evident that either the anion results are inaccurate or that the REDOX prediction equation is inadequate for the glycolic-nitric flowsheet REDOX prediction. In runs using the two HiFe slurries (GF34 and GF36), the predicted REDOX, although still lower than the measured REDOX, better agreed with the measured REDOX. One question it raises is whether additional terms are needed in this equation to adequately predict REDOX. It is also evident that additional work is needed to improve the current IC method, especially concerning oxalate and glycolate analyses. For instance, the measured glycolate was approximately twice that predicted (and much higher than is possible from the known addition of glycolic acid).

3.2.7 *SRAT pH profile*

Time dependent SRAT/SME pH data were collected for all runs. The graph below, Figure 3-15, shows the pH trends of all runs. The pH stays very stable throughout the SRAT and SME cycles, unlike the baseline flowsheet where the SME product pH may be as high as 10 or 11. In addition, the pH of the duplicate GF36 runs is included in Figure 3-16 to demonstrate the same pH profile was achieved in all three runs.

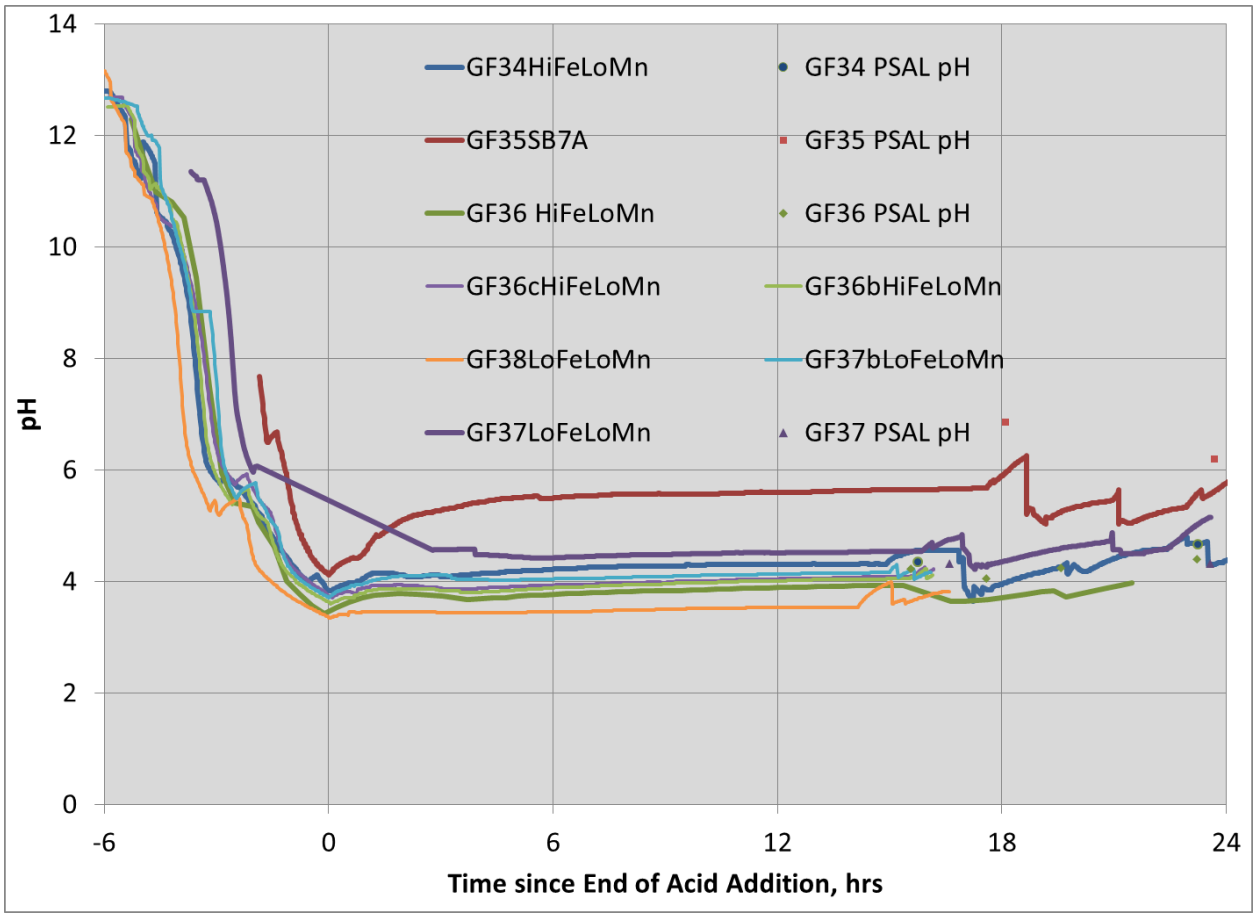

Figure 3-15. pH trends for SRAT and SME Cycles

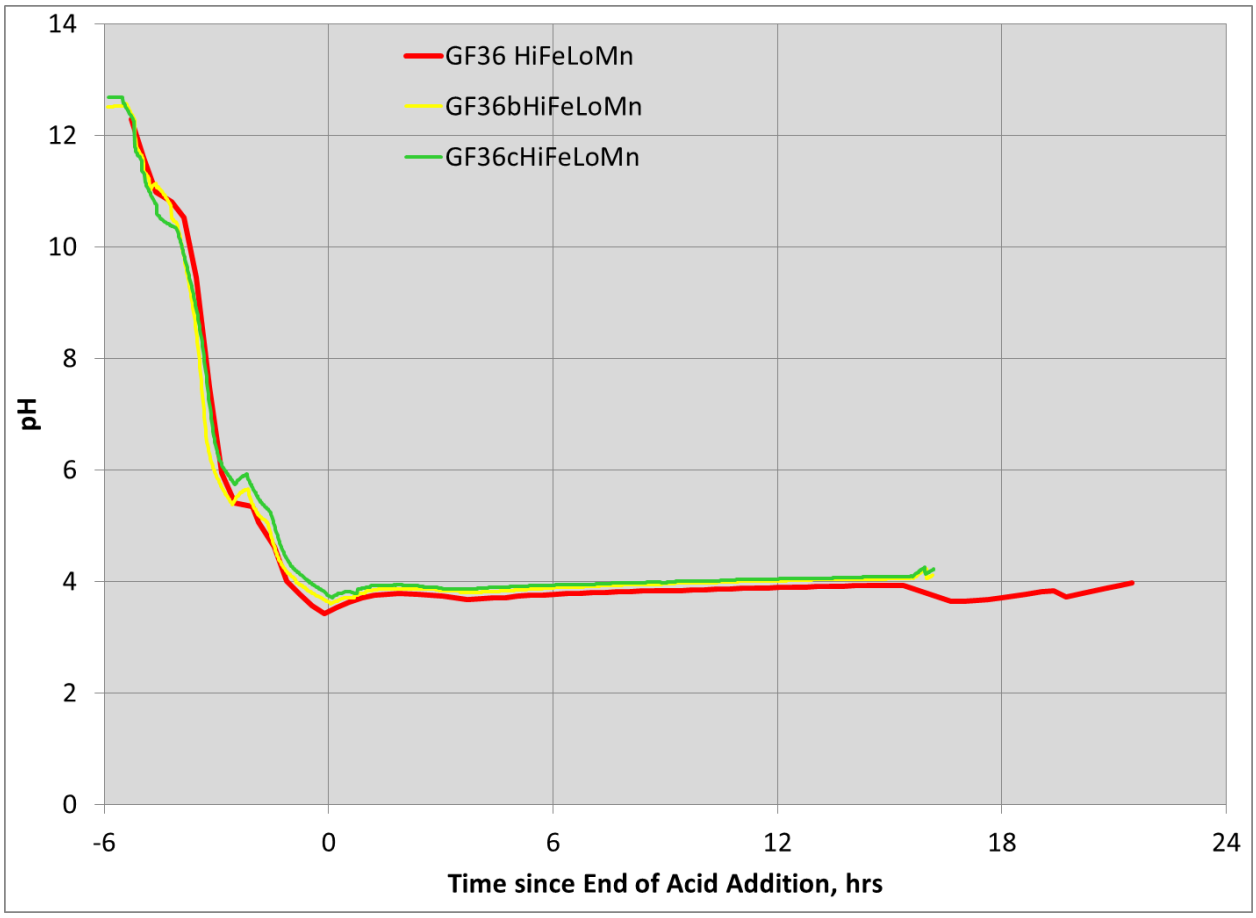

Figure 3-16. pH trends for Duplicate GF36 SRAT Cycles

3.2.8 *SRAT Condensate Data*

A composite sample was prepared for each of the runs by combining the condensate from the MWWT, FAVC, and SMECT to produce an "average" condensate sample. The sample was analyzed for elementals via ICP-AES, and anions via IC. The results are summarized in Table 3-33 and Table 3-34. The condensate was very low in anions and cations.

Table 3-33. Comparison of Composite Condensate Data, ICP-AES, mg/L supernate

Cation, mg/L	Ca	Fe	Si
GF34	1.785	0.428	99
GF35	0.456	<0.100	8.68
GF36	0.603	<0.100	25.9
GF37	0.641	<0.100	220

Less than detectable: Al, B, Ba, Cd, Cu, K, Li, Mg, Mn, Ni, P, Pb, Pd, Rh, Ru, S, Ti, Zn, Zr

Table 3-34. Comparison of Composite Condensate Data, IC (mg/L)

Anion	F	Cl	NO_2	NO_3	SO_4	C_2O_4	$C_2H_3O_3$	HCO_2	PO_4
GF34	<100	<100	<100	8045	133	<100	<100	<100	<100
GF35	<100	<100	<100	4635	<100	<100	<100	<100	<100
GF36	<100	<100	<100	5045	<100	<100	<100	<100	<100
GF37	<100	<100	<100	8535	<100	<100	<100	<100	<100

3.2.9 *Foaming*

Foaminess was not a concern in these runs. The antifoam strategy, 200 ppm before acid addition, 100 ppm after nitric acid addition, 500 ppm at the completion of acid addition and 100 ppm before the start of the SME cycle was more than enough antifoam to control foaming throughout testing. This is particularly significant since five different simulants containing very different insoluble solids compositions were used in the testing. Future testing should examine whether less antifoam can be used to control foaming.

3.2.10 *Heat Transfer Calculations*

The SRAT/SME apparatus used had two immersed heating rods to heat the slurry instead of the mantle that has been used in the past. Each heating rod has a four-inch heated section and has a maximum heat input of 750 watts. The temperature of the rod was limited to approximately 130°C by the temperature controller to prevent overheating the rod in the case of rod fouling. The use of the heating rods has several distinct advantages, including measurement of heating rod temperatures and heat input, allowing calculation of heat transfer coefficients. In addition, the heating rods more closely resemble the steam coils and can "foul" just like a heating coil.

The heat transfer coefficient of the rods was calculated as a function of time throughout the runs. The data are summarized in Figure 3-17. Note that the heat transfer coefficient was very consistent throughout the SRAT cycles. In run GF37 (LoFeLoMn), the heat transfer coefficient dropped from about 0.14 to 0.07. This run was very difficult to concentrate and the SME cycle concentration after the second frit addition was not finished due to breakage of the glassware. Calculation of the heat transfer coefficient is useful in predicting fouling. The power input to the rods is summarized in Figure 3-18.

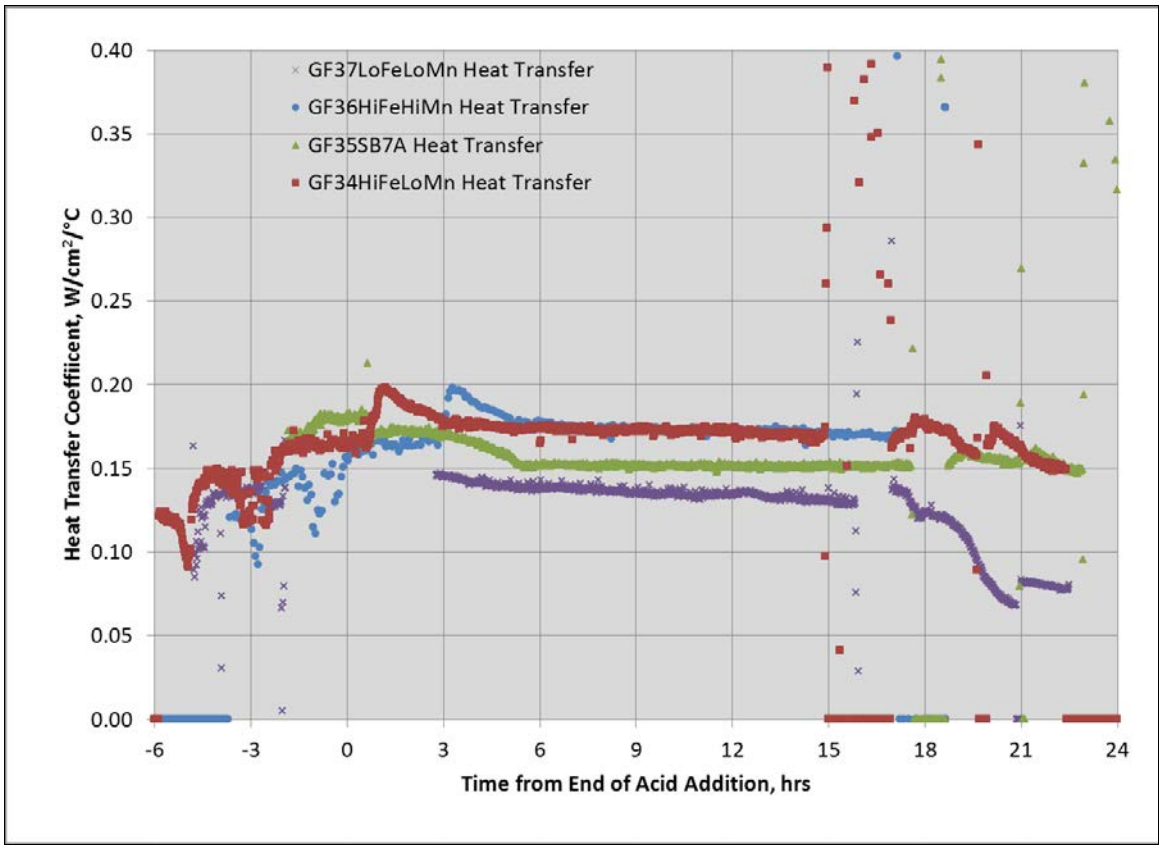

Figure 3-17. Heat Transfer Coefficient, W/cm^2/°C

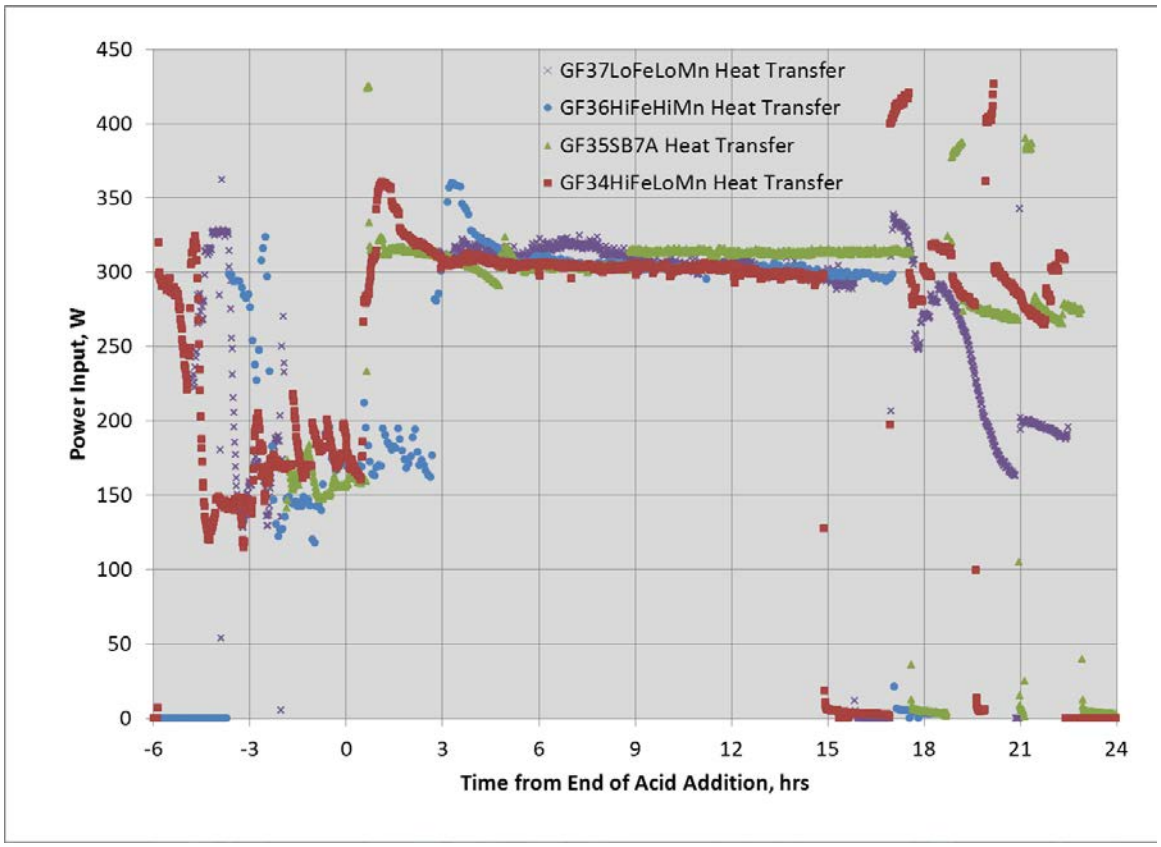

Figure 3-18. Power Input, W

Fouling was experienced in the problematic run GF37 (LoFeLoMn), and the fouled rod was photographed following the SME cycle (Figure 3-19). Note that neither the other rod nor the agitator was fouled.

Figure 3-19. Photograph of Fouled Heating Rod after Run GF37 SME

3.2.11 *Comparison of Identical Runs*

After completing the first four runs (GF34-GF37) and recovering relatively little mercury in the MWWT, four additional runs were completed. Run GF36 was duplicated in both the new (GF36b) and older (GF36c) kettle configurations to ensure that the equipment change was not responsible for the poor mercury recovery. In virtually every measure, these two runs were as close to identical as was feasible. The collection of mercury was also very similar in the two duplicate runs. However, the supernate was different in GF36 compared to GF36b and GF36c. For example, the iron and aluminum were higher in the GF36b and 36c and the supernate was also a darker color.

In order to easily compare the identical runs, it is important to put the analytical data on the same basis. Each rig is built separately and can have varying levels of leak tightness. In runs with a tighter seal, less water is lost through the agitator seal, joints and connections. As a result, the solids and ICP-AES supernate results were corrected to the same basis, the target total solid concentration for each run. For Run GF36, the target total solids concentration was 30.3 wt %. Total solids and anion concentrations in GF36b and GF36c were corrected as if these runs had also finished with a SRAT product at 27.9 wt % solids.

Table 3-35. GF36 Corrected Solids Concentrations

	Actual			Corrected		
Run	GF36	GF36b	GF36c	GF36	GF36b	GF36c
Total Solids, wt%	30.318	27.582	27.707	27.90	27.90	27.90
Insoluble Solids, wt%	17.035	13.701	13.275	15.68	13.86	13.37
Soluble Solids, wt%	13.283	13.881	14.432	12.22	14.04	14.53
Calcined Solids, wt%	16.684	15.037	15.145	15.35	15.21	15.25
Al, mg/L Supernate	411	2,280	2,255	447	2,254	2,239
Ba, mg/L Supernate	1.65	3.28	3.32	1.79	3.24	3.30
Ca, mg/L Supernate	2,390	3,345	3,485	2,597	3,307	3,461
Cr, mg/L Supernate	32.04	54.85	53.75	34.8	54.2	53.4
Cu, mg/L Supernate	11.9	25.9	24.6	12.9	25.6	24.4
Fe, mg/L Supernate	1,040	2,815	3,290	1,130	2,783	3,267
K, mg/L Supernate	272	16.4	5.23	296	16.2	5.19
Mg, mg/L Supernate	4,825	4,465	4,045	5,243	4,414	4,017
Mn, mg/L Supernate	1,330	1,280	1,154	1,445	1,265	1,146
Na, mg/L Supernate	26,550	28,150	25,850	28,851	27,829	25,671
Ni, mg/L Supernate	2,940	3,160	2,845	3,195	3,124	2,825
Pb, mg/L Supernate	0.61	2.29	2.01	0.663	2.264	1.996
Pd, mg/L Supernate	0.16	0.18	0.13	0.174	0.178	0.129
Rh, mg/L Supernate	10.7	18.36	15.02	11.6	18.2	14.9
Ru, mg/L Supernate	181	229	206	197	226	205
S, mg/L Supernate	572	453	482	622	448	479
Si, mg/L Supernate	17.4	132	68.8	18.9	130.5	68.3
Zr, mg/L Supernate	14.5	60.9	62	15.8	60.2	61.6

It should be noted that the corrected calcined solids analysis is very similar in all three runs. However, the ratio of soluble solids to total solids is much lower for GF36 than for GF36b or GF36c. In addition, both Fe and Al in supernate are much higher in GF36b and GF36c than in GF36. The solids identified in XRD were Al and Fe species. This is consistent with crystal formation post processing in GF36 but not GF36b or GF36c. It also was noted visually that the supernate for GF36 was much clearer than GF36b or GF36c.

Significant differences in these runs are summarized in Table 3-36. Note that the data is reported on slurry basis.

Table 3-36. Analyses of Interest of Duplicate Runs, Anions and Solids Concentrations Corrected

Run	GF36	GF36b	GF36c	GF37	GF37b	GF38
Formate, mg/kg slurry	<100	<100	<100	<100	<100	<100
Chloride, mg/kg slurry	622	591	602	821	590	583
Nitrite, mg/kg slurry	<100	<100	<100	<100	<100	<100
Nitrate, mg/kg slurry	57,500	56,650	56,350	56,550	52,500	56,900
Sulfate, mg/kg slurry	1,210	1,280	1,240	1,500	1,445	1,420
Oxalate, mg/kg slurry	3,955	3,190	3,210	2,755	2,420	2,655
Glycolate, mg/kg slurry	37,250	51,250	53,100	42,200	55,450	77,850
Formate, mg/L supernate	<100	<100	<100	<100	<100	<100
Chloride, mg/L supernate	858	736	783	913	772	746
Nitrite, mg/L supernate	<100	<100	<100	<100	<100	<100
Nitrate, mg/L supernate	86,350	74,000	74,300	82,150	70,950	77,350
Sulfate, mg/L supernate	2,170	1,530	1,610	2,740	1,845	1,795
Oxalate, mg/L supernate	3,250	4,060	4,240	3,860	3,035	3,605
Glycolate, mg/L supernate	46,700	64,550	70,750	61,350	72,500	98,150
Al, wt % CS	9.1	9.2	9.1	23.70	23.50	23.90
Ba	0.095	0.094	0.092	0.063	0.064	0.063
Ca	2.120	1.945	1.935	1.675	1.655	1.685
Cr	0.273	0.269	0.269	0.223	0.224	0.220
Cu	0.054	0.043	0.040	0.051	0.040	0.041
Fe	32.0	32.9	32.9	12.55	12.30	12.25
K	0.061	0.077	0.083	0.071	0.079	0.086
Mg	2.575	2.77	2.76	2.362	2.400	2.425
Mn	0.7055	0.640	0.631	0.6660	0.6005	0.5955
Na	13.5	13.4	13.2	15.27	14.15	14.45
Ni	2.69	2.73	2.73	2.37	2.35	2.37
Pb	0.056	0.049	0.041	0.058	0.050	0.039
Pd	<0.100	<0.010	<0.010	<0.100	<0.010	<0.010
Rh	0.033	<0.100	<0.100	0.047	<0.100	<0.100
Ru	0.032	<0.100	<0.100	0.030	<0.100	<0.100
S	0.276	0.264	0.269	0.294	0.283	0.260
Si	1.95	1.82	1.76	1.3	1.42	1.39
Sn	0.107	0.102	0.102	0.089	0.094	0.093
Zn	0.072	0.071	0.070	0.061	0.062	0.062
Zr	0.117	0.110	0.110	0.045	0.040	0.044
Al, mg/L	411	2,280	2,255	554	2,205	4,040
Ba	1.65	3.28	3.32	1.26	2.69	3.37
Ca	2,390	3,345	3,485	2,145	3,040	2,865
Cr	32.04	54.85	53.75	85.98	103.00	198.00
Cu	11.9	25.9	24.6	15.1	24.7	38.5
Fe	1,040	2,815	3,290	328	1,490	3,560
K	272	16.4	5.23	290	265	247
Mg	4,825	4,465	4,045	4,410	4,090	4,180
Mn	1,330	1,280	1,154	1,300	1,280	922
Na	26,550	28,150	25,850	30,400	29,800	28,500

Run	GF36	GF36b	GF36c	GF37	GF37b	GF38
Ni	2,940	3,160	2,845	3,165	3,180	3,965
Pb	0.61	2.29	2.01	2.31	4.15	18.95
Pd	0.16	0.18	0.13	0.18	<0.100	<0.100
Rh	10.70	18.36	15.02	11.97	36.05	78.25
Ru	181	229	206	289	330	453
S	572	453	482	672	599	513
Si	17.4	132.0	68.8	67.4	121.0	103.0
Sr	3.06	NA	NA	2.99	41.60	77.25
Zr	14.5	60.9	62.0	17.7	38.3	50.7

3.2.12 *Reanalysis of Anions*

Since the measured glass REDOX was much more reducing than predicted, the anions were reanalyzed by both Analytical Development (AD) and PSAL (Table 2-1). The accurate measurement of four anions, nitrate, glycolate, oxalate, and formate is necessary to predict redox. It is apparent from the PSAL reanalysis results that nitrate ion concentration is a very robust analysis, but that the oxalate and glycolate concentrations vary during reanalysis. In fact, a number of unreported glycolate results were so high that they greatly exceeded the maximum concentration of glycolate possible based on the glycolic acid added.

Table 3-37. Anion and TOC Analyses for Runs GF36b, 36c, 37b and 38, mg/kg

Sample ID	Lab ID	Cl	NO3	SO4	C2O4	C2H3O3	TOC Calc	TOC
12-GF36b-6160A	**PSAL**	**736**	**74,000**	**1,530**	**4,060**	**64,550**	**21,770**	**19,700**
12-GF36b-6160A.	**PSAL**	**717**	**72,450**	**1,555**	**4,130**	**61,750**	**20,893**	**19,700**
12-GF36b-6160C	**AD**	**545.0**	**57,100**	**1,030**	**2,440**	**33,900**	**11,517**	**19700**
12-GF36c-6184A	**PSAL**	**783**	**74,300**	**1,610**	**4,240**	**70,750**	**23,804**	**28,600**
12-GF36c-6184A	**PSAL**	**774**	**74,550**	**1,645**	**3,655**	**72,050**	**24,061**	**28,600**
12-GF36c-6184C	**AD**	**589.0**	**56,000**	**1,010**	**1,940**	**34,400**	**11,541**	**28,600**
12-GF37b-6217A	**PSAL**	**772**	**70,950**	**1,845**	**3,035**	**72,500**	**24,062**	**24,500**
11-GF37b-6217C	**AD**	**559.0**	**51,700**	**1,250**	**1,340**	**35,900**	**11,857**	**24,500**
12-GF38-6249A	**PSAL**	**746**	**77,350**	**1,795**	**3,605**	**98,150**	**32,428**	**26,200**
12-GF38-6255C	**AD**	**321.0**	**58,100**	**1,160**	**2,390**	**54,500**	**18,098**	**26,200**

4.0 Conclusions

Testing was completed to demonstrate the viability of the newly developed glycolic/nitric flowsheet for processing in the Defense Waste Processing Facility's (DWPF) Chemical Process Cell (CPC). The Savannah River National Laboratory (SRNL) initiated a sludge matrix study to evaluate the impact on CPC processing. Four sludge simulants were designed to cover a broad insoluble solid composition range to bracket future sludge batches. The first pair of sludge parameters was high iron/low aluminum versus low iron/high aluminum (referred to as HiFe or LoFe in this report). The second pair of sludge parameters was high calcium-manganese/low nickel, chromium, and magnesium versus low calcium-manganese/high nickel, chromium, and magnesium (referred to as HiMn or LoMn in this report). In addition, a simple supernate simulant was prepared to match the composition of the matrix simulants.

Four planned experiments (GF34 to GF37) and four additional experiments (GF36b, GF36c, GF37b and GF38) were completed to demonstrate the glycolic-nitric flowsheet viability. Also, four supernate experiments (GF39a-GF39d) were performed to better understand the reaction sequence, particularly the reduction and stripping of mercury.

Composition and physical property measurements were made on the Sludge Receipt and Adjustment Tank (SRAT) and Slurry Mix Evaporator (SME) products. Composition measurements were made on the composited condensates from the Mercury Water Wash Tank (MWWT), and Formic Acid Vent Condenser (FAVC), on the ammonia scrubber solution, and on SRAT samples pulled throughout the SRAT cycle. Updated values for glycolate and formate loss, nitrite-to-nitrate conversion, and oxalate formation were found that can be used in the acid calculations for future sludge matrix process simulations with the glycolic-nitric flowsheet.

Preliminary results of the initial testing indicate:

- Hydrogen generation rate was below detection limits (<7.6E-4 lb/hr DWPF-scale or <0.001 vol%) throughout all SRAT cycles.
- Hydrogen generation rate was below 0.0258 lb/hr DWPF-scale throughout all SME cycles. Hydrogen was produced in the SME cycles because formic acid was added with the frit slurry.
- Mercury was both reduced and stripped without formic acid. The mercury concentration of the SRAT product was below 0.8 wt % limit in four of the runs and below 0.92 wt % in the other four runs.
- Nitrite in the SRAT product was <100 mg/kg slurry for all runs
- Foaminess was not an issue using the nominal antifoam addition strategy in these tests.
- High wt % total solids were achieved while staying within rheological limits which makes the glycolic acid/nitric acid flowsheet an improvement for processing more viscous sludges. However, there may be a tradeoff between excessive dissolution of metals and thinner rheology.
- The pH remains steady throughout processing (i.e. no pH rebound) potentially leading to more consistent processing during the CPC. The SRAT product pH varied from 3.5-4.5 for the 100% acid stoichiometry runs, significantly lower than is typical of the baseline nitric acid/formic acid flowsheet.
- The testing apparatus has been significantly modified to improve processing with high viscosity slurries. Testing of the old style and new style rig identified no differences in CPC processing, including steam stripping of Hg.

5.0 Recommendations

The glycolic-nitric flowsheet is recommended as a viable flowsheet alternative to the baseline DWPF flowsheet. In the testing that has been performed to date, this flowsheet meets or outperforms the current flowsheet in minimizing off-gas generation, removing mercury, and producing a rheologically thinner product. Previous testing with glycolic/formic acid mixtures demonstrated a wide processing window regarding both the glycolic-formic ratio and acid stoichiometry. The addition of glycolic acid leads to SRAT products that are rheologically less viscous which means that more concentrated products can be produced, leading to potentially higher waste throughput per batch. In addition, the combination of lower pH processing and the

complexing power of glycolic acid leads to the dissolution of more metals, which may minimize deposits in the CPC processing vessels and prevent the fouling of steam coils. Follow on testing is recommended in the following areas:

- Improve glycolate and oxalate analyses. The majority of the glycolate results reported were correct. However, there are issues with anion and cation deposition on the Ion Chromatograph's (IC) column, causing higher than expected glycolate and oxalate in blanks and some samples. Both Process Science and Analytical Laboratory (PSAL) and Analytical Development (AD) have reported results that have varied significantly from expectations. Modification to the sample preparation method is likely needed to improve analytical accuracy and minimize the cleaning and replacement of the IC column. An alternative to the IC measurement of glycolate should also be considered.
- Determine the appropriate REDOX model for the glycolic-nitric flowsheet. The REDOX model may need more terms due to the more extensive reduction of some metals, including Mn and Fe. In addition, accurate measurement of glycolate (and possibly oxalate) and nitrate is needed to accurately predict REDOX. REDOX testing of the matrix sludges should be repeated using acceptable frits that meet Product Composition Control System (PCCS) limits.
- Testing should be completed with alternate forms of ruthenium to determine whether the elimination of the chloride added as ruthenium chloride would improve the reduction and stripping of the mercury. Testing should be completed with the baseline and glycolic-nitric flowsheets.
- Test the glycolic-nitric flowsheet at acid stoichiometries of less than 100%. Demonstration of this flowsheet at an acid stoichiometry of <100% is recommended and might be useful for mercury stripping.
- Demonstrate the glycolic-nitric flowsheet with actual waste in SRNL Shielded Cells SRAT and SME processing, to include periodic slurry sampling throughout the SRAT and SME processing along with a glass REDOX measurement.
- Increase both the nitric and glycolic acid flowrate to the same scaled molar flowrate as formic acid to minimize glycolic-nitric flowsheet batch time.
- Complete a supernate experiment without nitrite to determine whether nitrite is needed to reduce mercury.
- Measure SME condensate anions and cations in future glycolic-nitric flowsheet runs.

6.0 Acknowledgements

The authors would like to thank a number of SRNL employees who supported this testing.

Thanks to Jon Duvall, Vickie Williams, Phyllis Workman, David Healy, Tony Burckhalter, and Beverly Walls for their excellent support during these around the clock runs.

Thanks to Whitney Riley, Beverly Walls, Phyllis Workman and Pat Simmons for their excellent and timely analysis of the hundreds of samples that were submitted as part of this study.

Thanks to Tom White, Amy Ekechukwu, and David Missmer for the AD analysis of samples for IC, TOC and XRD.

Thanks to Frances Williams and John Pareizs for their support of the GC calibration, analysis, and post run processing.

Thanks to Jackie Best for her excellent administrative support.

7.0 References

[1] Pickenheim, B.R., M.E. Stone, SRAT Alternative Reductant Feasibility Assessment – Phase I, SRNL-STI-2009-00120, Savannah River National Laboratory, Aiken, SC, February 2009.

[2] Pickenheim, B.R., M.E. Stone, J.D. Newell, Glycolic-Formic Acid Flowsheet Development, SRNL-STI-2010-00523, Rev 0, Savannah River National Laboratory, Aiken, SC, November 2010.

[3] D.P. Lambert, B.R. Pickenheim, M.E. Stone, J.D. Newell, D.R. Best, Glycolic - Formic Acid Flowsheet Final Report for Downselection Decision, SRNL-STI- 2010-00523, Rev 1, Savannah River National Laboratory, Aiken, SC, March 2011.

[4] Fellinger, T.L., "*Alternate Reductant Flowsheet Development – Phase I*", HLW-DWPF-TTR-2012-0003, Revision 0, October 2011.

[5] Lambert, D.P., Task Technical and Quality Assurance Plan for Glycolic Acid Flowsheet Development, SRNL-RP-2011-01586, Savannah River National Laboratory, Aiken, SC, November 2011.

[6] D. C. Koopman, D. P. Lambert, Initial Characterizations and SRAT Simulations of Four Sludge Matrix Study Simulants, SRNL-STI-2009-00606, Revision 0, Savannah River National Laboratory, Aiken, SC, December 2009

[7] Lambert, D.P., Acid Calculation Spreadsheet for DWPF Simulations, Revision 1, SRNL-PSE-2006-00176, Savannah River Site, Aiken, SC 29808 (2006). Acid Calculation

[8] Koopman, D.C., A.I. Fernandez, B.R. Pickenheim, Preliminary Evaluations of Two Proposed Stoichiometric Acid Equations, Revision 0, Savannah River Site, Aiken, SC 29808 (2009).

[9] Stone, M. E., Lab-Scale CPC Equipment Set-up, SRNL-ITS-2006-000742011-00127, Savannah River Site, Aiken, SC 29808 (2011).

[10] Manual L29, Procedure ITS-0094, Rev. 6, Laboratory Scale Chemical Process Cell Simulations, Savannah River Site, Aiken, SC 29808, November 2011.

[11] Glycolic/Nitric Acid Flowsheet Development Notebook, SRNL-NB-2012-00039, Savannah River Site, Aiken, SC 29808 (2012). Notebook

[12] Jantzen, C. M. and M. E. Stone, Role of Manganese Reduction/Oxidation (REDOX) on Foaming and Melt Rate in High Level Waste Melters, WSRC-STI-2006-00066, Savannah River Site, Aiken, SC, 29808 , March 2007.

[13] Jantzen, C.M., J.R. Zamecnik, D.C. Koopman, C.C. Herman, and J.B. Pickett, Electron Equivalents Model for Controlling Reduction-Oxidation (REDOX) Equilibrium during High Level Waste (HLW) Vitrification, WSRC-TR-2003-00126, Savannah River Site, Aiken, SC 29808 (2003).

[14] Lambert, D. P., Koopman, D. C., Glycolic-Formic Acid Flowsheet Sludge Matrix Study, SRNL-STI-2011-00275, Savannah River Site, Aiken, SC, 29808 (June 2011).

[15] D. C. Koopman, D. P. Lambert, Initial Characterizations and SRAT Simulations of Four Sludge Matrix Study Simulants, SRNL-STI-2009-00606, REVISION 0, Savannah River National Laboratory, Aiken, SC, December 2009.

[16] Best, D.R., Anion Analysis by Ion Chromatography for the Alternate Reductant Program for the Defense Waste Processing Facility, SRNL-STI-2010-00389, Savannah River National Laboratory, Aiken, SC, June 2010.

[17] Manual L29, Procedure ITS-0052, Rev. 2, Heat Treatment of Waste Slurries for REDOX (Fe2+/∑Fe) and Chemical Composition Measurement.

[18] Zamecnik, J.R., Behavior of Mercury during DWPF Chemical Process Cell, SRNL-STI-2012-00051, REVISION 0, Savannah River National Laboratory, Aiken, SC, April 2012.

[19] Koopman, D. C., Rheology Protocols for DWPF Samples, WSRC-RP-2004-00470, Savannah River Site, Aiken, SC, 29808 (October 2004).

Appendix A. Acid Spreadsheet Inputs

Table A-1. Sludge Analyses for Acid Calculations,

Run #	GF34	GF35	GF36	GF36b	GF36c	GF37	GF37b	GF38	Units
Mass without trim chemicals	2,900.0	2,900.0	2,900.0	2,900.0	2,900.0	2,900.0	2,900.0	2,900.0	g slurry
Weight % Total Solids	23.70	18.47	22.81	22.81	22.81	23.07	23.07	23.07	wt%
Weight % Calcined Solids	17.81	13.56	16.95	16.95	16.95	16.00	16.00	16.00	wt%
Weight % Insoluble Solids	16.70	13.01	16.35	16.35	16.35	16.05	16.05	16.05	wt%
Density	1.185	1.144	1.180	1.180	1.180	1.176	1.176	1.176	kg / L slurry
Supernate density	1.057	1.051	1.055	1.055	1.055	1.057	1.057	1.057	kg / L supernate
Nitrite	17,900	9,605	17,800	17,800	17,800	18,100	18,100	18,100	mg/kg slurry
Nitrate	13,550	5,880	13,400	13,400	13,400	13,250	13,250	13,250	mg/kg slurry
Formate	0	0	0	0	0	0	0	0	mg/kg slurry
Sulfate	1,770	1,345	1,575	1,575	1,575	1,585	1,585	1,585	mg/kg slurry
Chloride	116	0	131	131	131	127	127	127	mg/kg slurry
Phosphate	0	0	0	0	0	0	0	0	mg/kg slurry
Oxalate	300	7,220	275	275	275	294.5	294.5	294.5	mg/kg slurry
Slurry TIC	2,751	1,066	2,492	2,492	2,492	2,403	2,403	2,403	mg/kg slurry
Supernate TIC	1,080	664	1,310	1,310	1,310	1,280	1,280	1,280	mg/L supernate
Base Equivalents) pH = 7	0.5903	0.580	0.562	0.562	0.562	0.522	0.522	0.522	MolesBase/L slurry
Coal/Carbon source	0.000	0.000	0.000	0.000	0.000	0.000	0.000	0.000	wt% dry basis
Manganese	4.040	5.115	0.690	0.690	0.690	0.662	0.662	0.662	wt % calcined basis
Mercury	0.0000	0.0000	0.0000	0.0000	0.0000	0.0000	0.0000	0.0000	wt% dry basis
Magnesium	0.448	0.413	2.970	2.970	2.970	2.420	2.420	2.420	wt % calcined basis
Sodium	12.500	14.700	12.900	12.900	12.900	14.200	14.200	14.200	wt % calcined basis
Potassium	0.110	0.120	0.076	0.076	0.076	0.096	0.096	0.096	wt % calcined basis
Cesium	0.000		0.000	0.000	0.000	0.000	0.000	0.000	wt % calcined basis
Calcium	3.840	0.831	2.115	2.115	2.115	1.970	1.970	1.970	wt % calcined basis
Strontium	0.000	0.000	0.000	0.000	0.000	0.000	0.000	0.000	wt % calcined basis
Nickel	0.214	3.310	2.600	2.600	2.600	2.310	2.310	2.310	wt % calcined basis
Supernate Manganese	0	0.000	0	0	0	0	0	0	mg/L supernate

Table A-2. SRAT Processing Assumptions

Run #	GF34	GF35	GF36	GF36b	GF36c	GF37	GF37b	GF38	Units
Conversion of Nitrite to Nitrate in SRAT Cycle	30.00	30.00	30.00	30.00	30.00	30.00	30.00	30.00	gmol NO_3^-/100 gmol NO_2^-
Destruction of Nitrite in SRAT and SME cycle	100.00	100.00	100.00	100.00	100.00	100.00	100.00	100.00	% of starting nitrite destroyed
Destruction of Formic acid charged in SRAT	0.00	0.00	0.00	0.00	0.00	0.00	0.00	0.00	% formate converted to CO_2 etc.
Destruction of Glycolic acid charged in SRAT	30.00	30.00	30.00	30.00	30.00	30.00	30.00	30.00	% glycolate converted to CO_2 etc.
Conversion of Glycolic acid to Oxalate	3.00	3.00	3.00	3.00	3.00	3.00	3.00	3.00	% glycolate converted to C2O4
Destruction of Oxalate charged	0.00	0.00	0.00	0.00	0.00	0.00	0.00	0.00	% of total oxalate destroyed
Percent Acid in Excess Stoichiometric Ratio	103.97	100.00	106.07	106.07	106.07	100.00	100.00	125.00	%
SRAT Product Target Solids	27.90	27.90	27.90	27.90	27.90	27.90	27.90	27.90	%
Nitric Acid Molarity	10.304	10.304	10.304	10.304	10.304	10.304	10.304	10.304	Molar
Formic Acid Molarity	23.552	23.552	23.552	23.552	23.552	23.552	23.552	23.552	Molar
Glycolic Acid Molarity	11.930	11.930	11.930	11.930	11.930	11.930	11.847	11.847	Molar
DWPF Nitric Acid addition Rate	4.572	4.572	4.572	4.572	4.572	4.572	4.572	4.572	gallons per minute
DWPF Formic Acid addition Rate	3.948	3.948	3.948	3.948	3.948	3.948	3.976	3.976	gallons per minute
REDOX Target	0.100	0.100	0.100	0.100	0.100	0.100	0.100	0.100	Fe^{+2} / ΣFe
Ag metal	0.0014	0.0014	0.0014	0.0014	0.0014	0.0014	0.0014	0.0014	total wt% dry basis
wt% Hg dry basis	1.5000	1.5000	1.5000	1.5000	1.5000	1.5000	1.5000	1.5000	total wt% dry basis
Pd metal	0.0790	0.0790	0.0790	0.0790	0.0790	0.0790	0.0790	0.0790	total wt% dry basis
Rh metal	0.0380	0.0380	0.0380	0.0380	0.0380	0.0380	0.0380	0.0380	total wt% dry basis
Ru metal	0.2170	0.2170	0.2170	0.2170	0.2170	0.2170	0.2170	0.2170	total wt% dry basis
Cr metal	0.0000	0.0000	0.0000	0.0000	0.0000	0.0000	0.0000	0.0000	total wt% dry basis
Ba metal	0.0000	0.0000	0.0000	0.0000	0.0000	0.0000	0.0000	0.0000	total wt% dry basis
Cd metal	0.0000	0.0000	0.0000	0.0000	0.0000	0.0000	0.0000	0.0000	total wt% dry basis
Gd metal	0.0000	0.0000	0.0000	0.0000	0.0000	0.0000	0.0000	0.0000	total wt% dry basis
Wt% Coal/carbon	0.0000	0.0000	0.0000	0.0000	0.0000	0.0000	0.0000	0.0000	total wt% dry basis
Oxalate	0.1235	3.8086	0.1176	0.1176	0.1176	0.1246	0.1246	0.1246	total wt% dry basis

Run #	GF34	GF35	GF36	GF36b	GF36c	GF37	GF37b	GF38	Units
Dilution Water	250.00	250.00	250.00	250.00	250.00	250.00	250.00	250.00	g
Acid flush water	20.00	20.00	20.00	20.00	20.00	20.00	20.00	20.00	g
Mass of SRAT cycle samples	450.00	450.00	450.00	450.00	450.00	0.00	450.00	450.00	g
Active Agent In Antifoam Solution	10	10	10	10	10	10	10	10	wt%
Basis Antifoam Addition for SRAT	100	100	100	100	100	100	100	100	mg/kg slurry
Number of basis antifoam additions	8	8	8	8	8	8	8	8	
SRAT air purge	230	230	230	230	230	230	230	230	scfm
SRAT boil-up rate	5000	5000	5000	5000	5000	5000	5000	5000	lbs/hr
SRAT total boil-up (reflux)	60,000	60,000	60,000	60,000	60,000	60,000	60,000	60,000	lbs
SRAT Steam Stripping Factor	750	750	750	750	750	750	750	750	g steam/g mercury

Table A-3. SME Processing Assumptions

Run #	GF34	GF35	GF36	GF37	**Units**
Frit type	418	418	418	418	
Destruction of Formic acid in SME	0.00	0.00	0.00	0.00	% Formate converted to CO_2 etc.
Destruction of Nitrate in SME	5.00	5.00	5.00	5.00	% Nitrate destroyed in SME
Destruction of Glycolate in SME	5.00	5.00	5.00	5.00	% glycolate converted to CO_2 etc.
Assumed SME density	1.400	1.400	1.400	1.400	kg / L
Basis Antifoam Addition for SME cycle	100	100	100	100	mg/kg slurry
Number of basis antifoam additions added	3	3	3	3	
Sludge Oxide Contribution (Waste Loading)	36.00	36.00	36.00	36.00	%
Frit Slurry Formic Acid Ratio	1.50	1.50	1.50	1.50	g 90 wt% FA/100 g Frit
Target SME Solids total Wt%	45.0	45.0	45.0	45.0	wt%
Number of frit additions in SME Cycle	2	2	2	2	
# DWPF Canister decons simulated	0.0	0.0	0.0	0.0	
Volume of water per deconed can	1,000	1,000	1,000	1,000	gal at DWPF scale
Water flush volume after frit slurry addition	0.0	0.0	0.0	0.0	gal
SME air purge	74	74	74	74	scfm

Appendix B. Off-gas Results

Raw off-gas data from the GCs are presented in this Appendix for the eight SRAT cycles and four SME cycles from the process simulations with slurry simulants.

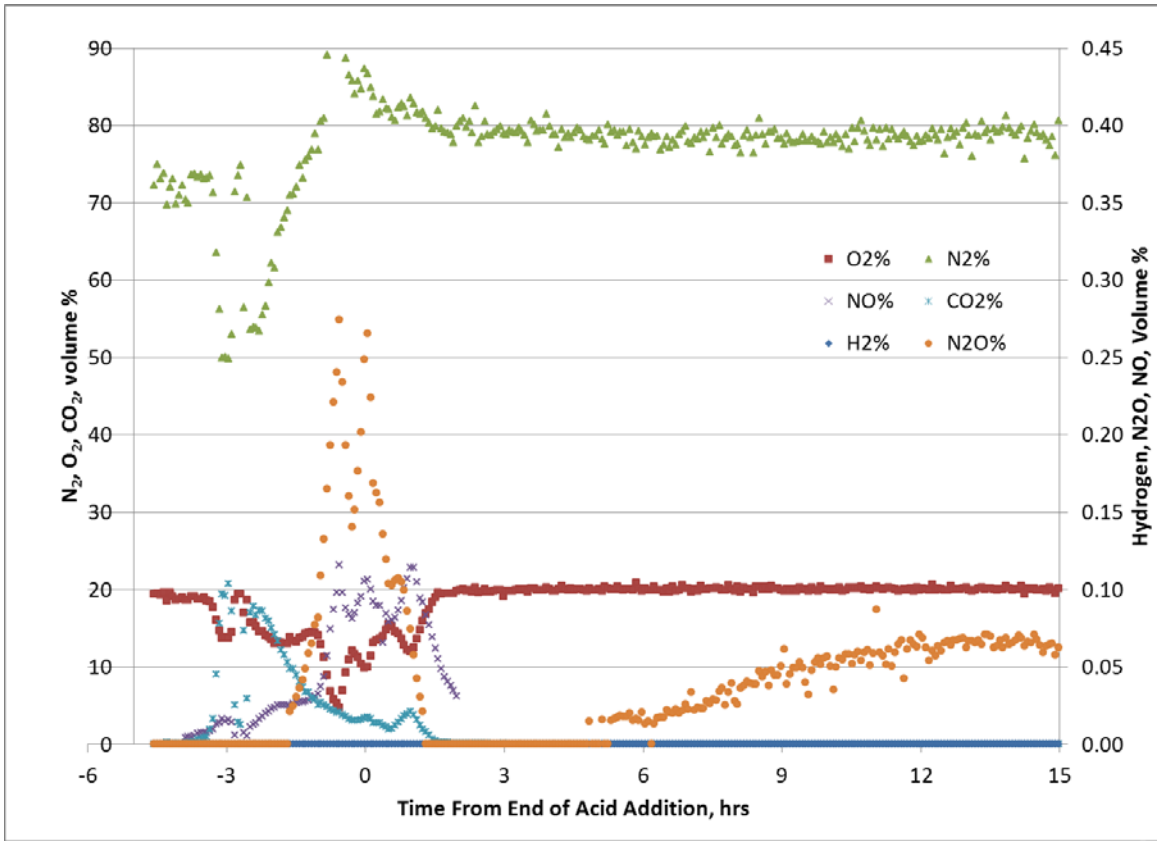

Figure B-1. GF34 SRAT Off-gas Data

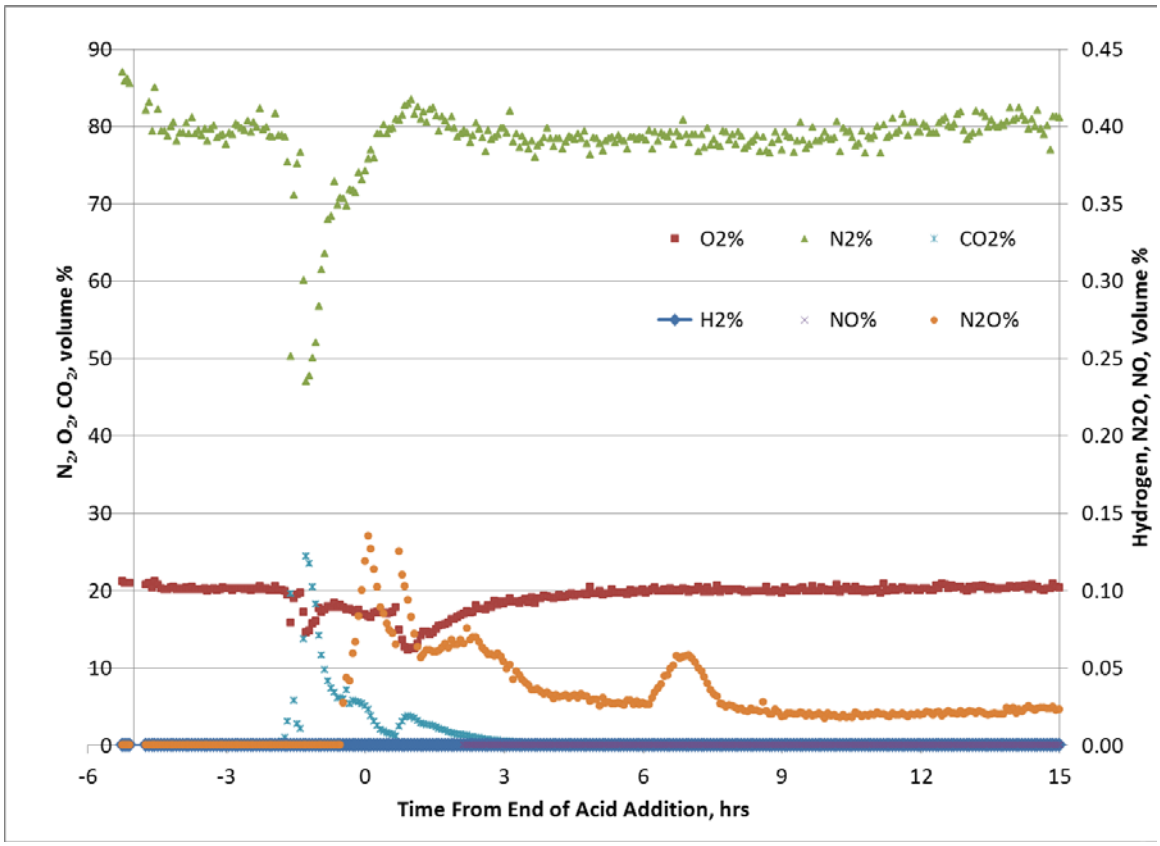

Figure B-2. GF35 SRAT Off-gas Data

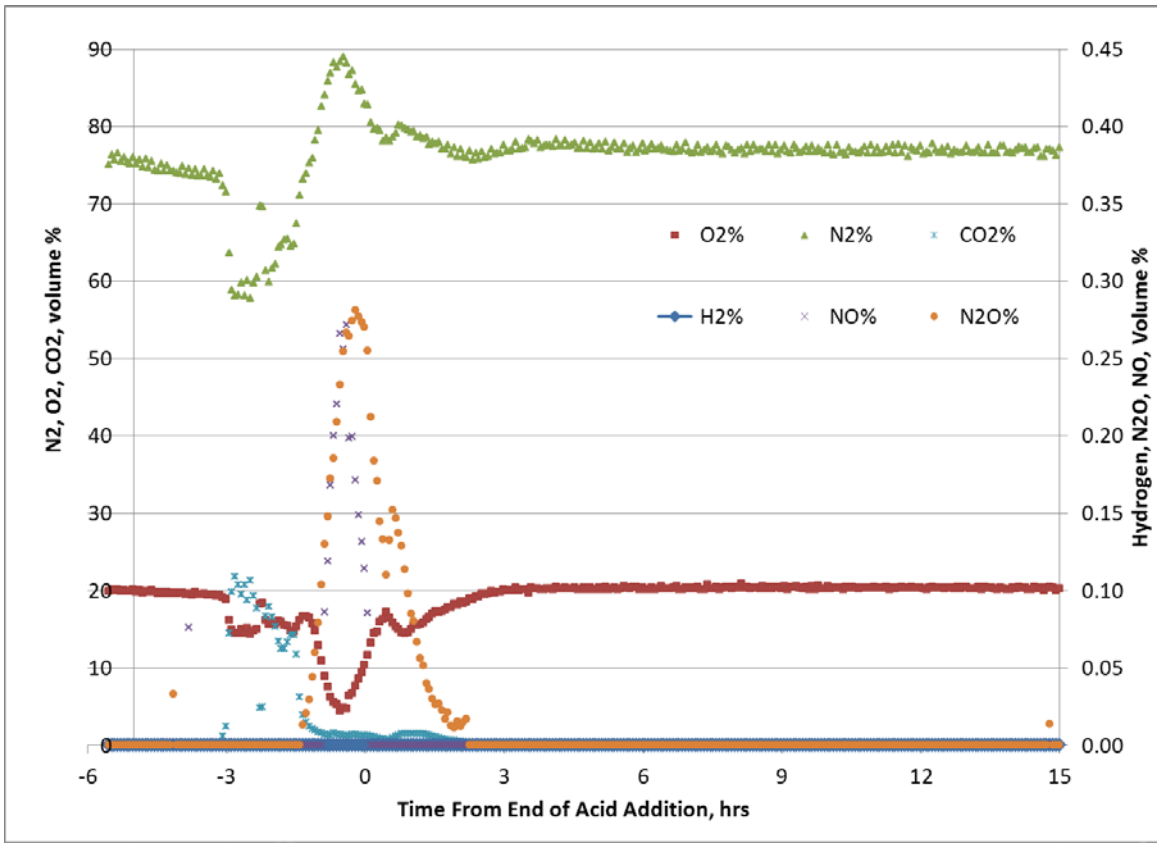

Figure B-3. GF36 SRAT Off-gas Data

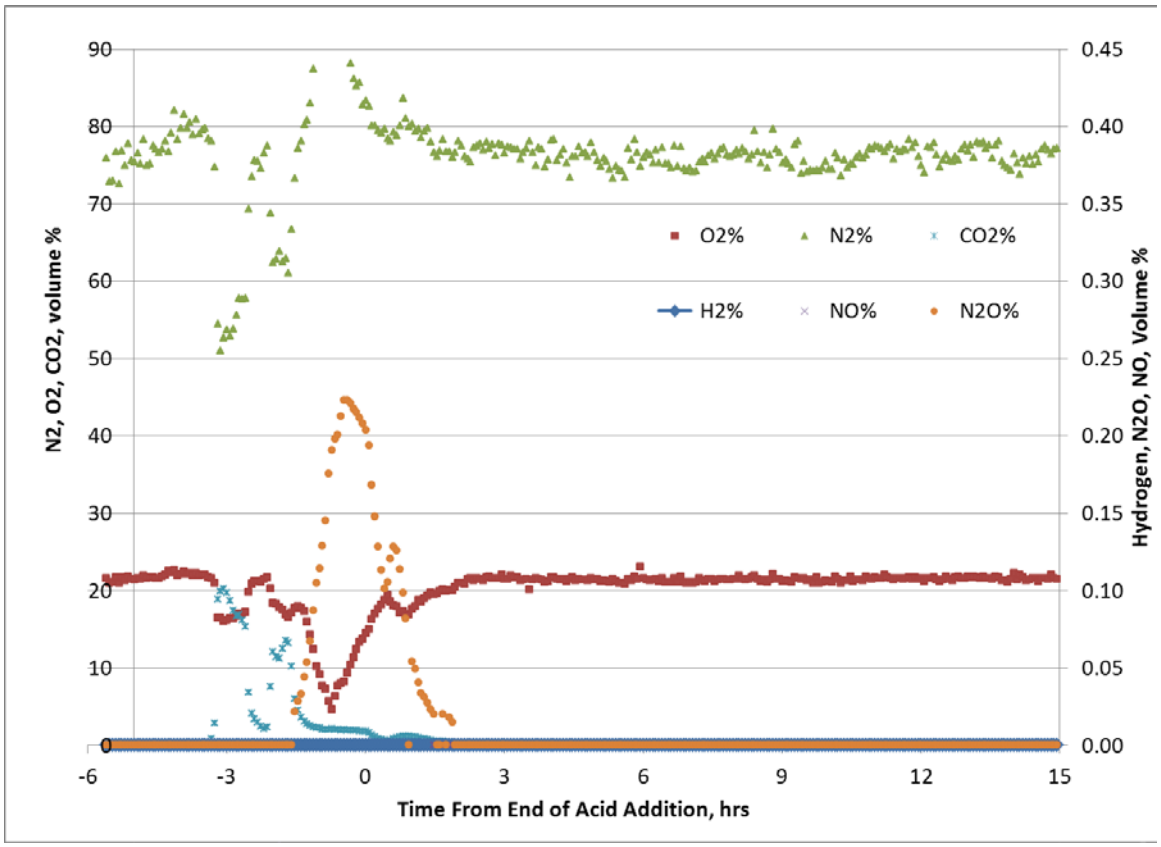

Figure B-4. GF36b SRAT Off-gas Data

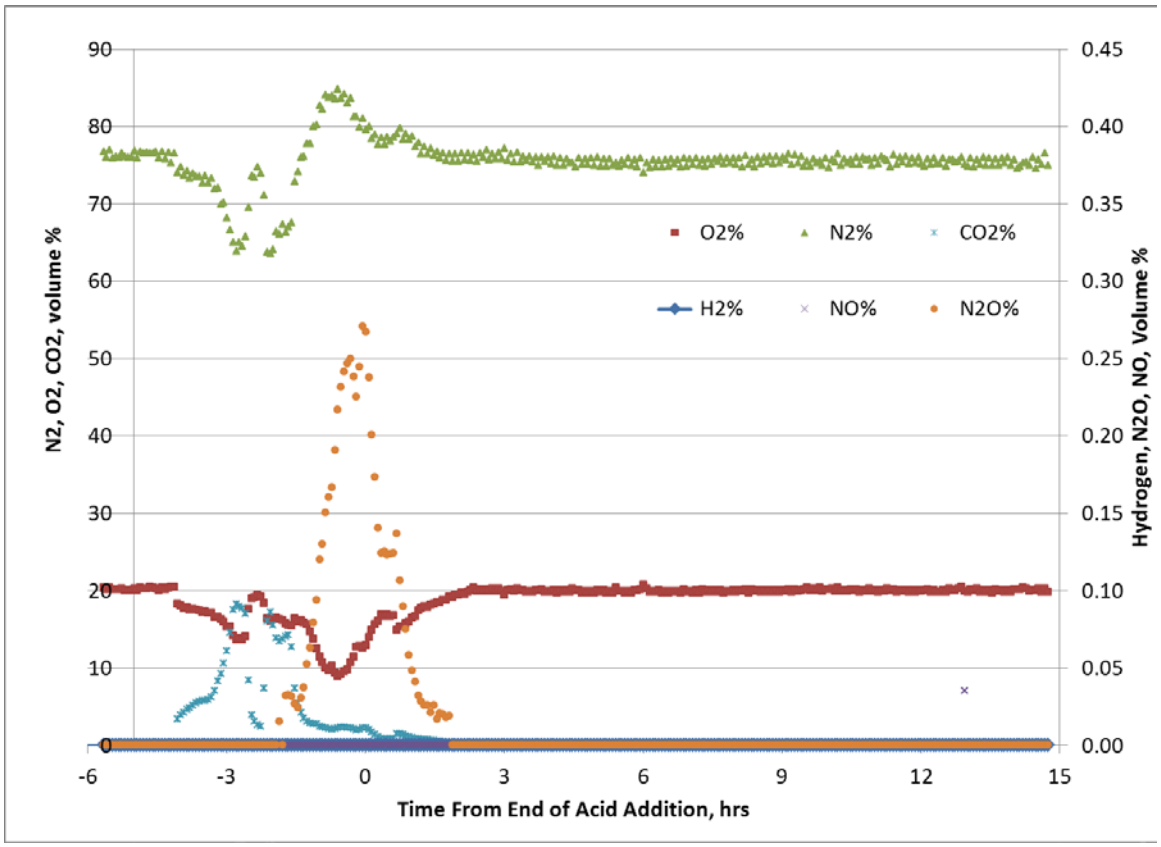

Figure B-5. GF36c SRAT Off-gas Data

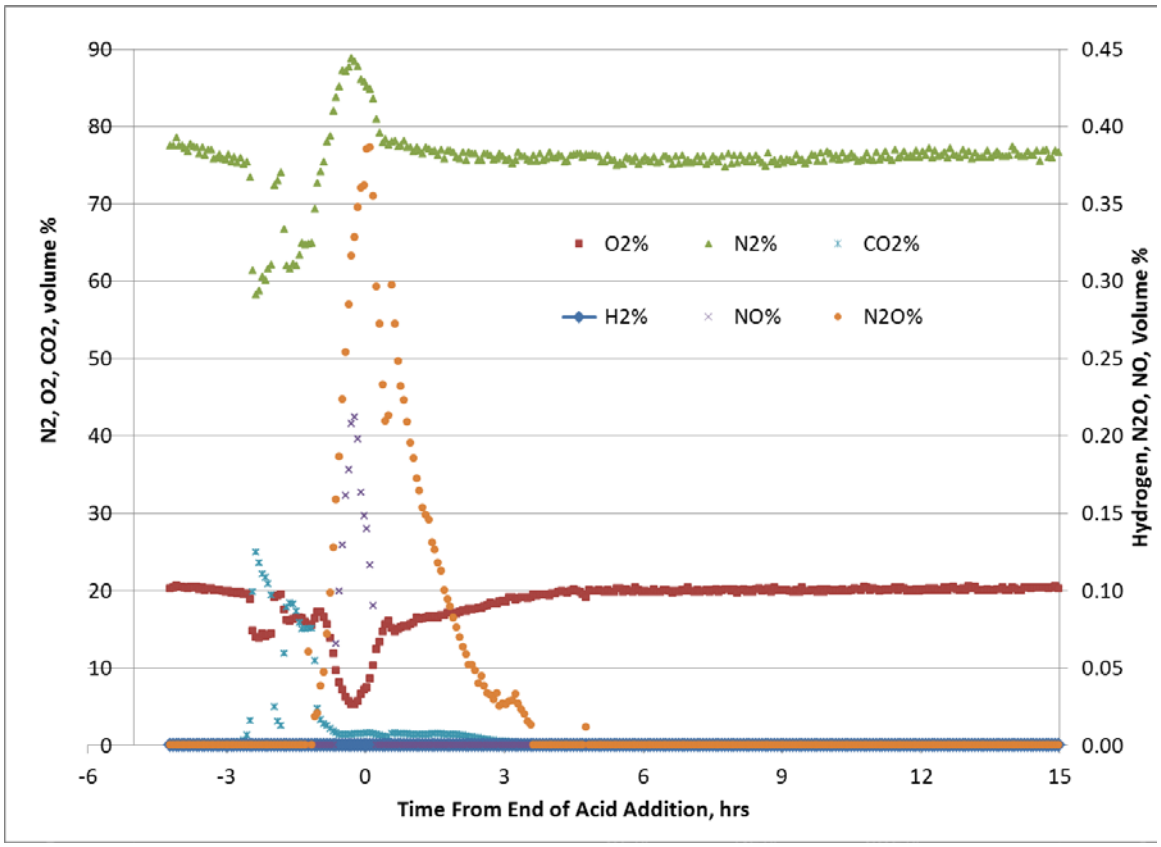

Figure B-6. GF37 SRAT Off-gas Data

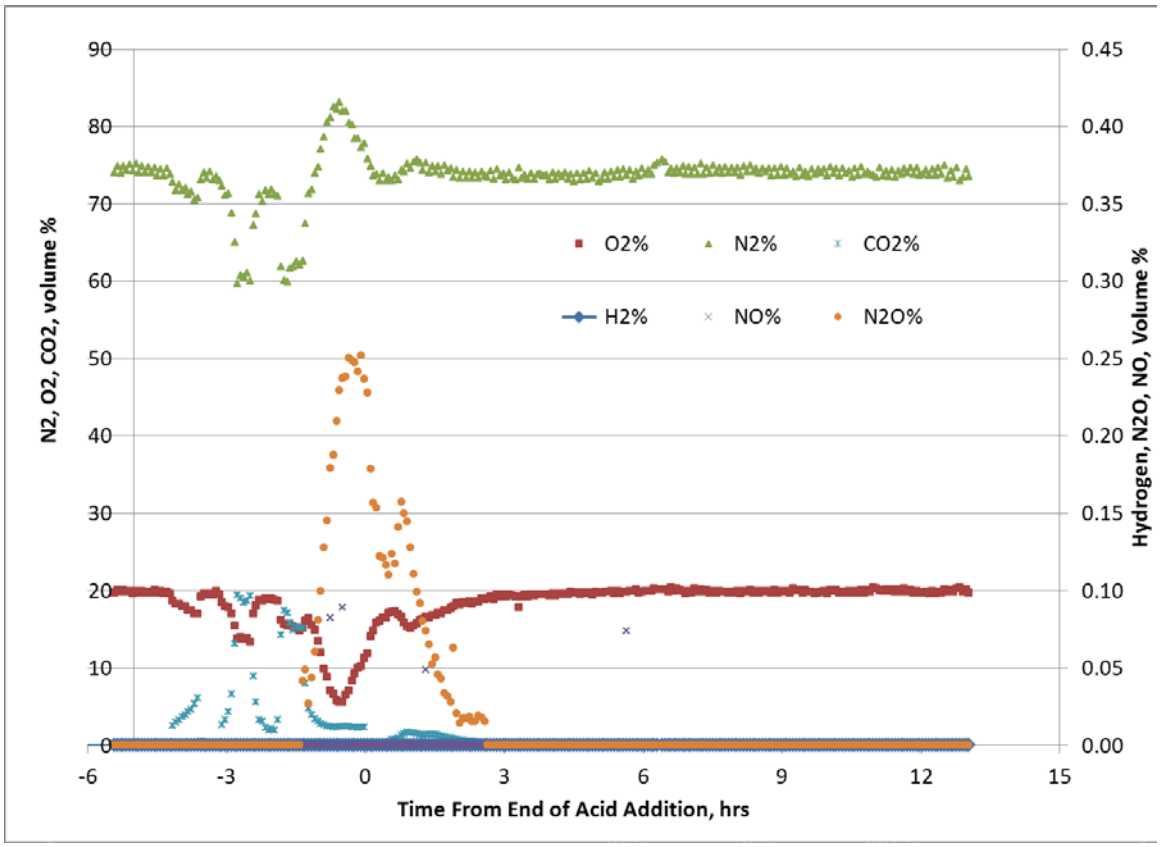

Figure B-7. GF37b SRAT Off-gas Data

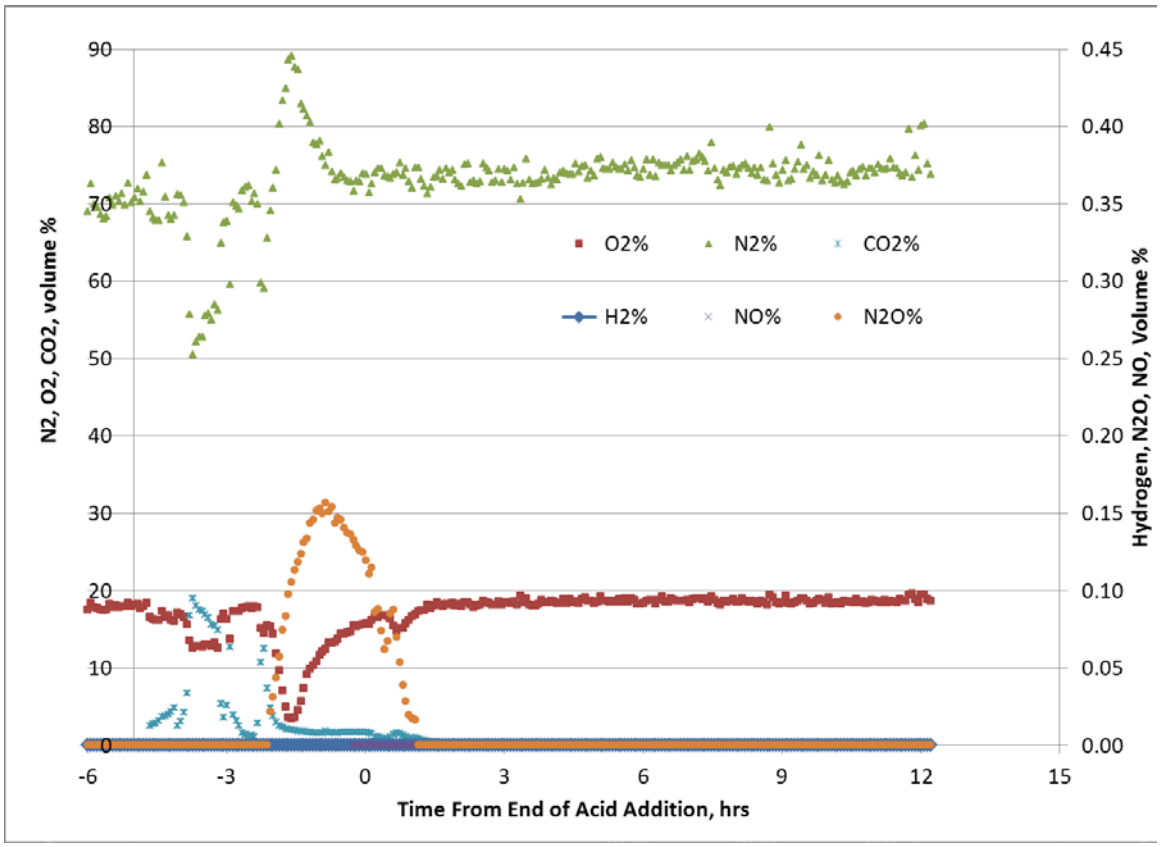

Figure B-8. GF38 SRAT Off-gas Data

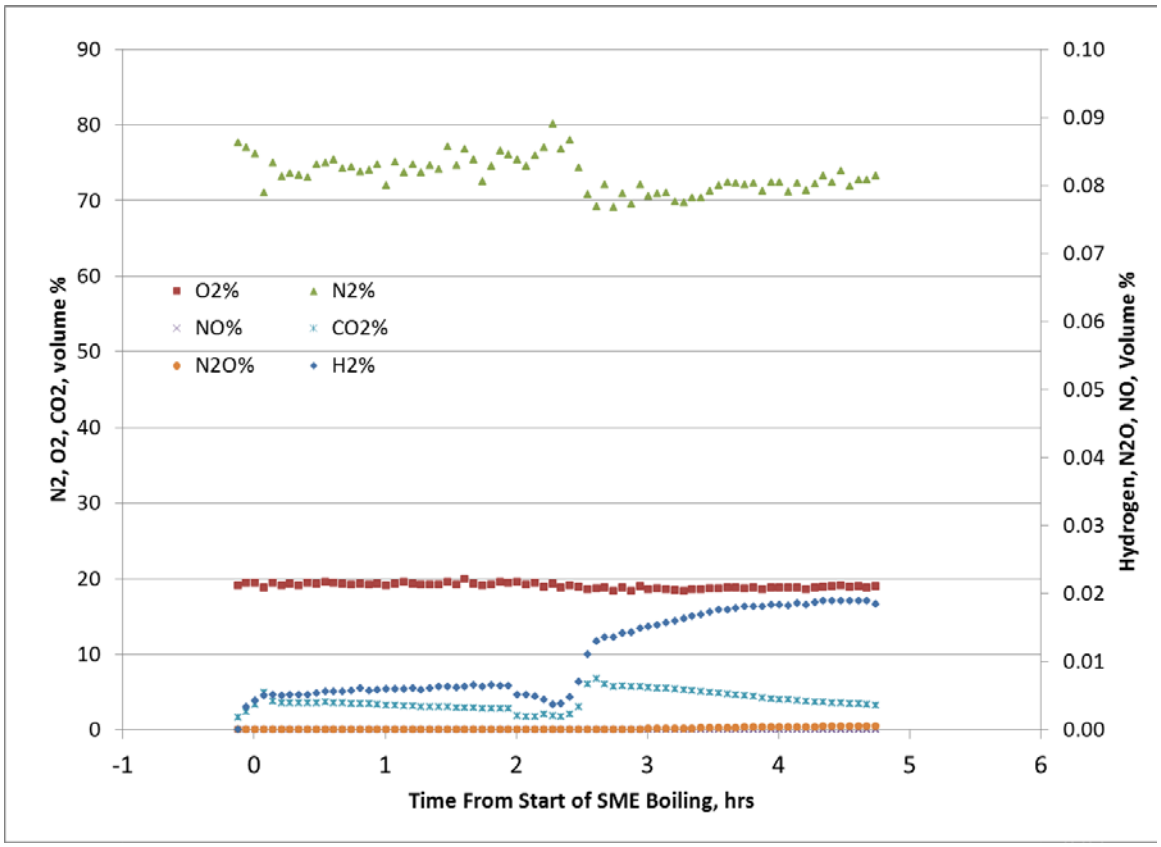

Figure B-9. GF34 SME Off-gas Data

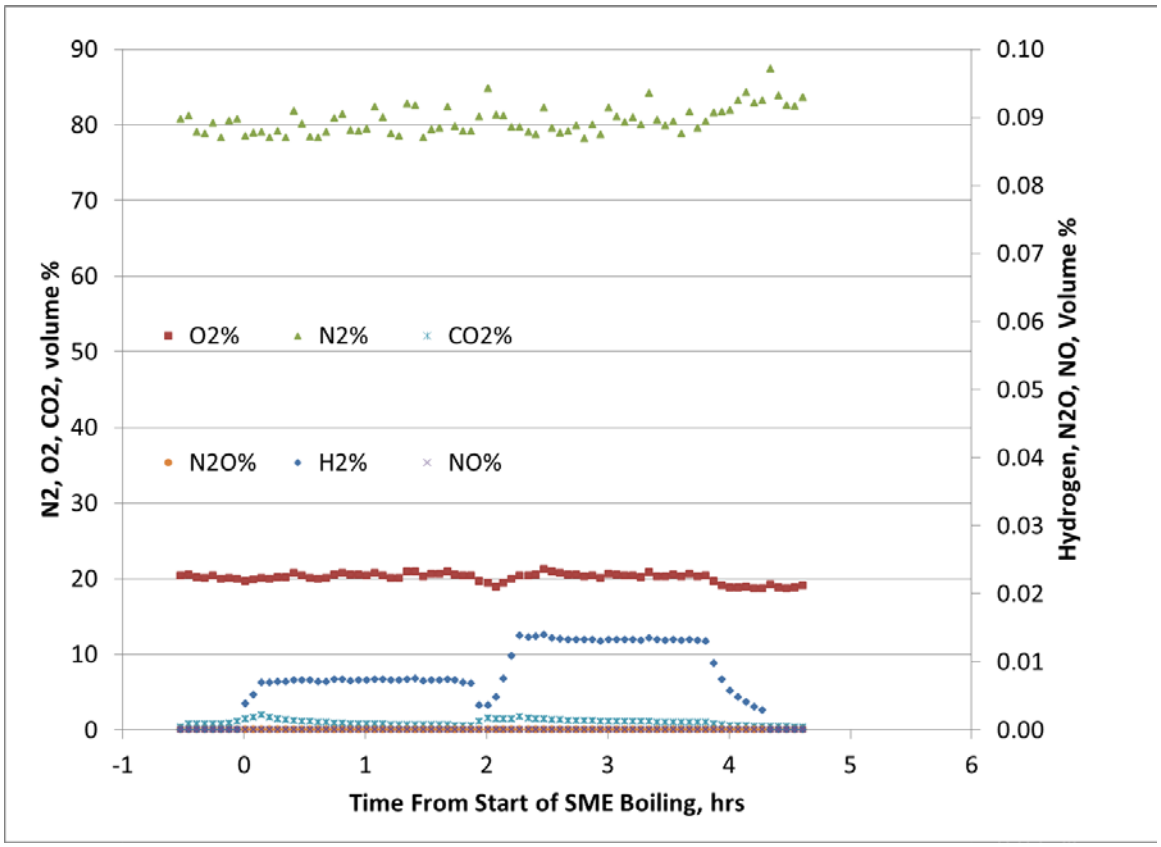

Figure B-10. GF35 SME Off-gas Data

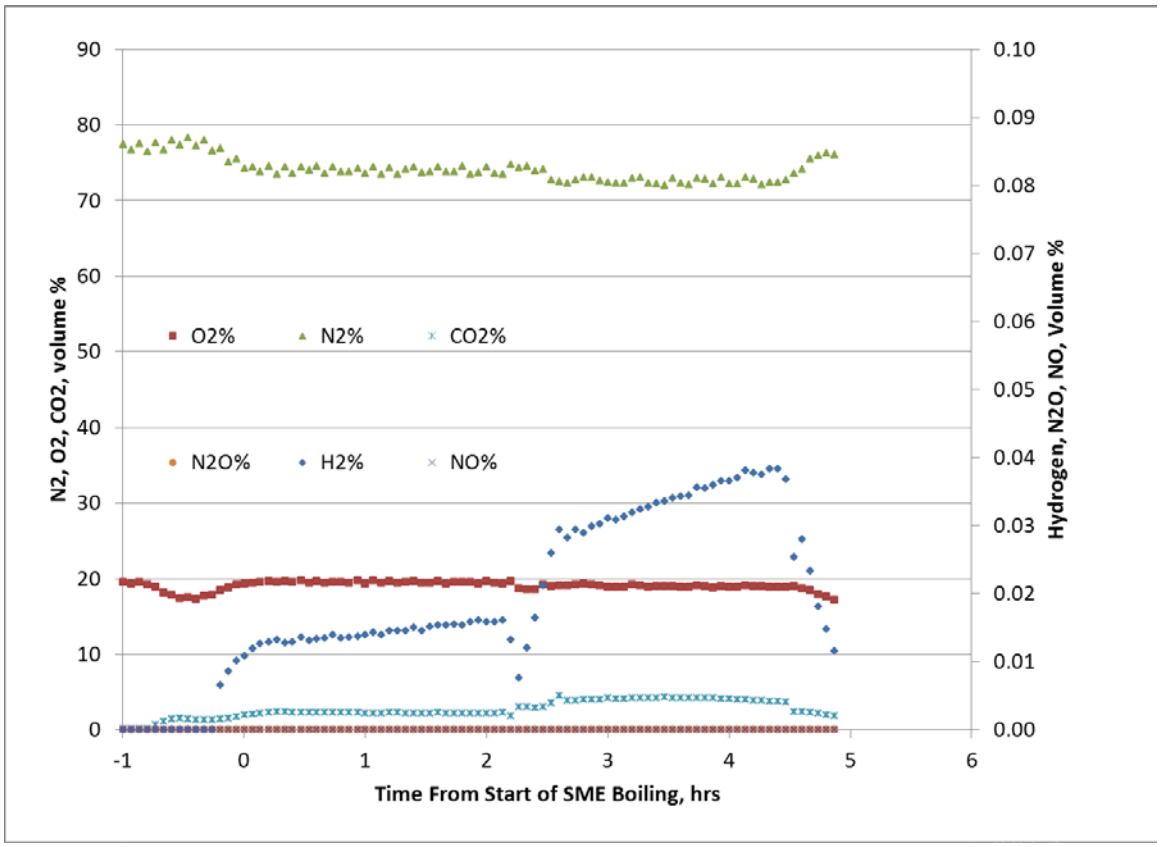

Figure B-11. GF36 SME Off-gas Data

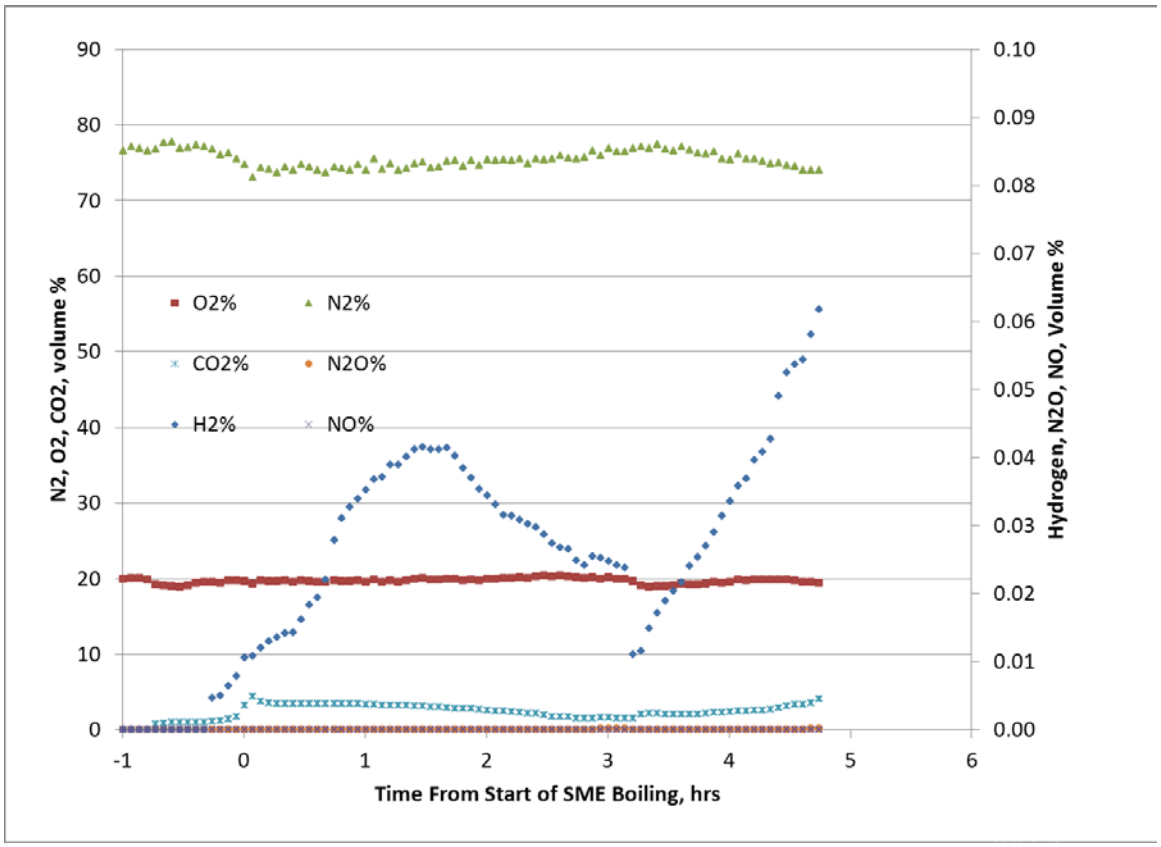

Figure B-12. GF37 SME Off-gas Data

Appendix C. X-ray Defraction (XRD) Results of SRAT and SME Solids

This Appendix contains X-ray diffraction data for samples of the _____

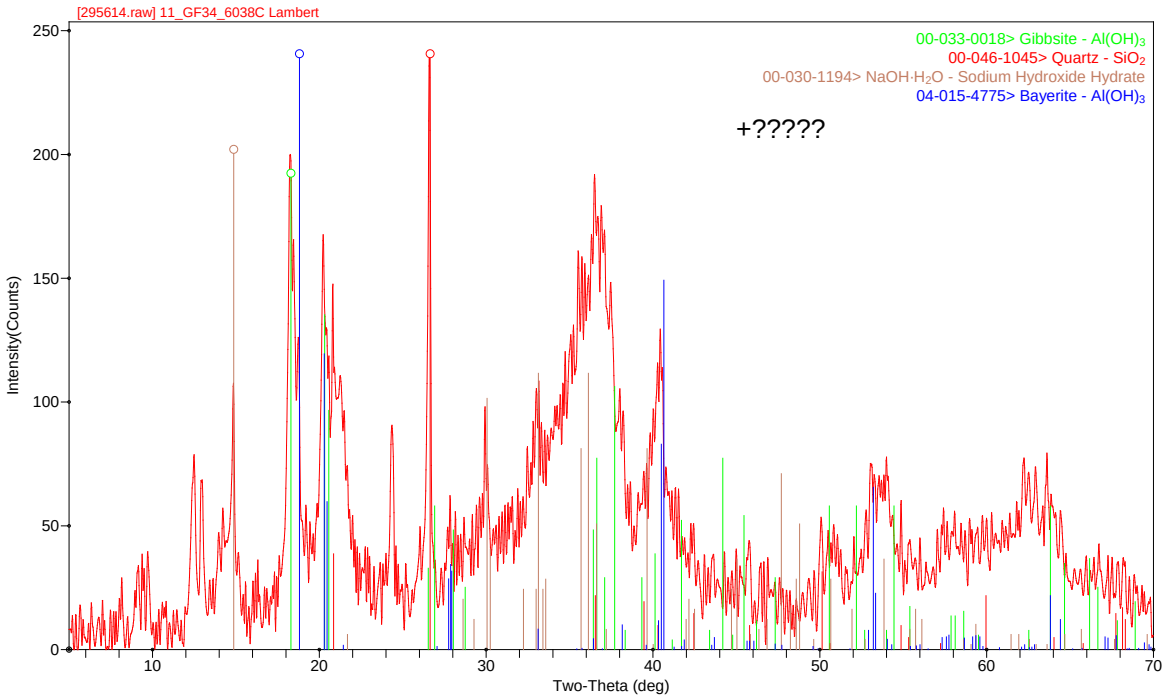

* The NaOH*H2O is questionable. There is a phase in this sample that could not be identified.

Figure C-1. GF34 SRAT Product

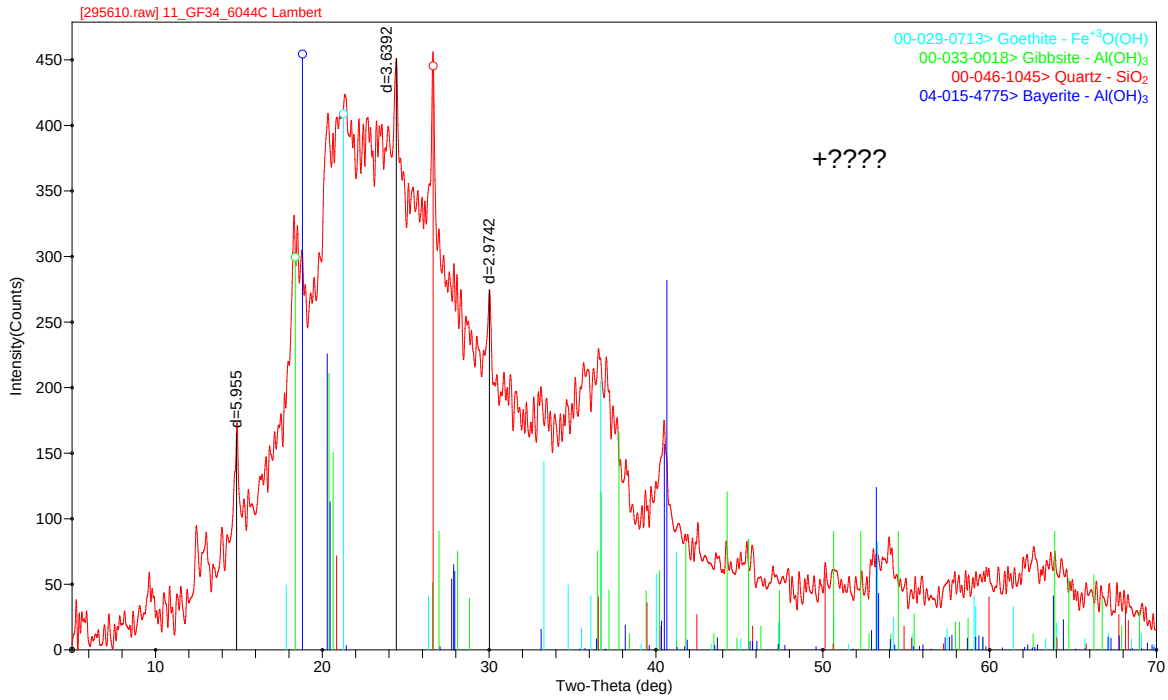

Figure C-2. GF34 SME Product XRD

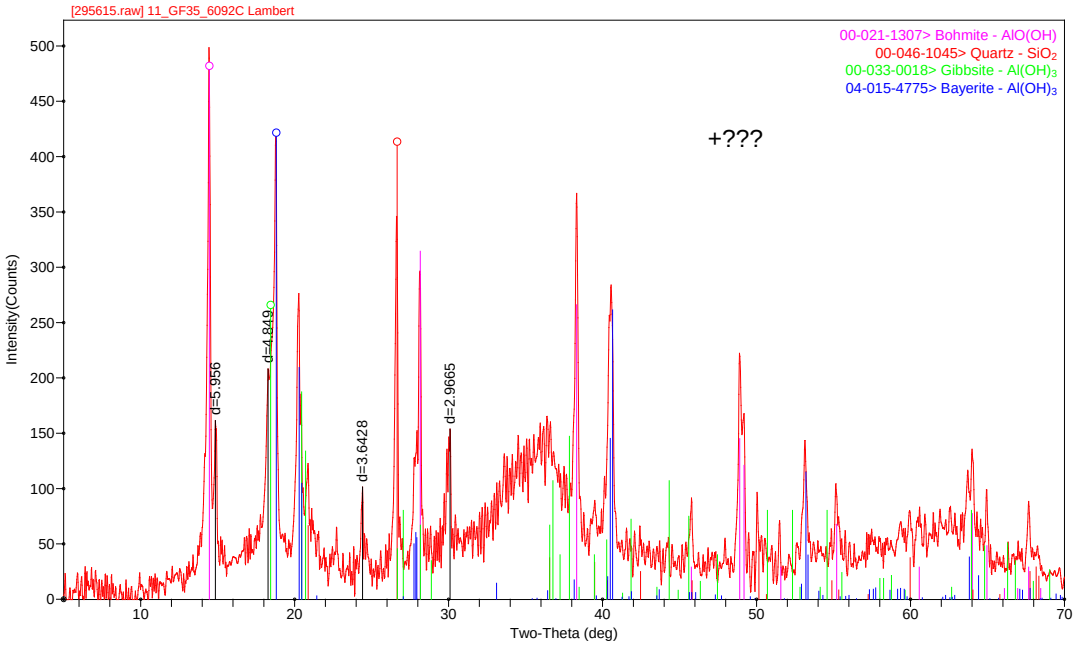

Figure C-3. GF35 SRAT Product XRD

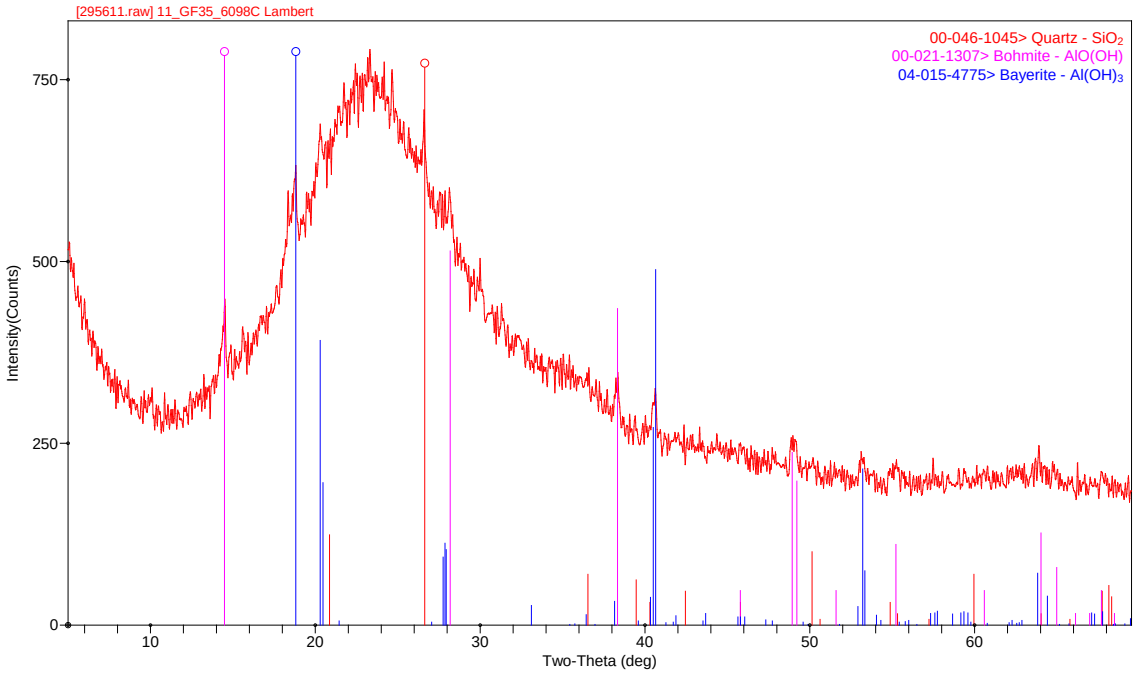

Figure C-4. GF35 SME Product

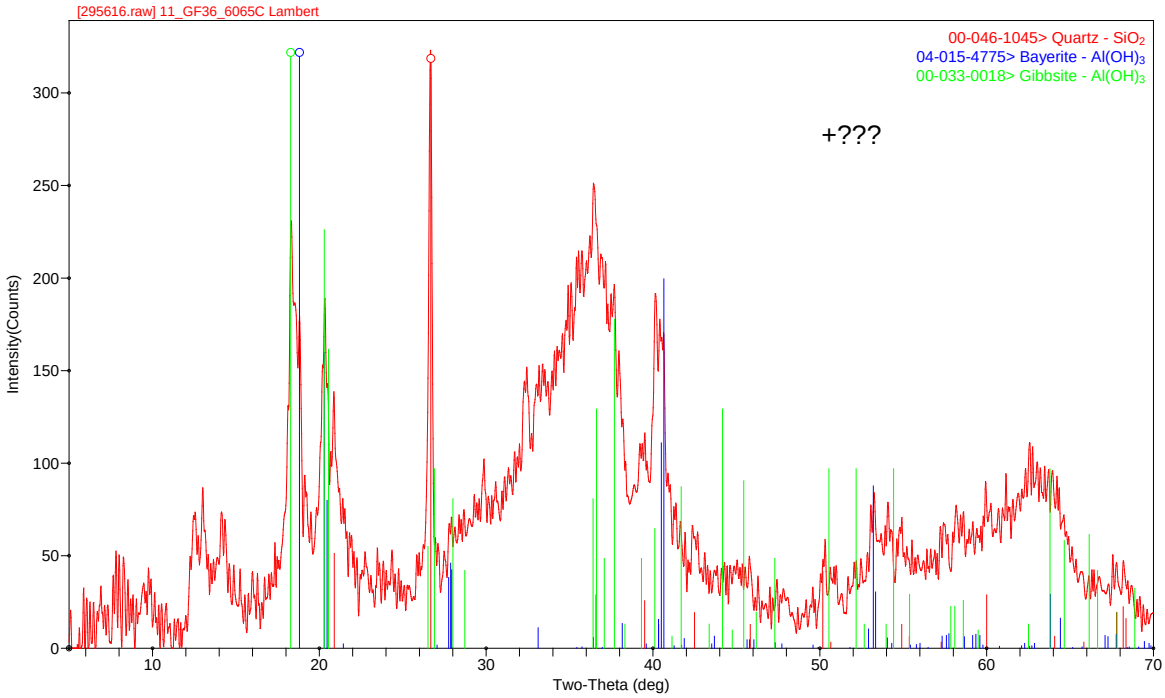

Figure C-5. GF36 SRAT Product

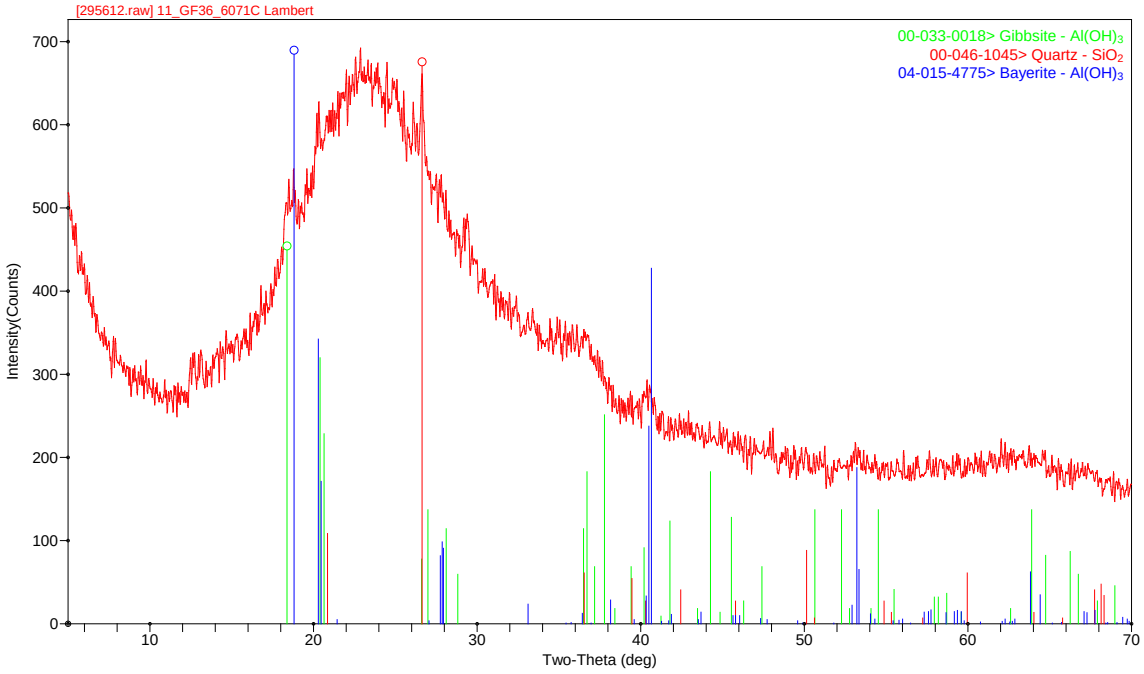

Figure C-6. GF36 SME Product

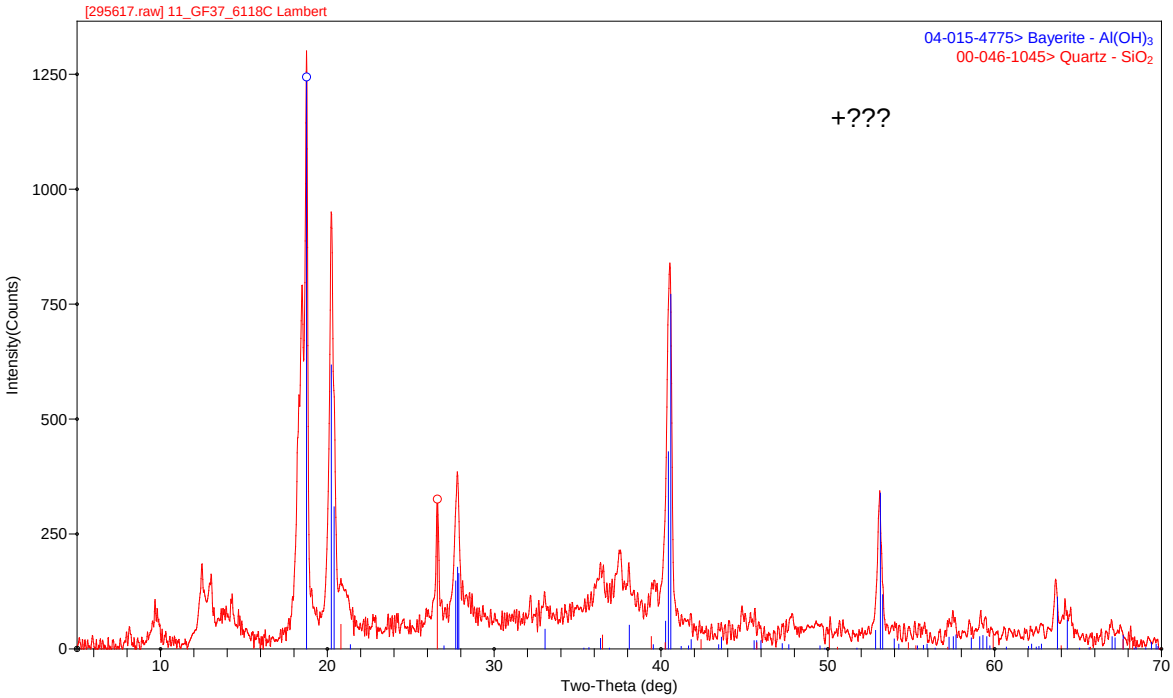

Figure C-7. GF37 SRAT Product

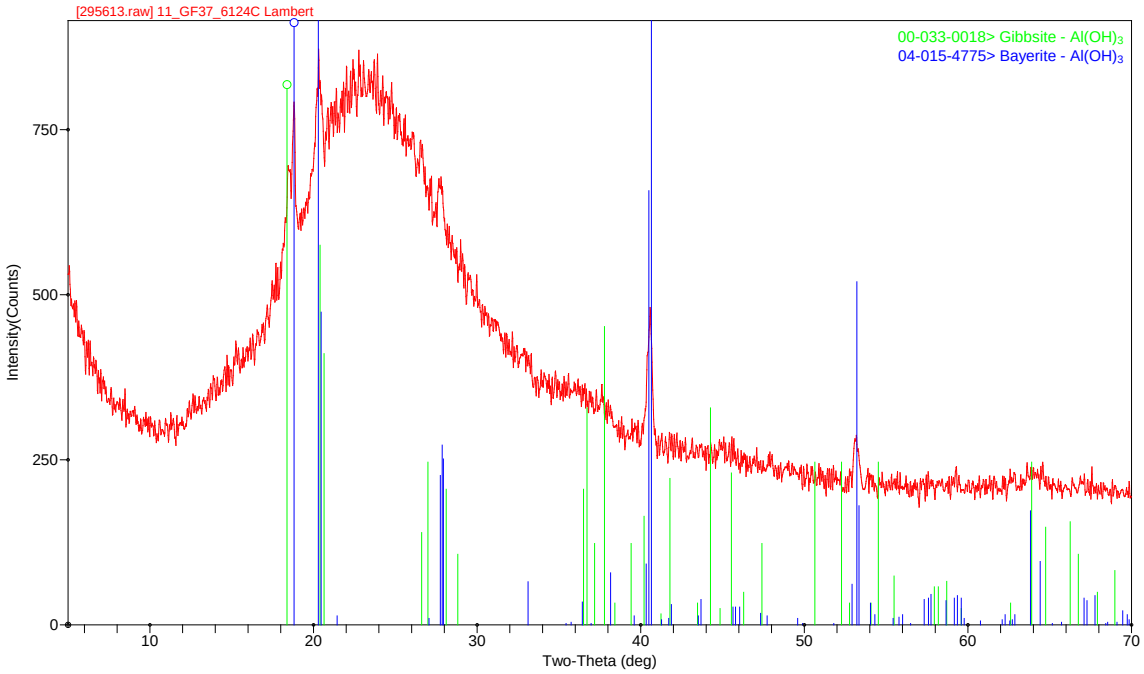

Figure C-8. GF37 SME Product

Appendix D. Supernate Study Results

This Appendix includes data collected from experiments using a supernate simulant instead of sludge as describe in Section 3.1.

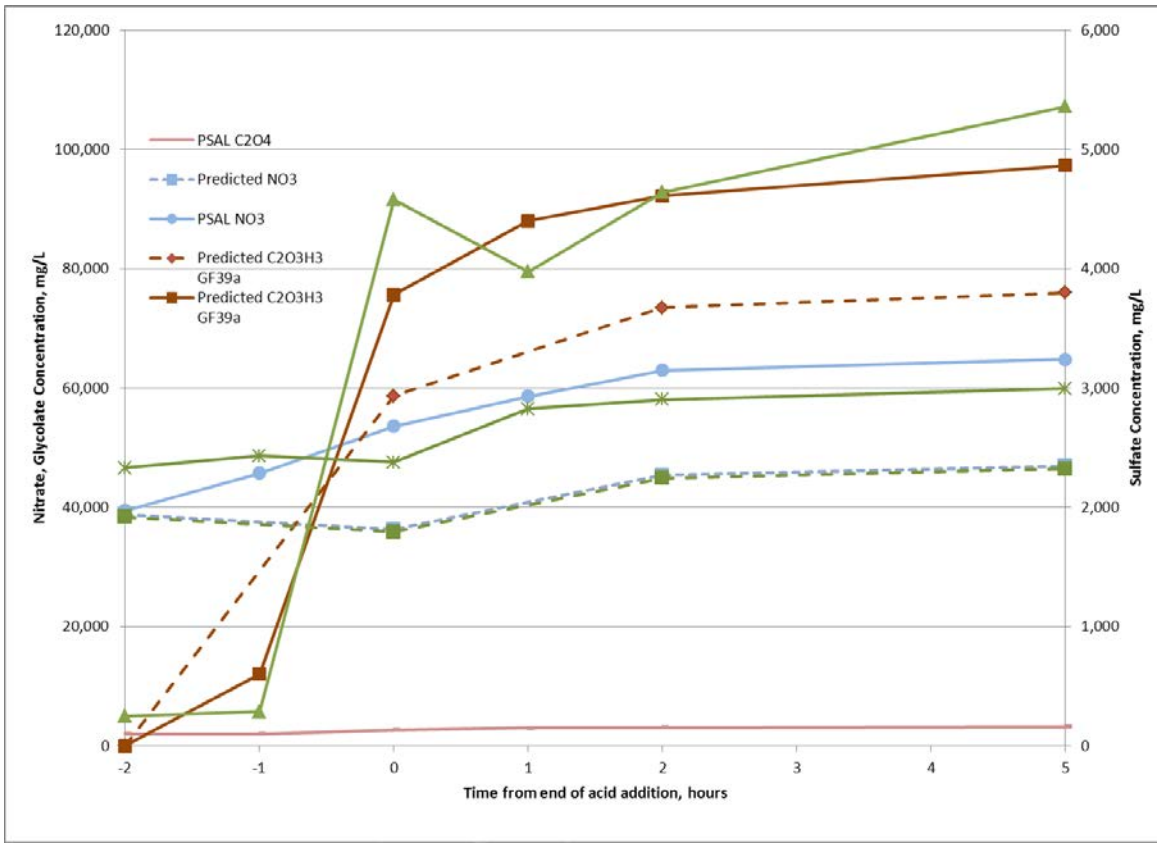

Figure D-1. GF39a Supernate Anion Results

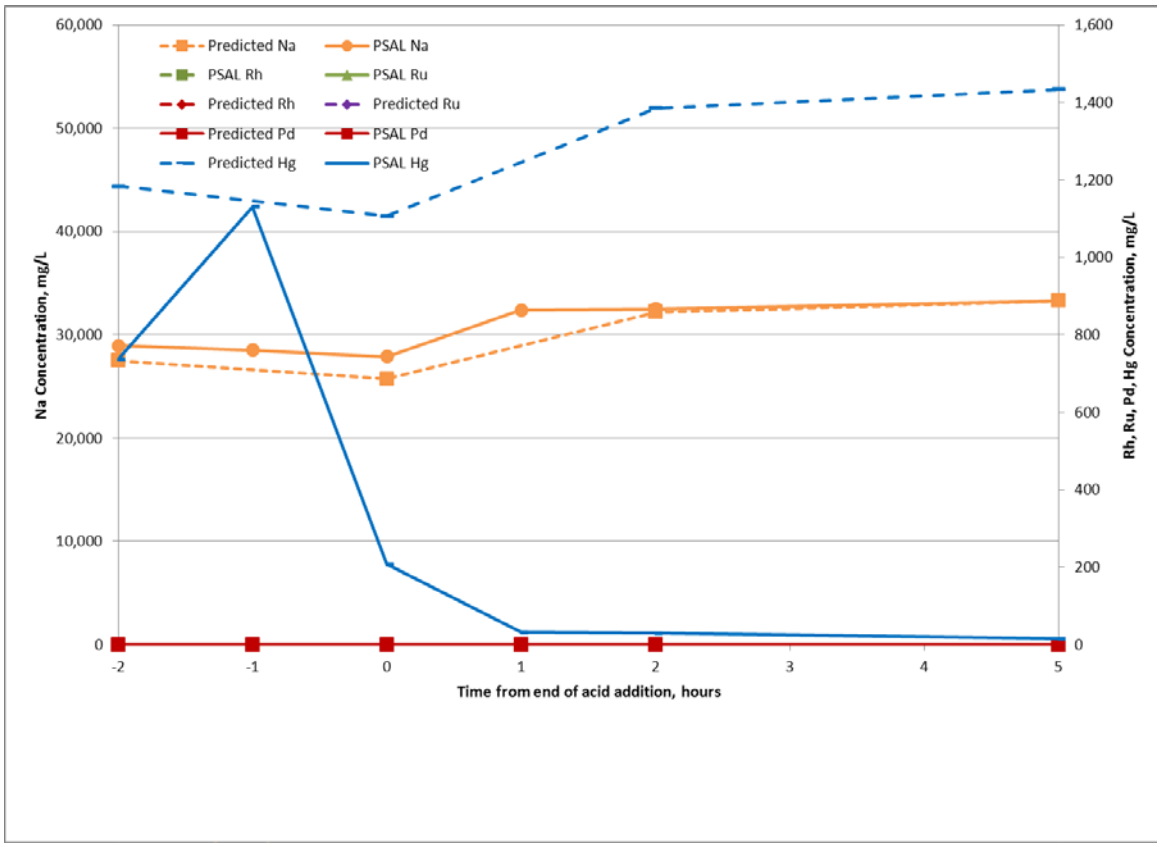

Figure D-2. GF39a Supernate Cation Results

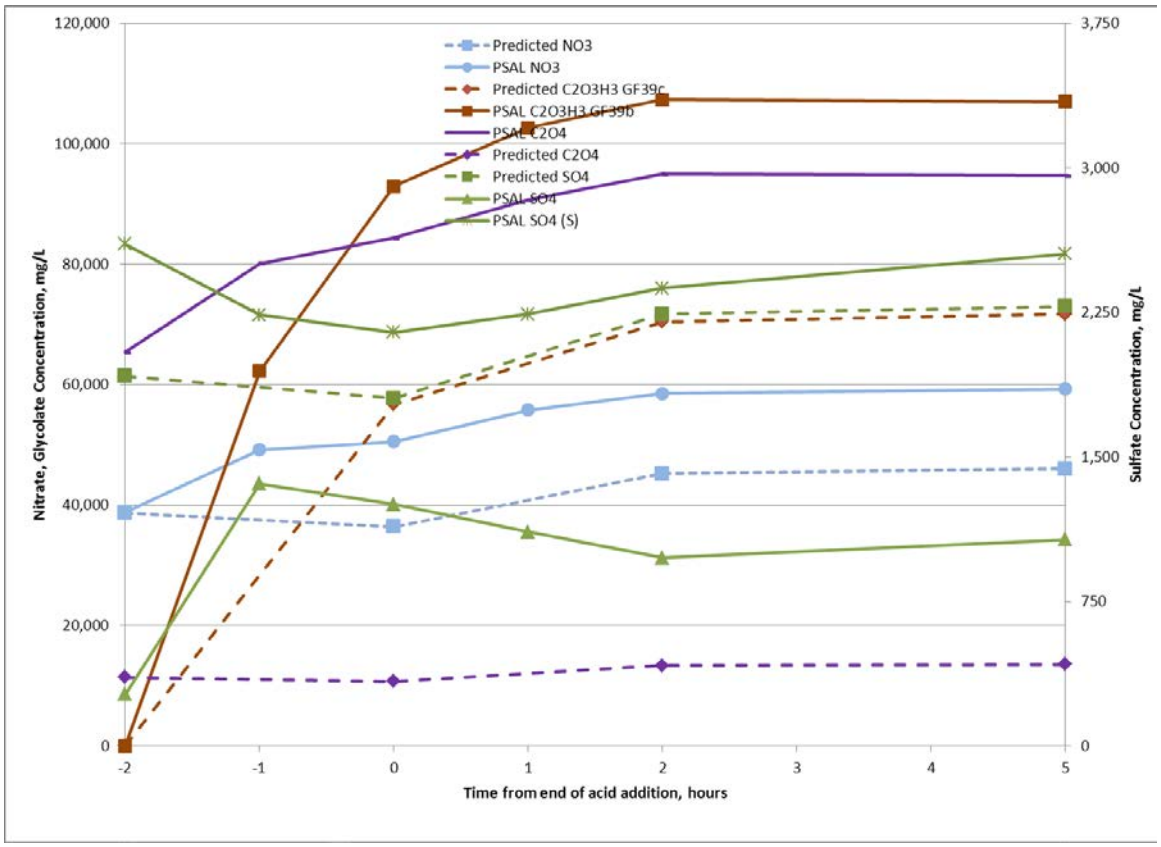

Figure D-3. GF39c Supernate Anion Results

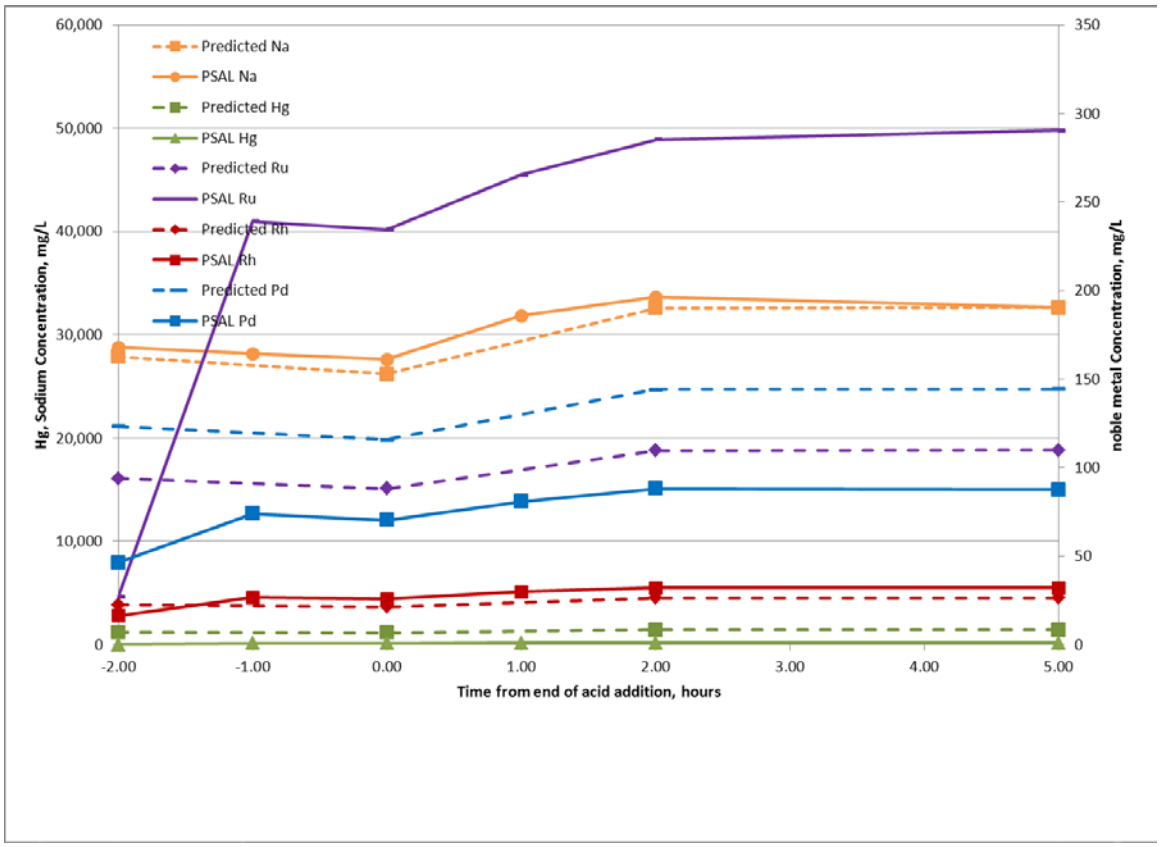

Figure D-4. GF39c Supernate Cation Results

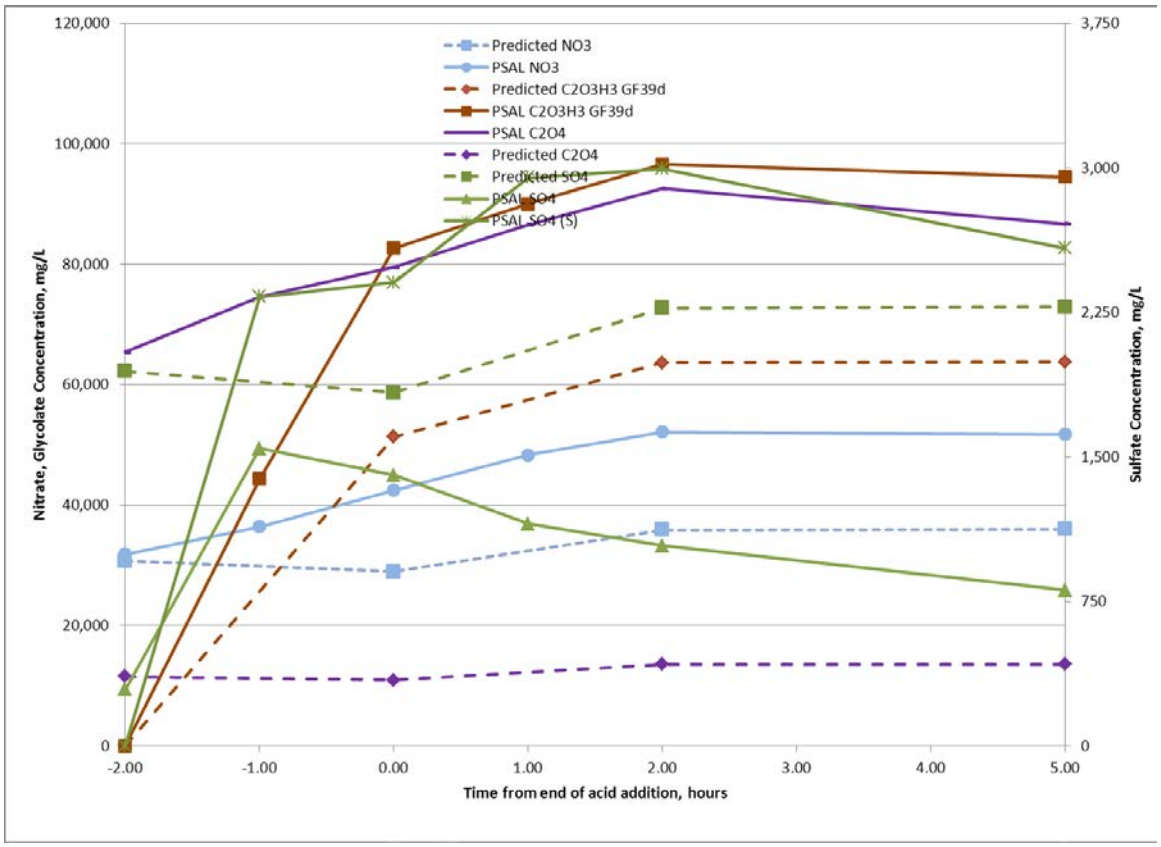

Figure D-5. GF39d Supernate Anion Results

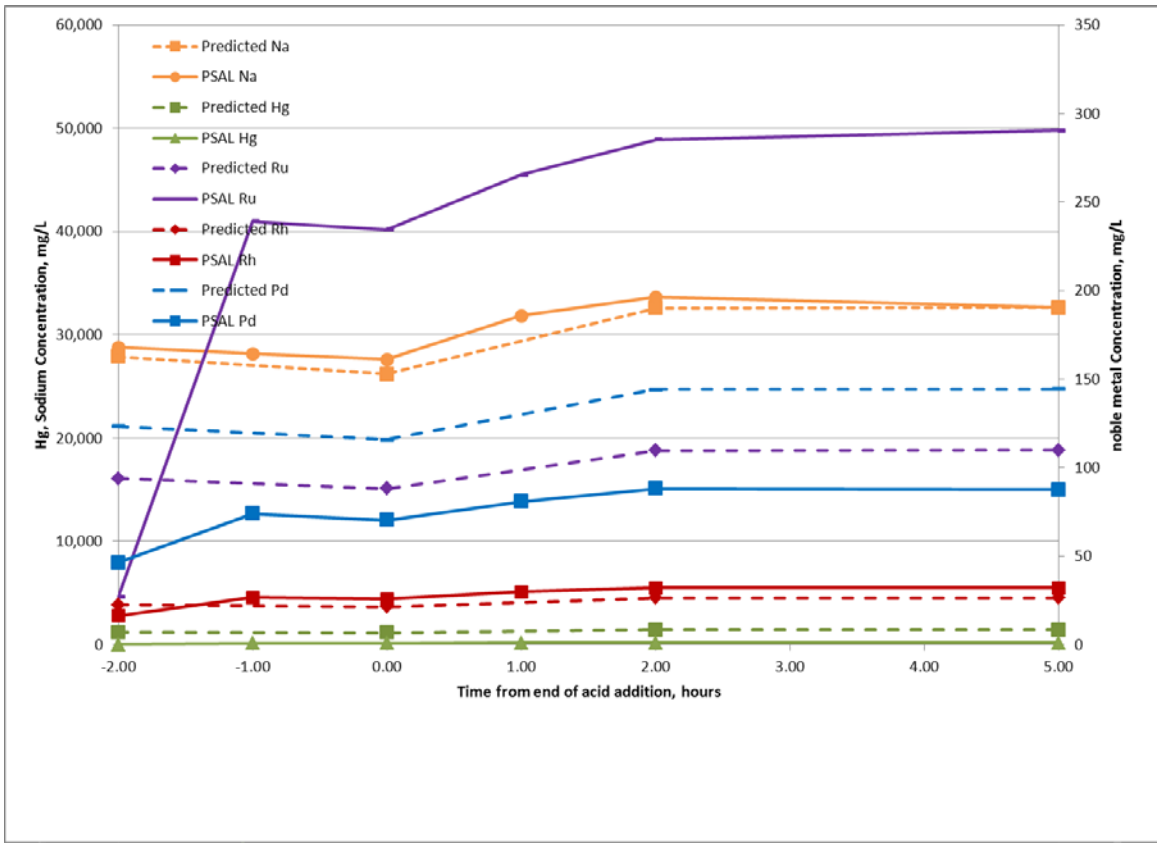

Figure D-6. GF39d Supernate Cation Results

Distribution:

K. M. Fox, 999-W
A. P. Fellinger, 773-41A
S. D. Fink, 773-A
B. J. Giddings, 786-5A
C. C. Herman, 999-W
S. L. Marra, 773-A
F. M. Pennebaker, 773-42A
W. R. Wilmarth, 773-A
Records Administration (EDWS)
C. J. Bannochie, 773-42A
J. M. Bricker, 704-27S
T. L. Fellinger, 704-26S
A. Samadi-Dezfouli
J. M. Gillam, 766-H
B. A. Hamm, 766-H
E. W. Holtzscheiter, 704-15S
J. F. Iaukea, 704-30S
M. T. Keefer, 766-H
M. A. Rios-Armstrong, 241-156A
D. W. McIlmoyle, 766-H
T. A. Le, 766-H
J. E. Occhipinti, 704-S
D. K. Peeler, 999-W
J. W. Ray, 704-S
H. B. Shah, 766-H
D. C. Sherburne, 704-S
A. V. Staub, 704-27S
M. E. Stone, 999-W
P. R. Jackson, DOE-SR, 703-46A
K. H. Subramanian, 766-H
C. E. Duffey, 704-61H
A. W. Wiggins, 704-60H